Cyprus University of Technology

Faculty of Geotechnical Sciences and Environmental management

Doctoral Dissertation

STUDY OF MAILLARD REACTIONS WITH COUPLED CHROMATOGRAPHIC AND SPECTROSCOPIC TECHNIQUES

Aristodimos Ioannou

Limassol, September 2017

CYPRUS UNIVERSITY OF TECHNOLOGY

FACULTY OF GEOTECHNICAL SCIENCES AND ENVIRONMENTAL MANAGEMENT

DEPARTMENT OF ENVIRONMENTAL SCIENCE AND TECHNOLOGY

Doctoral Dissertation

STUDY OF MAILLARD REACTIONS WITH COUPLED CHROMATOGRAPHIC AND SPECTROSCOPIC TECHNIQUES

Aristodimos Ioannou

Limassol, September 2017

Approval Form

Doctoral Dissertation

STUDY OF MAILLARD REACTIONS WITH COUPLED CHROMATOGRAPHIC AND SPECTROSCOPIC TECHNIQUES

Presented by

Aristodimos Ioannou

Supervisor: Prof. Constantinos Varotsis

Signature _____

Member of the committee: Prof. Demetrios Anglos

Signature _____

Member of the committee: Prof. Dimitris Tsaltas

Signature _____

Cyprus University of Technology

Limassol, September 2017

Copyrights

The present study was performed in the laboratory of Environmental Biocatalysis and Biotechnology at the Cyprus University of Technology and would like to thank the lab members, starting from my supervisor, Prof. Constantinos Varotsis, whom I warmly thank for the award of the subject, the allocation of the laboratory and the laboratory equipment for conducting experiments, as well as for the valuable help and knowledge he gave me and for the excellent cooperation we have had all these difficult nonetheless productive years. I would also like to thank my fellow doctoral students, Antonis Nicolaides and Anastasia Adamou for the solidarity shown over the years that we worked together. I would also like to thank my wife Marilena Loizou for all her support and patience throughout my studies. Finally I would like to dedicate this to the newest member of our family our little son Ioannis Ioannou.

ABSTRACT

The present research work was aimed to study model Maillard reactions by a combination of analytical techniques such as HPLC, UV-vis and ATR-FTIR spectroscopies. The Maillard reaction involves a complex network of chemical reactions that occur in food after processing at high temperatures. A further purpose of this study was to develop simple spectroscopic methods of application of the spectroscopic properties of the food constituents.

The reaction of asparagine and fructose at high temperature was studied by the coupling technique of HPLC-ATR-FTIR. The coupling of high performance liquid chromatography (HPLC) with FTIR detection provides a further capability for confirming chemical system changes in a new experimental layout.

Furthermore, the formation of the Amadori products was identified by employing a combined analytical technique of Solid Phase Extraction (SPE) and Attenuated Total Reflection-Fourier Transform Infrared Spectroscopy (ATR-FTIR).

The isolation of reaction products of asparagine with reducing sugars at alkaline pH and high temperature was probed by a combination of high performance liquid chromatography (HPLC) coupled with a Fraction Collector. The reaction products were analyzed by UV-vis and Fourier transform infrared (FTIR) spectrophotometry. The UV-vis and FTIR spectra of the isolated Maillard reaction products showed structure-sensitive changes as depicted by deamination events and formation of asparagine-saccharide conjugates. Evidence for Cu (II) metal ion complexation with the Maillard reaction products is supported by UV-Vis and FTIR spectroscopy.

The same model system was utilized to investigate the interaction of Maillard reaction products formed by the reactions of saccharide-derived compounds creating intermediates with proteins, more specifically with hemoglobin and myoglobin. The spectral events upon addition of discrete MRPs to hemoglobin and myoglobin were monitored. This led to the formation of a modified protein adduct known as a hemichrome.

Additionally, fluorescence spectroscopy was employed as a complementary technique to study the reaction of hemoglobin with MRPs from an asparagine-sugar model system. The modification of hemoglobin by MRPs was illustrated through tryptophan-specific changes in the fluorescent spectra.

TABLE OF CONTENTS

LIST OF TABLES

LIST OF FIGURES

LIST OF ABBREVIATIONS

Asn:	Asparagine
ATR:	Attenuated Total Reflection
Fruc:	Fructose
FTIR:	Fourier Transform Infrared
Gluc:	Glucose
HATR:	Horizontal Attenuated Total Reflection
HPLC:	High Performance Liquid Chromatography
Hb:	Hemoglobin
Mb:	Myoglobin
MR:	Maillard reaction
SPE:	Solid Phase Extraction
Trp	Tryptophan
UV-vis:	Ultra Violet-visible

1 Introduction

1.1 The Maillard reaction

The term Maillard reaction, or non-enzymatic browning, was named after its inventor, Louis-Camille Maillard. The Maillard reaction (MR) is one of the most important chemical reactions in food processing, with influence on several aspects of food quality such as flavor, color and nutritional value. In food science, Maillard Reaction (MR) is essential because of color and flavor formation in a vast range of processed foods. It occurs wherever non-enzymatic browning is induced by heat-treatment during food processing. Most unprocessed foods contain the necessary starter reactants which are amino acids/proteins and reducing sugar. Thus, the Maillard reaction is a collective term for the reaction between amines and carbonyl compounds, especially reducing sugars.

The Maillard reaction is a series of subsequent and parallel reactions (**Figure 1**) and it typically consists of three major stages: the early, the advanced, and the final stage [1].

i) The early stage: The early stage involves the condensation of a free amino group (from free amino acids and/or proteins) with a reducing sugar to form Amadori or Heyns rearrangement products via an N-substituted glycosylamine. The nucleophilic attack by a free amino group on the aldehyde of glucose initially forms a carbinolamine. The carbinolamine subsequently dehydrates to a Schiff base. Next, the Schiff base undergoes a slow rearrangement to form the Amadori product (**Figure 2**).

ii) The advanced stage: The advanced stage is the degradation of the Amadori or Heyns rearrangement products via different alternative routes. These involve a number of possible reaction routes involving deoxyosones, fission or Strecker degradation. Complex series of reactions including dehydration, elimination, cyclization, fission and fragmentation result in a pool of flavour intermediates and flavour compounds [2]. The Schiff base and Amadori adduct also undergo facile oxidation, especially in the presence of transition metal ions, and fragment to yield shorter chain sugars and reactive intermediates, such as glyoxal (GO) and methylglyoxal (MGO). Amadori product will degrade to form reactive dicarbonyl compounds such as 3-deoxyglucosone, glyoxal, methylglyoxal that can again react with amino compounds leading to the generation of AGEs. The Strecker degradation is an important pathway in which amino acids react

with dicarbonyl compounds to generate numerous reactive intermediates. Strecker degradation is also a suggested route of formation of the toxic compound acrylamide.

iii) The final stage: The final stage is characterized by the formation of brown nitrogenous polymers and co-polymers (**Figure 1**). The color compounds can be grouped into two general classes: a) low molecular weight compounds, which comprise between two and four linked rings of heterocyclic compounds, and b) the melanoidins, which have much higher molecular weights.

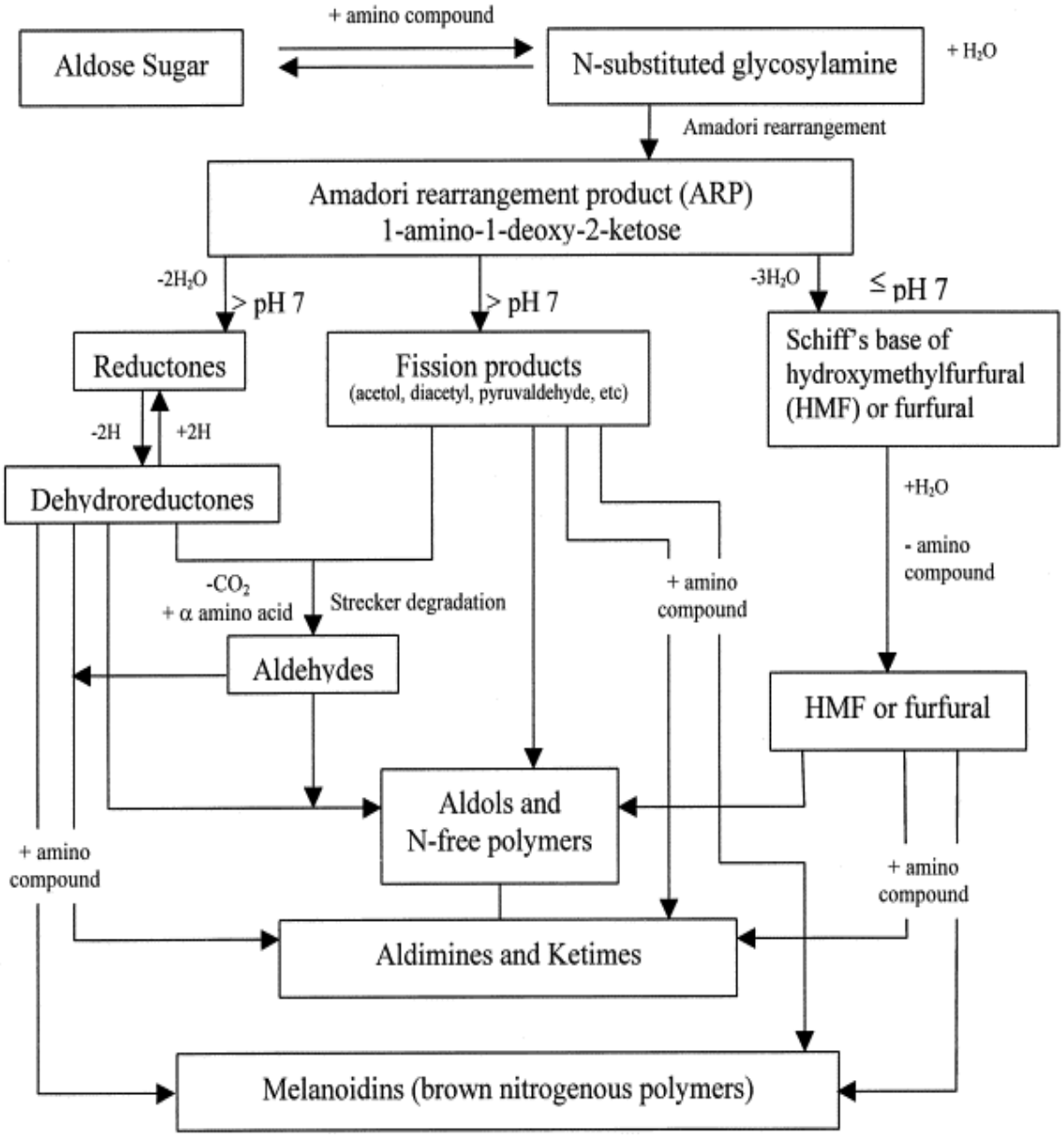

Figure 1. Overview of the Maillard reaction network of chemical reactions (Adapted from [1]).

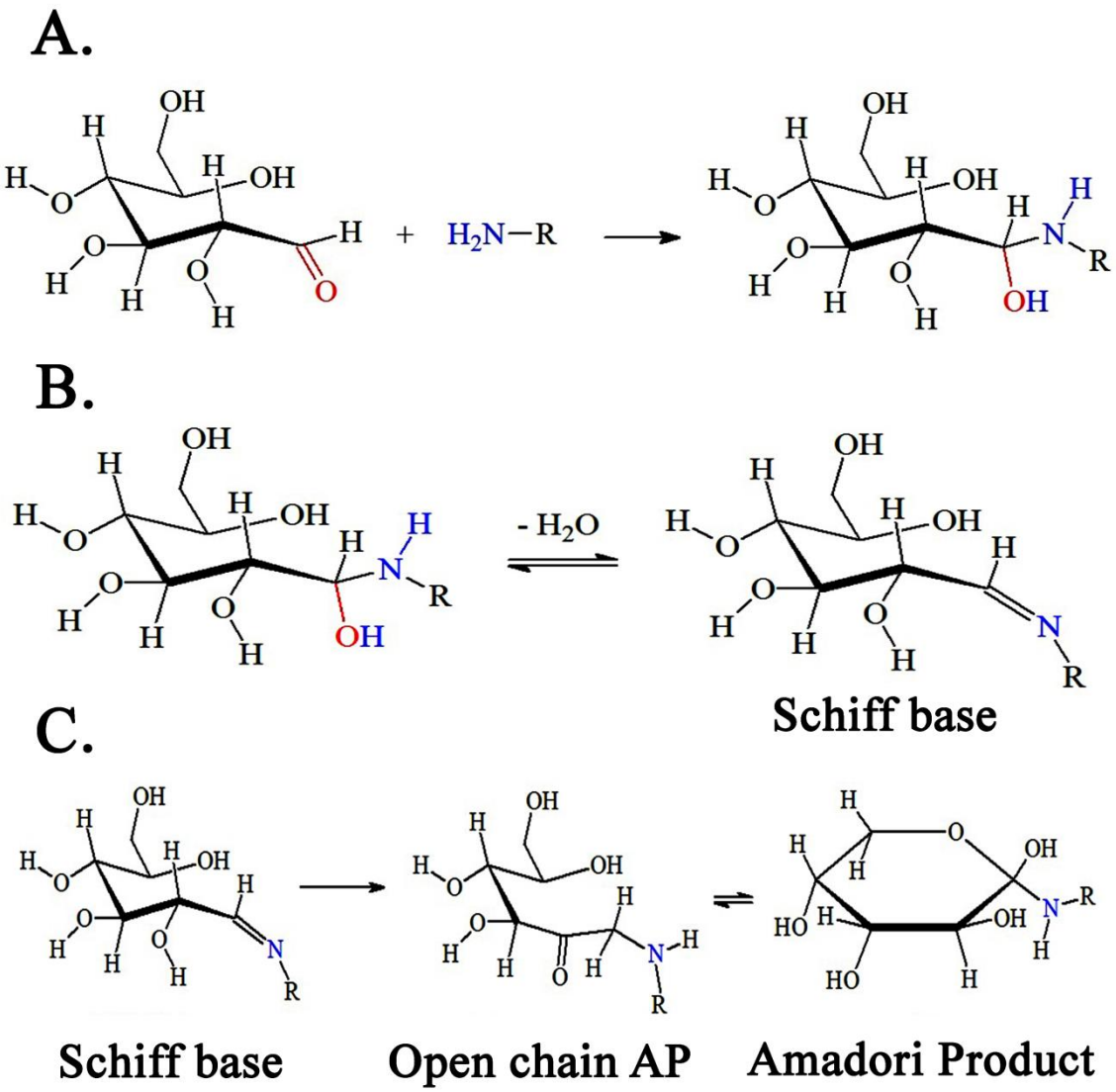

Figure 2. Reaction between glucose and the amino group of amino acids, proteins or peptides **A.** Carbinolamine formation by the nucleophilic attack by a free amino group on the aldehyde of glucose. **B.** Schiff base formation after dehydration. **C.** Amadori Product formation from the Schiff base.

All these reactions can occur simultaneously, affected by each other as well as by reaction parameters. Color formation increases with increasing temperature, with time of heating, with increasing pH and by intermediate moisture content (water activity, a_w = 0.3-0.7). As a general rule, browning occurs slowly in dry systems at low temperatures and is relatively slow in high-moisture foods.

1.2 Acrylamide and the Maillard reaction

The Maillard reaction can cause both enhancement and deterioration of food quality. Maillard reaction products (MRPs) containing anti-oxidant, anti-allergenic, anti-microbial and cytotoxic properties are amongst others mostly detected. Special attention has been on the high anti-oxidant capacity of MRPs in model systems and foods. Traditionally, the main focus has been on components affecting color, flavor, and taste development as these play an important role on food quality. However, another aspect of the Maillard reaction has gained more attention in recent years: the formation of mutagens and carcinogens [3]. The discovery of acrylamide in foods has revisited the interest in the Maillard reaction.

There is an increasing demand from both consumers and regulatory organizations for high quality, healthy and safe food and food scientists attempt to develop new processes based on the existing and emerging knowledge of the complex Maillard reaction network. A parallel aim is to produce functional food ingredients without the use of harmful chemicals and time-consuming purification procedures. Thus, the exact determination of MRPs with their advantageous or harmful properties is of key importance.

1.3 Factors affecting acrylamide formation

The Maillard reaction and hence acrylamide formation is dependent upon several factors, such as concentrations of reactants and reactant type, pH, time, temperature, and water activity. Temperature is the most important parameter affecting the Maillard reaction. However, different combinations of reaction parameters can give either a synergistic or an antagonistic effect towards formation of acrylamide. For example, reaction time and temperature were found to be covariant parameters: acrylamide was preferably formed by reacting glucose and asparagine at 120 °C for 60 min, whereas 160 °C was required at shorter reaction time of 5 min [4]. It is now generally accepted that acrylamide is an intermediate of the Maillard reaction rather than an end product, which implies that it is also subject to a degradation reaction. The formation and elimination reactions seem to occur simultaneously. The actual acrylamide level in any food product reflects the balance between formation and elimination reactions.

Another important factor affecting rate of formation/elimination reaction of acrylamide is the type of reactants involved. The higher yield of acrylamide at pH 5.5 with fructose compared to pH 6.8 with glucose suggests that in food systems, the type of reducing sugar as well as pH can play a role in lowering acrylamide formation [5]. Pyrolysis and kinetics of acrylamide release in amorphous and crystalline glucose/asparagine models indicated the importance of the physical state in acrylamide formation. In amorphous systems, acrylamide was generated in higher concentrations and at lower temperatures as compared to the crystalline samples [6]. The formation of acrylamide reached its maximum when the amount of sugars was completely consumed [7]. This supported previous findings showing that a carbonyl source is needed for the formation of acrylamide from asparagine [8-9] (**Figure 3**).

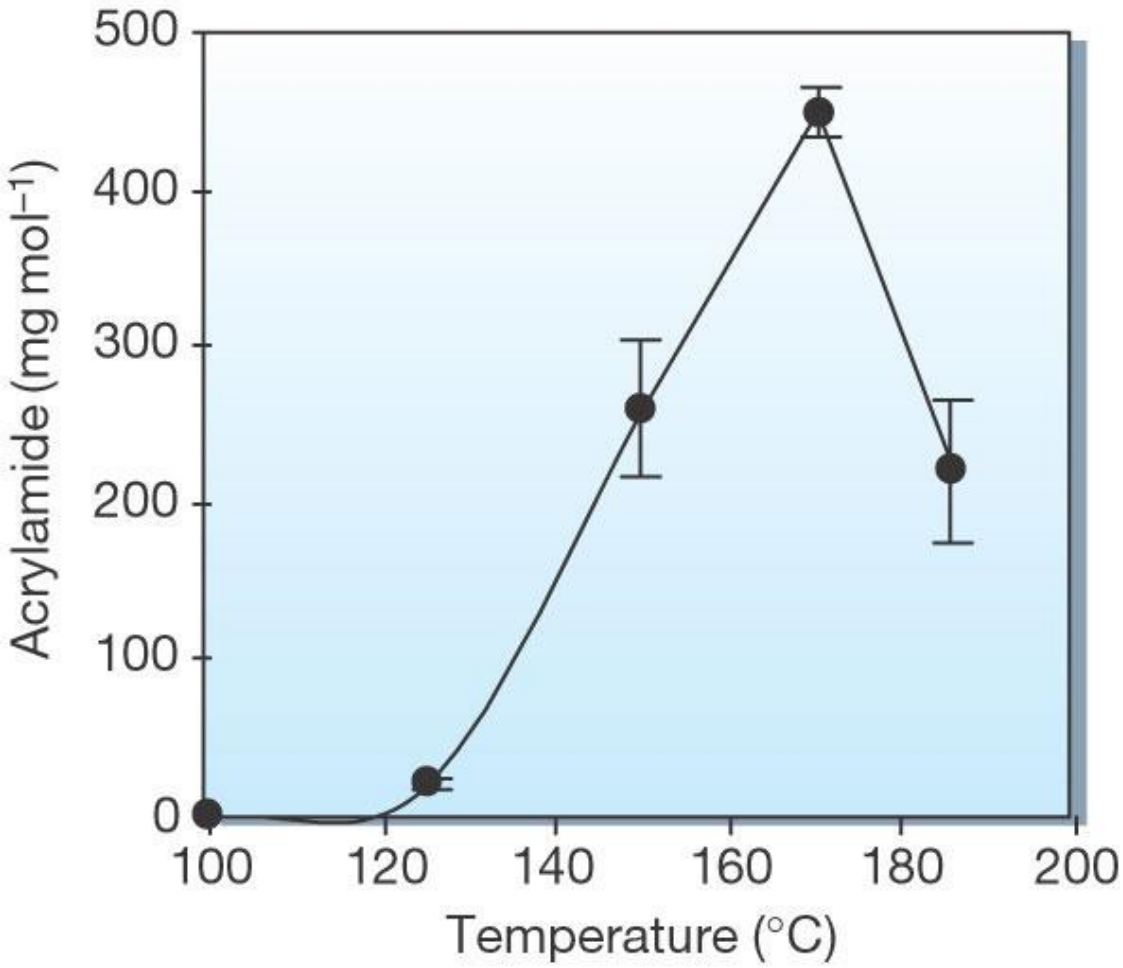

Figure 3. Temperature-dependent formation of acrylamide (mg per mol of amino acid) from asparagine and glucose [8].

In a study involving a heated potato food system it was shown that the dependence on pH of the acrylamide content exhibited a maximum around pH 8 and in particular, lower pH was shown to enhance elimination and decelerate formation of acrylamide [10]. The effect of pH on acrylamide formation and elimination kinetics was also modeled in an asparagine-glucose model system where by increasing acidity, the reaction rate constants at a reference temperature of 160 °C for both acrylamide formation and elimination can significantly be reduced, whereas the temperature dependence of both reaction rate constants was increased [11].

The presence of ammonium hydrogen carbonate led to increases in acrylamide and α-dicarbonyls from glucose and fructose, respectively [12]. The effects of mono- and divalent cations on the formation of acrylamide were studied in a fructose-asparagine model system at high temperatures and it was shown that added divalent cations, such as Ca^{2+}, were found to prevent acrylamide formation completely, whereas monovalent cations, such as Na^{+}, almost halved the acrylamide formed in the model system [13].

1.4 Pathways of acrylamide formation

1.4.1 The asparagine pathway

The formation of acrylamide follows a number of possible routes in concurrence with the Maillard reactions system in food products, in which the asparagine route is the major one for formation of acrylamide. Current data indicate that the Maillard reaction is an important reaction route for acrylamide formation. Acrylamide has been shown to originate from the Maillard reaction of the amino acid asparagine with reducing sugars as well as carbonylic compounds deriving from either the Maillard reaction or lipid oxidation processes [9,12,14-15] during heating. Maillard reactions involving asparagine can produce acrylamide and can explain the increased concentrations of acrylamide in certain plant-derived foods after cooking [8]. Asparagine and glutamine were the only amino acids tested that formed acrylamide, and the higher yield of acrylamide from asparagine demonstrated that it is the predominant amino acid responsible for forming acrylamide [9]. The side chain amide group of asparagine is incorporated into the amide bond of acrylamide. Experiments with uniformly isotope-substituted asparagine (all carbons and nitrogens were isotope substituted) heated with

d-glucose showed that all three acrylamide carbon atoms, as well as the one nitrogen atom, came from asparagine [9]. An additional experiment with 13C6-d-glucose and unsubstituted asparagine in the model system resulted in only unsubstituted acrylamide [9].

1.4.2 Mechanism of acrylamide formation in food

Glycoconjugates, such as N-glycosides and related compounds formed in the early phase of the Maillard reaction have been proposed as key intermediates leading to acrylamide formation [16]. This hypothesis was supported by the work of Zyzak et al., 2003 and Yaylayan et al., 2003. Both groups provided evidence of the importance of Schiff base of asparagine which is formed after a dehydration step (**Figure 4**). The Schiff base is formed early in the Maillard reaction as the result of elimination of water from the conjugate of glucose and asparagine [9,14]. The key mechanistic step seems to be the decarboxylation of the Schiff base leading to intermediates that can directly release acrylamide (**Figure 4**). However, some researchers have discussed the fact that at high temperature conditions, formation of the Schiff base is accordingly rate determining, while at lower temperatures, decarboxylation becomes rate determining [18].

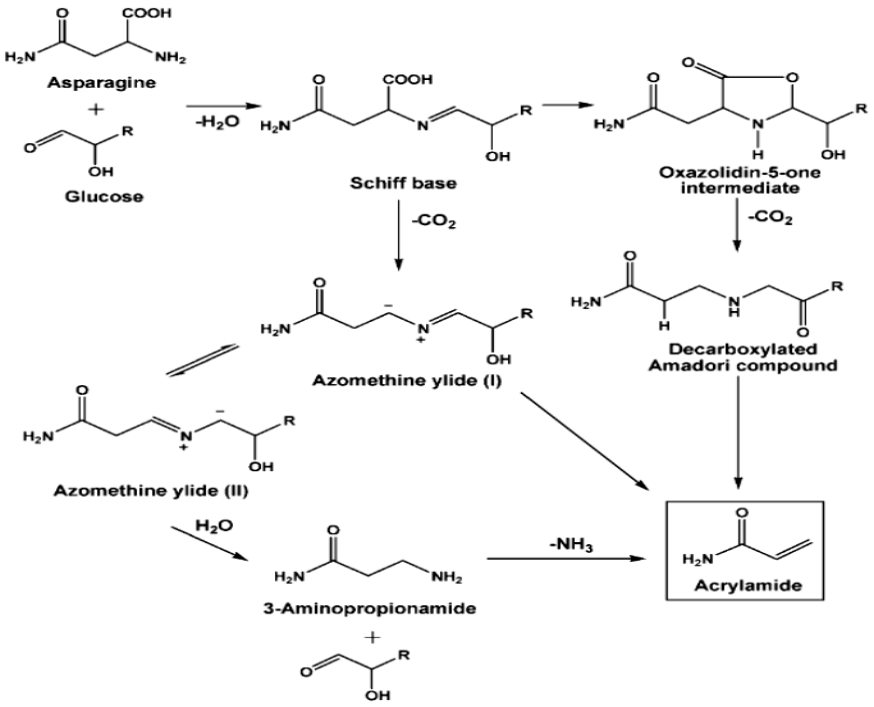

Figure 4. Proposed formation mechanism of acrylamide formation via the asparagine pathway.

Some key intermediates in the asparagine pathway are only predicted, and therefore, the chemical interactions leading to acrylamide remains largely hypothetical. To fill in the gaps under the currently proposed routes, the mechanism of acrylamide formation in food was further demonstrated by comparing the two major hypothetical pathways, i.e. via (i) the Strecker aldehyde route and (ii) glycoconjugates of asparagine [14]. Model studies have shown that the N-glycosyl of asparagine generated 20 times more acrylamide, compared to α-dicarbonyls and the Amadori compound of asparagine and that the Strecker alcohol of acrylamide, 3-hydroxypropanamide, generates 20 times less amounts of acrylamide compared with hydroxyacetone [14]. It is therefore concluded that α-hydroxy carbonyl compounds, such as fructose and glucose are more effective than other carbonylic compounds in generating acrylamide.

1.4.3 Key intermediates in acrylamide formation

The decarboxylated Schiff base and decarboxylated Amadori product are both key intermediates contributing to the formation of acrylamide (**Figure 5**). Their relative importance was determined when both of the intermediates were synthesized and their relative abilities to generate acrylamide under dry and wet heating conditions were investigated [19] (**Figure 6**).

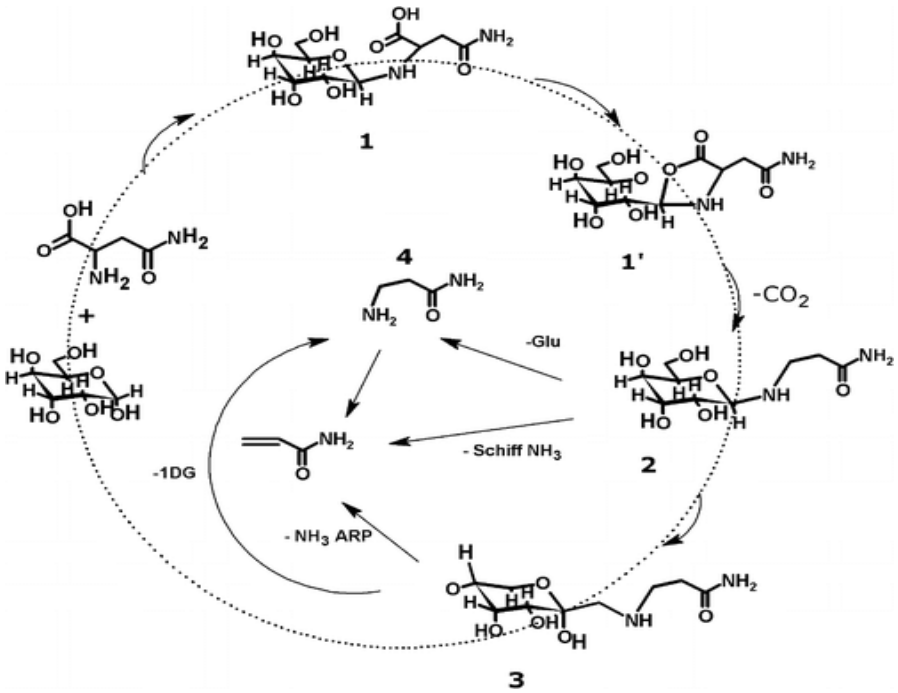

Figure 5. Proposed reactive intermediates involved in the generation of acrylamide. (Glu, glucose; ARP, Amadori rearrangement product; 1-DG, 1-deoxyglucosone).

Recently, azomethine ylides (**Figure 4**) have been implicated as intermediates in the Maillard reaction [17,20,21] on the basis of evidence from spectroscopic [22,23] and isotope labeling studies [15,23] using different model systems at various temperatures. One of their precursor intermediate is oxazolidin-5-one which was recently monitored by FTIR in a dry model reaction system [23]. This intermediate is thought to initiate further isomerization reactions which propagate the Maillard reaction. The azomethine ylides are known to undergo 1,3-cycloaddition reactions with dipolarophiles [24] to form pyrroles and this was used as an indirect evidence of their existence in the Maillard reaction. More importantly, they can undergo dimerization reaction leading to the formation of a piperazine moiety [25].

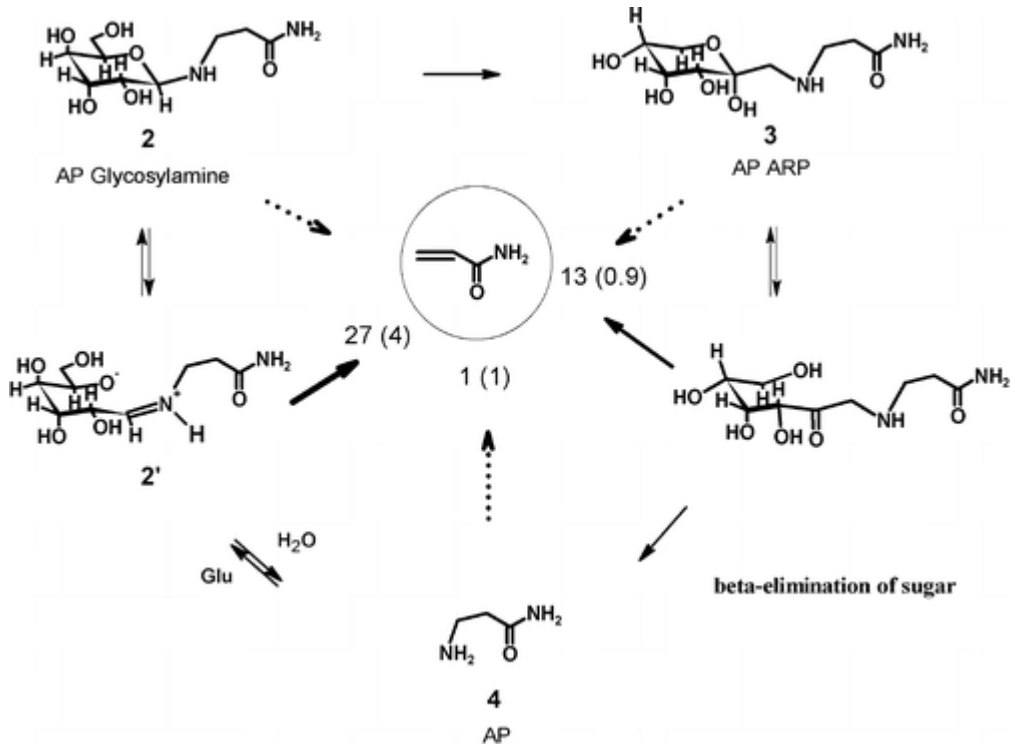

Figure 6. Reactive precursors and their relative abilities to generate acrylamide in wet and dry (values in parentheses) model systems. (Glu, glucose; AP, 3-aminopropionamide; ARP, Amadori rearrangement product) [19].

3-Aminopropionamide was first identified as a transient intermediate during acrylamide formation from asparagine [9]. In addition to that 3-aminopropionamide can be formed in foods by enzymatic decarboxylation of asparagine [26], and in reactions between asparagine and pyruvic acid [14], and it is a very effective precursor of acrylamide formation under certain reaction conditions.

1.5 The significance of aqueous and dry systems

As the pathway shown in **Figure 4**, the first critical step is the amino-carbonyl reaction between asparagine and a carbonyl substance, preferably reducing sugars, resulting in the relative N-glycosyl conjugation and forming the Schiff base as a key intermediate after dehydration under elevated temperatures. The well-studied initial reaction steps have been difficult to describe kinetically, mainly because the Schiff base is difficult to be determined quantitatively [18]. Decarboxylation of the initially formed Schiff base of glucose with asparagine is one of the critical steps in the pathway of conversion of asparagine into acrylamide.

Both the N-glycosyl conjugation and the Schiff base are relatively stable under low-moisture systems. N-glycosides were synthesized by condensation of reducing sugars and amino acids in anhydrous methanol under basic pH conditions [14]. In aqueous systems, however, the Schiff base may be hydrolyzed to the precursors or be rearranged to the Amadori compound (**Figure 4**), which is not an efficient precursor during acrylamide formation. Even under low-moisture conditions, this reaction is hypothesized to be the main pathway initiating the early Maillard reaction stage that leads to 1- and 3-deoxyosones, which further decompose, generating color and flavor. This is in accordance with the relatively low transformation yield of asparagine to acrylamide.

In dry systems, the open-form Schiff bases are prone to undergo intramolecular cyclization to form either 5-oxazolidinone or glycosylamines, unlike in high-moisture systems where they tend to undergo Amadori rearrangement, the more stable isomer. Alternatively, Schiff base may decarboxylate either directly via the Schiff betaine or via the intermediary oxazolidine-5-one to generate the azomethine ylide I, which provides the decarboxylated Amadori product after tautomerization. The decarboxylated Schiff

base (azomethine ylide) and decarboxylated Amadori product are both key intermediates contributing to the formation of acrylamide.

There is sufficient experimental evidence in favour of a reaction mechanism based on (i) a Strecker-type degradation of the Schiff base leading to azomethine ylides, followed by (ii) a β-elimination reaction of the decarboxylated Amadori compound to afford acrylamide. Acrylamide formation takes place in the early stages of the Maillard reaction and is highly interrelated with browning [27]. Acrylamide was concluded to be formed in a reaction step prior to browning. The rate of formation of acrylamide at temperatures above 120 ˚C appears to be of zero order with respect to glucose and first order with respect to asparagine, which indicates that a simple collision between the reactant molecules is not rate determining. This is in contrast to the browning reaction determined as the melanoidin content, the rate of which is highly dependent on the concentration of glucose [28].

Imines or Schiff bases formed through the interaction of reducing sugars with amino acids are known to play a critical role not only in initiating the Maillard reaction but also in its propagation through isomerization reactions. Imines formed subsequent to carbonyl–amine reactions between amino acids and reducing sugars tend to undergo various chemical transformations depending on the nature of the carbonyl moiety such as Amadori rearrangement, the Strecker reaction, or cyclizations to generate N-containing heterocyclic compounds. Preceding these transformations, imines are also susceptible to isomerization reactions, further increasing the diversity of Maillard reaction products. Isomerization reactions can proceed either through oxazolidin-5-one formation in dry systems to generate decarboxylated imine isomers or through transamination reactions (**Figure 4**).

In a recent study acrylamide generation was examined through oxazolidin-5-one formation in the glucose–asparagine model system [19]. Further work revealed FTIR spectroscopic evidence for the formation of this intermediate in a phenylalanine-glycoaldehyde model system [23]. The sampling methods were developed in order to enhance the sensitivity of the detection specific towards the detection of the oxazolidin-5-one intermediate in the absence of water. An equimolar mixture of glycoaldehyde and phenylalanine was briefly heated in toluene at a high temperature and the sample was applied and evaporated on a temperature-controlled ATR crystal. An alternative in the

same study used methanol as a solvent to form a melt of one of the reactants with the addition of the powdered amino acid on the ATR crystal [23].

There are only few studies utilizing the monitoring ability of the FTIR technique to elucidate the reaction network in the acrylamide formation pathway. FTIR is more often used as a complementary technique mainly to chromatographic and/or mass spectroscopic techniques employed to study the mechanism of formation of acrylamide. There is also no developed FTIR analysis method to detect acrylamide either in simple model systems or food systems. This is probably due to the low sensitivity of the existing FTIR techniques compared to chromatographic and mass spectroscopic techniques.

However, Attenuated Total Reflection (ATR)-Fourier transform infrared (FTIR) spectroscopy techniques have potential qualitative and quantitative applications for food analyses. FTIR-ATR provides a simple and reproducible means of sample handling in the form of liquids; the analyses are nondestructive with fast sampling. The application of ATR-FTIR for the rapid and simultaneous determination of both reactants and products exploits the potential of this technique towards constructing a chemical fingerprints. Fingerprinting instrumental techniques like UV-vis and mid infrared spectroscopy have become more popular especially for qualitative analyses.

1.6 Fluorescence from the Maillard reaction

The fluorescent compounds formed in the frame of Maillard reactions have been considered intermediates during pigment formation and are useful in helping to detect early stages of the reaction when there is no color formation [29-30]. In the initial stage of the MR, the Amadori compounds are thought to exhibit no fluorescent, but in advanced MR stages these compounds can form cross-links with further protein molecules or with other amino groups, resulting in fluorescent polymeric aggregates or advanced glycation end products (AGEs). Thus, fluorescent compounds may be free in the matrix or linked to the protein fraction and this often dictates the analytical methodology of their detection.

In biological systems, the fluorescent AGEs are thought as final products and are useful indicators of the level of the damage of biomolecules in a prolonged time frame. The incidence of this reaction in vivo has adverse effects on the functionality of biomolecules and biological structures, and it has been investigated in relation to aging and disorders such as diabetes. Likewise, the functional loss in foods can be due to color/flavor development, texture changes as a result of protein cross-linking or nutritional damage. A characteristic example in foods is milk, where measurements of fluorescence at different wavelengths or the fluorescence of advanced Maillard products and soluble tryptophan (FAST) index have been employed to evaluate the progress of MR resulting from thermal treatments or processing [31-35]. The FAST method is based on the quantification of protein denaturation.

The Hodge's scheme the Maillard reaction as previously discussed is generally divided into three stages [1]. The first stage involves sugar-amine condensation and isomerization (Amadori/Heinz rearrangements) with no pigments formed at this stage. The second stage involves the reaction of Amadori compounds to form sugar dehydration and fragmentation products and amino acid degradation via the Strecker reaction. Later, in the final stage, the Amadori products degrade into α- dicarbonyl compounds that continually react with the amino groups to form stable intra- and intermolecular cross-linking and are responsible for the formation of browning chromophores.

The complete classification of the scheme of the Maillard reaction is difficult in the sense that kinetic consideration of the reaction pathways depend on the specific experimental conditions. The rate of the initial amino-carbonyl condensation and the nature of the MRPs are directed by the immediate chemical environment of the reactants defined by a number of factors (water content, pH, presence and type of buffer salts, temperature, etc). Extensive data in the literature [13, 36-40] have pointed towards the hypothesis that fluorescent and colored compounds are not identical, and that the maximum of fluorescence increase was followed by the increase of pigment formation. Fluorescent compounds may also be converted into AGEs and then into brown pigments, or can directly react to form brown pigments.

In terms of kinetics, fluorescent products will accumulate if the limiting step of the reaction was the transformation of fluorescent products into pigments (**Figure 7a**). Conversely, it may be that the limiting step is the fluorescent products development, and then we would have conversion the fluorescent products into pigments rather than accumulating (**Figure 7b**). Another scheme could be the parallel reactions dictating production of fluorophores and pigments (**Figure 7c**). Owing to the high influence of the environmental and compositional factors governing Maillard reactions, it is obvious that it is not always possible to establish a universal mechanism. It is likewise probable that consecutive and parallel reactions may co-exist. Favorable conditions for consecutive reactions and the formation of limiting concentration of fluorescent products include the presence of phosphate buffer, neutral pH and presence of highly reactive species. Non-favorable conditions for the Maillard reaction include low pH and presence of retardant buffers or salts [41].

The temperature requirements of reactions involved in lipid oxidation and Maillard reactions are different. Lipid oxidation, having low activation energy values, is less temperature-dependent than Maillard reaction (which has higher activation energy values). At lower temperatures, lipid oxidation may be significant, while Maillard reaction progresses slowly [42].

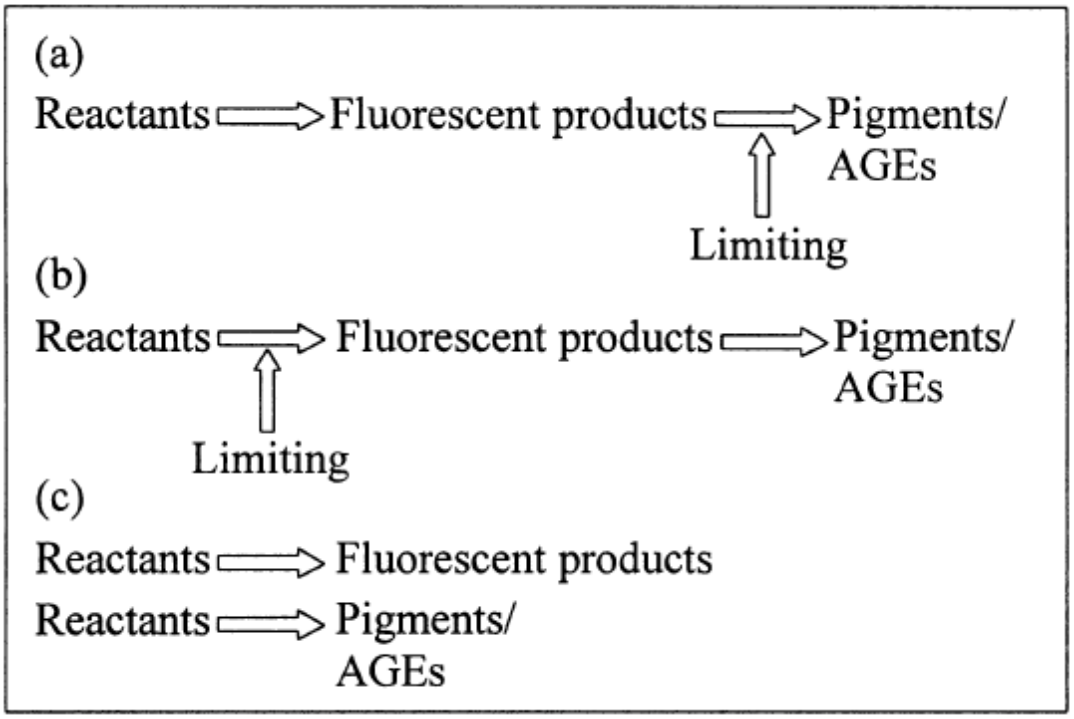

Figure 7. Proposed kinetic considerations for the formation of fluorescent and pigment compounds in the Maillard reaction. (a) Consecutive reactions, limiting step is the passage from fluorescent to pigment compounds (favourable conditions); (b) Consecutive reactions, limiting step is the passage from reactants to fluorescent compounds (unfavourable conditions); (c) Parallel reactions (any condition) [43].

A series of consecutive and parallel reactions may occur in the same reaction pool. As a result, the separation of the three defined initial, intermediate, and final stages is considered a generalization and a simplistic overall scheme. Yaylayan (1997) introduced the pool concept [2]. Both reactants and products from the first stage are included in pool 1. Pool 2 is composed by dehydration and fragmentation products derived from pool 1, and by the independent degradation of sugars and amino acids. Reactants and products from both pools can further react and can be found at the end of the reaction along with the final products. Fluorescent compounds are presented in this scheme as the result of these last interactions (**Figure 8**).

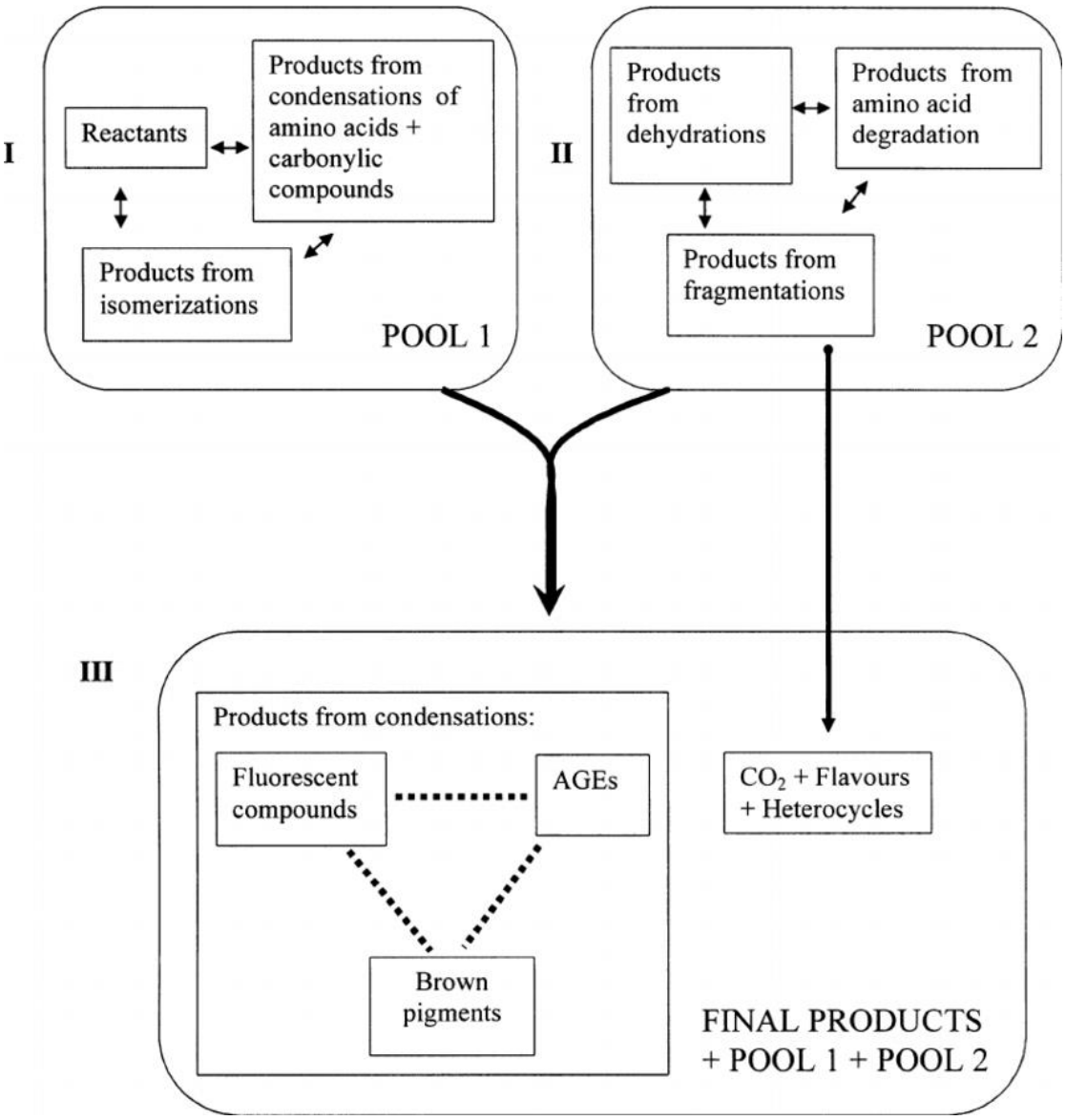

Figure 8. Conceptual scheme of the Maillard reaction with the pool approach introduced by Yaylayan (1997).

1.7 Potentially hazardous MRP compounds

Alongside to the positive effects, several unfavorable concerns of thermal processes have been recently addressed. The loss of temperature-sensitive compounds for example vitamins in addition to essential amino acids (lysine, tryptophan) and/or the formation of undesired and off-flavors are well established occurrences resulting in loss in the nutritional value and sensorial quality of heated foods. Nevertheless, the main concerns

resulting from the application of high temperatures arise from the creation of hazardous chemical substances, termed as food-borne toxicants i.e. compounds that are not naturally present in foods, but that may be developed during elevated temperatures or certain storage conditions and that reveal detrimental effects. Well acknowledged examples of these foodborne toxicants are heterocyclic amines, nitrosamines and polycyclic aromatic hydrocarbons.

The example of acrylamide has become a case study due to its high toxicological potential and its extensive occurrence in foods. The toxicological effects of acrylamide have been studied in animal models and humans. Exposure to acrylamide leads to DNA damage and at high doses neurological and reproductive effects have been observed. Carcinogenicity to humans has not been demonstrated in epidemiological studies, although it is classified as a carcinogenic compound. Acrylamide has been classified as a "probable human carcinogen" [44]. In addition, it is classified as a germ cell mutagen. The highly effective neurotoxic effects of acrylamide are mediated most probably by direct inhibition of neurotransmission or by kinesin-based fast axonal transport. In either case, however, the binding of electrophilic acrylamide or glycidamide to nucleophilic sites on proteins seems to make up the biochemical cause of these effects.

The high chemical reactivity of acrylamide arises primarily through its ethylenic double bond but also a reactive site on the acrylamide molecule itself is the amide group. The limited conjugation involving any π-electrons means that acrylamide lacks a strong chromophore for UV detection and does not fluoresce. Acrylamide exhibits both weakly acidic and basic properties. It is known to react as an electrophile by 1, 4-addition to nucleophiles such as SH and NH_2 groups in biomolecules [45]. The presence of amino acids with a nucleophilic side chain considerably decreased free acrylamide, due to Michael-type addition reactions. Many of these reactions are reversible, and the rate of reaction depends on the strength of the nucleophile. Examples are the addition of ammonia, amines, phosphines and bisulphites. Alkaline conditions favor the addition of mercaptans, sulfides, ketones, nitroalkanes, and alcohols to acrylamide. The highest reactivity was noted for cysteine, leading to the formation of the mono-addition product cysteine-S-β-propionamide, as well as to the double addition product [46].

Compounds that are highly reactive like acrylamide and short lived in the body can be demonstrated through their stable reaction products with biomacromolecules such as

proteins. There are six human proteins which are known to bind to acrylamide. A number of studies have identified potential acrylamide targets and potential mechanisms. In addition to experimental work computational studies have also been employed to predict potential targets. By means of molecular docking methodology, interactions between acrylamide and its human targets were studied providing novel information on putative cysteines to which acrylamide could be bound in both mouse and human protein [47]. It has been discovered that acrylamide is metabolized by cytochrome P450 2E1 to the epoxide glycidamide, which also possesses electrophilic reactivity [48].

1.8 Biological effects of Maillard reaction products

Protein nutritional loss, as a result of the reduction of essential amino acids or the decrease in their bioavailability, is a well-established nutritional concern of the Maillard reaction [49-50]. This is thought to occur through the decrease in the availability of several amino acids, mainly lysine in certain foods and also significantly lower protein absorption and digestibility. Protein cross-linking, a possible cause of solubility loss of milk proteins, like caseins and lactoglobulins, may occur via advanced Maillard reaction products (methylglyoxal or dehydroalanine). Another detrimental effect is the lowering of the bioavailability of minerals by MRPs, since these species have the capacity to chelate minerals leading to a decrease in mineral solubility [51]. One of the main health concerns is the substantial decrease on dietary iron availability when diets rich in MRPs were consumed [52]. Magnesium and calcium bioavailability was also shown to be affected by the existence of dietary MRPs [53-54]. Another example in the literature is the peptide-bound Maillard products N^{ε}-hippuryl-N-fructosyllysine and N^{ε}-hippuryl-N-carboxymethyllysine which can form complexes with copper ions [55]. These observations lead to the hypothesis that such binding by dietary metal-chelating compounds in vivo may negatively impact the biological and nutritional exploitation of essential trace elements and inhibit active sites of metalloenzymes. Similar observations were illustrated in other studies as well [56-57]. Other investigations have shown that lysinoalanine, a food processing related, cross-linked amino acid can also strongly chelate essential metal ions [58-60].

Genotoxic and mutagenicity of MRPs is still a controversial topic. Even though there are studies demonstrating that some MRPs have the potential to cause mutations, other researchers find no association between MRPs and genotoxicity [61]. It has been shown that in vitro, mixtures of melanoidins have negligible mutagenic effects [62], whereas the thermal damage marker compound 5-hydroxymethylfurfural (HMF) is reflected as possibly carcinogenic to humans and epidemiological studies have established a relationship between acrylamide intake and the incidence of tumors [63].

The formation of advanced glycation end products (AGEs) is normally observed during ageing and is located both intra- and extra-cellularly [64]. AGEs develop cross-links with proteins that severely impair protein functionality and irreversibly modify the functionality of a wide range of biological structures [65]. AGEs accumulate in numerous tissues such as skin, neural, vascular, renal and cardiac tissues, collagens and crystalline lens. Two recent studies, demonstrated that the amount of AGEs in plasma proteins are increased in diabetic patients [66-67]. The elevated blood glucose levels lead to the manifestation of glycation reactions between glucose and proteins, as a consequence of which is the excessive deposition of AGEs [68]. In the case of renal failure patients, AGEs buildup occurs due to the limited ability to degrade and eliminate these compounds from the body and furthermore to increased exposure to oxidative stress [69]. Other negative aspects of AGEs include their contribution in neurodegenerative diseases, for example Alzheimer's and Parkinson [70-71], arthritis [72], loss of bone mass [73] and enhancement of modifications in the structure and function of DNA and RNA [74].

A lot of emphasis has been given on the adverse effects of MRPs; nevertheless several authors highlight and endorse MRPs as compounds that may promote positive health effects. Food derived AGEs/MRPs are undoubtedly affected by digestive enzymes and also by the bacteria of the gut [75]. There is increasing evidence to suggest that MRPs are beneficial towards intestinal microbiota [76]. Anaerobic bacteria, predominantly Bifidobacteria strains, were able to utilize bread melanoidins as carbon source [77]. Likewise, Maillard Reaction products in roasted cocoa beans were able to inhibit the growth of E. coli and Enterobacteriaceae [78]. Water-soluble melanoidins isolated from roasted malt induced the liver detoxifying enzymes NADPH cytochrome-c reductase and glutathione-S-transferase in intestinal Caco-2 cells [79]. These results advocate that

melanoidins may enable the conjugation, metabolic fate, and elimination of toxic xenobiotics catalyzed by these enzymes. Additionally, MRPs display antioxidant activity [78, 80-83]. Melanoidins from roasted coffee and biscuits yielded protective effects against oxidative stress on human hepatoma cells [84-85]. Some in vivo experiments showed suppression of lipid peroxidation by a MRPs rich diet. This mechanism probably came through an increase in plasma antioxidant activity, and not through modification of the antioxidant enzymes activity such as superoxide dismutase, glutathione peroxidase and catalase [86].

In summary, understanding the chemical, biological and toxicological consequences of Maillard reactions, both in vitro and in vivo, is important towards improved and safer foods and enhanced human health. **Figure 9** presents a summary of the main biological effects related to Maillard Reaction Products (MRPs)/Advanced Glycation End Products (AGEs).

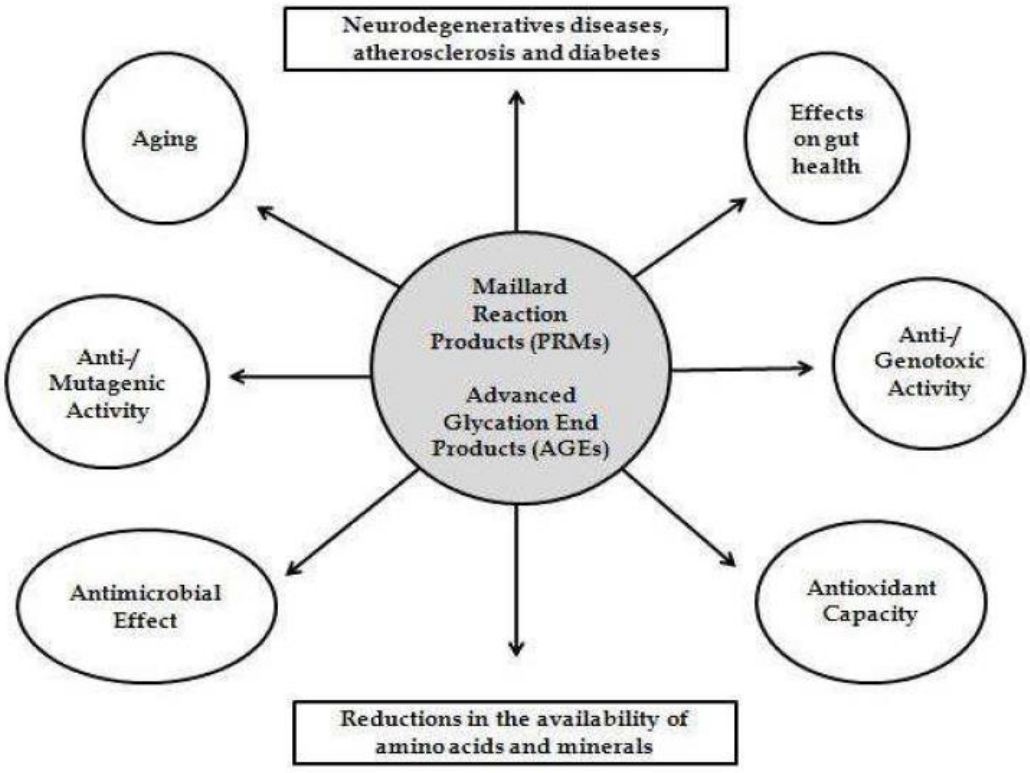

Figure 9. Biological effects of the Maillard Reaction Products and Advanced Glycation End Products (AGEs) [87].

1.9 Why is Maillard reaction still important

It is a fact that a great majority of the chemistry of the Maillard reaction has been elucidated in the last decades and an increasing volume of scientific data exists in the literature about the complexity of Maillard reaction. The Maillard reaction is, along with lipid oxidation, the hot topic contributing to the quality of processed foods. Therefore the efforts for its understanding and control are of extremely important towards the development of novel and functional foods. Apart from the food science area relevance, an understanding of the reaction mechanisms is necessary for the biological concerns relating to the consumption of MRPs.

The classical example of acrylamide came from an environmental accidental incident. Acrylamide became a major toxicological issue because of a large water leakage during the building of a railway tunnel in Sweden in 1997. The grouting material used to seal the tunnel walls containing monomeric acrylamide and N-methylolacrylamide leaked to the environment and spread into streams, ground water and wells, causing concern about exposure to residents in the area and also to the tunnel workers. Quantification of reaction products (adducts) with the protein haemoglobin (Hb) in blood showed that tunnel workers had received high exposures and several of them developed peripheral nerve symptoms. As a consequence of the environmental contamination, cattle in the area were taken away and local food products were destroyed; nevertheless acrylamide was never discovered in food products produced in the contaminated area. The observation that acrylamide used as a sealing adjuvant in tunnel construction in Sweden was responsible for adverse health effects in exposed humans eventually led researchers to an association of acrylamide with food [88]. They found that rats on a fried diet had significantly higher levels of the hemoglobin (Hb) adduct of acrylamide, measured as N-(2-carbamoylethyl)valine, than those fed a control diet. Analysis of the heat-treated feed revealed the presence of acrylamide in amounts that paralleled those of the Hb adducts. The suggestion was made that heat-treated food is probably the major source of acrylamide for humans. This was confirmed by the same authors 2 years later since they demonstrated high levels of acrylamide in heat processed commercial foods and in foods cooked at high temperatures, especially in carbohydrate rich foods [89].

The issue of the dietary AGEs is extensively discussed in recent years as a now established origin of dietary related diseases. The demonstration of the interaction of these AGEs with endogenous receptors (RAGEs) is responsible for triggering biochemical pathways sustaining inflammation and oxidative stress. There is controversy about the relevance of dietary AGEs in this process since there are also endogenously formed AGEs. However, it is now generally accepted that some risks exist that are associated to dietary AGEs consumption for specific high risk individuals, for instance those with renal diseases, uremic and diabetics.

The common link between the diseases of concentration, like diabetes and atherosclerosis, is that of the non-enzymatic chemical modification of proteins that is primarily the result of carbonylamine chemistry or more broadly, the reaction of nucleophilic groups on proteins (e.g. the side chains of lysine, arginine, histidine and cysteine) with electrophilic carbohydrates and lipids and their derivatives (e.g. hydroxyaldehydes, dicarbonyls, hydroxyalkenals). In both Maillard reactions and metabolism there are common intermediates derived from carbohydrates and lipids. However, there are characteristic compounds that are unique Advanced Lipoxidation End-products (**ALEs**) like malondialdehyde (MDA) and acrolein adducts to lysine, hydroxynonenal (HNE) adducts to lysine, histidine and cysteine and hexanoic acid amide derivatives of lysine. There is to date no evidence for enzymatic reversal of ALE formation. Some of these ALEs like MDA-Lys and and HNE-Lys have carbonyl groups which participate in further reactions which have not been studied in detail. It is also been recently demonstrated that asparagine is decarboxylated in the presence of alkanals, alkenals, and alkadienals, among other lipid derivatives. It is therefore of great value for one to investigate the reaction pathways by which some lipid oxidation products such as 2,4-decadienal for example are able to convert asparagine into other potentially reactive species like acrylamide.

1.10 References

[1] Hodge, J. E. (1953). Dehydrated Foods, Chemistry of Browning Reactions in Model Systems. *Journal of Agricultural and Food Chemistry,* **1**, pp. 928-943.

[2] Yaylayan, V. A. (1997). Classification of the Maillard reaction: A conceptual approach. *Trends in Food Science & Technology,* **8**, pp. 13-18.

[3] Arvidsson, P., van Boekel, M. A. J. S., Skog, K., Jägerstad, M. (1998). The Maillard Reaction in Foods and Medicine Formation of Mutagenic Maillard Reaction Products. In: O'Brien, J., Nursten, H. E., Crabbe, M. J., Ames J. M. eds, *Woodhead Publishing Series in Food Science, Technology and Nutrition*, pp. 219-224.

[4] Robert, F., Vuataz, G., Pollien, P., Saucy, F. O., Alonso, M. I., Bauwens, I., Blank, I. (2004). Acrylamide Formation from Asparagine under Low-Moisture Maillard Reaction Conditions. 1. Physical and Chemical Aspects in Crystalline Model Systems. *Journal of Agricultural and Food Chemistry,* **52**, pp. 6837-6842.

[5] Knol, J. J., Linssen, J. P. H., Van Boekel, M. A. J. S. (2005). Unravelling the kinetics of the formation of acrylamide in the Maillard reaction of fructose and asparagine by multiresponse modelling. *Food Chemistry*, **120,** pp. 1047-1057.

[6] Robert, F., Vuataz, G., Pollien, P., Saucy, F., Alonso, M. I., Bauwens, I., Blank, I. (2005). Acrylamide Formation from Asparagine under Low Moisture Maillard Reaction Conditions. 2. Crystalline vs Amorphous Model Systems. *Journal of Agricultural and Food Chemistry*, **53**, pp. 4628-4632.

[7] Knol, J. J., Van Loon, W. A. M., Linssen, J. P. H., Ruck, A. L., Van Boekel, M. A. J. S., Voragen, A. G. J. (2005). Toward a Kinetic Model for Acrylamide Formation in a Glucose-Asparagine Reaction System. *Journal of Agricultural and Food Chemistry*, **53**, pp. 6133-6139.

[8] Mottram, D. S., Wedzicha, B. L., Dodson, A. T. (2002). Acrylamide is formed in the Maillard reaction. *Nature,* **419,** pp. 448-9.

[9] Zyzak, D. V., Sanders, R. A., Stojanovic, M., Tallmadge, D. H., Eberhart, B. L., Ewald, D. K., Gruber, D. C., Morsch, T. R., Strothers, M. A., Rizzi, G. P., Villagran, M. D. (2003). Acrylamide Formation Mechanism in Heated Foods. *Journal of Agricultural and Food Chemistry*, **51**, pp. 4782-4787.

[10] Rydberg, P., Eriksson, S., Tareke, E., Karlsson, P., Ehrenberg, L., Tornqvist, M. (2003). Investigations of Factors That Influence the Acrylamide Content of Heated Foodstuffs. *Journal of Agricultural and Food Chemistry,* **51**, pp. 7012-7018.

[11] De Vleeschouwer, K., Van Der Plancken, I., Van Loey, A., Hendrickx, M. E. (2006). Impact of pH on the Kinetics of Acrylamide Formation/Elimination Reactions in Model Systems. *Journal of Agricultural and Food Chemistry,* **54**, pp. 7847-7855.

[12] Amrein, T. M., Andres, L., Manzardo, G. G. G., Amado, R. (2006). Investigations on the Promoting Effect of Ammonium Hydrogencarbonate on the Formation of Acrylamide in Model Systems. *Journal of Agricultural and Food Chemistry,* **54**, pp. 10253-10261.

[13] Gokmen, V., Senyuva, H. Z. (2007). Acrylamide formation is prevented by divalent cations during the Maillard reaction. *Food Chemistry,* **103**, pp. 196-203.

[14] Stadler, R. H., Robert, F., Riediker, S., Varga, N., Davidek, T., Devaud, S. P., Goldmann, T., Hau, J. R., Blank, I. (2004). In-Depth Mechanistic Study on the Formation of Acrylamide and Other Vinylogous Compounds by the Maillard Reaction. *Journal of Agricultural and Food Chemistry,* **52**, pp. 5550-5558.

[15] Hidalgo, F. J., Delgado, R. M., Navarro, J. L., Zamora, R. (2010). Asparagine Decarboxylation by Lipid Oxidation Products in Model Systems. *Journal of Agricultural and Food Chemistry,* **58**, pp. 10512-10517.

[16] Stadler, R. H., Blank, I., Varga, N., Robert, F., Hau, J., Guy, P. A., Robert, M. C., Riediker, S. (2002). Food chemistry: Acrylamide from Maillard reaction products. *Nature,* **419**, pp. 449-450.

[17] Yaylayan, V. A., Wnorowski, A., Perez Locas, C. (2003). Why Asparagine Needs Carbohydrates To Generate Acrylamide. *Journal of Agricultural and Food Chemistry,* **51**, pp. 1753-1757.

[18] Hedegaard, R. V., Frandsen, H., Skibsted, L. H. (2008). Kinetics of formation of acrylamide and Schiff base intermediates from asparagine and glucose. *Food Chemistry,* **108**, pp. 917-925.

[19] Perez Locas, C., Yaylayan, V. A. (2008). Further Insight into Thermally and pH-Induced Generation of Acrylamide from Glucose/Asparagine Model Systems. *Journal of Agricultural and Food Chemistry*, **56**, pp. 6069-6074.

[20] Rizzi, G. (2008). The Strecker Degradation of Amino Acids: Newer Avenues for Flavor Formation. *Food Reviews International*, **24**, pp. 416-435.

[21] Zhang, Y., Ren, Y., Zhang, Y. (2009b). New Research Developments on Acrylamide: Analytical Chemistry, Formation Mechanism, and Mitigation Recipes. *Chemical Reviews*, **109**, pp. 4375-4397.

[22] Chu, F. L., Yaylayan, V. A. (2008). Post-Schiff Base Chemistry of the Maillard Reaction. *Annals of the New York Academy of Sciences*, **1126**, pp. 30-37.

[23] Chu, F. L., Yaylayan, V. A. (2009). FTIR monitoring of oxazolidin-5-one formation and decomposition in a glycolaldehyde phenylalanine model system by isotope labeling techniques. *Carbohydrate Research*, **344**, pp. 229-236.

[24] Tsuge, O., Kanemasa, S., Alan, R. K. (1989). Recent Advances in Azomethine Ylide Chemistry. In: *Advances in Heterocyclic Chemistry*. Academic Press.

[25] Guerra, P. V., Yaylayan, V. A. (2010). Dimerization of Azomethine Ylides: An Alternate Route to Pyrazine Formation in the Maillard Reaction. *Journal of Agricultural and Food Chemistry*, **58**, pp. 12523-12529.

[26] Granvogl, M., Schieberle, P. (2006). Thermally Generated 3-Aminopropionamide as a Transient Intermediate in the Formation of Acrylamide. *Journal of Agricultural and Food Chemistry*, **54**, pp. 5933-5938.

[27] Ehling, S., Shibamoto, T. (2005). Correlation of Acrylamide Generation in Thermally Processed Model Systems of Asparagine and Glucose with Color Formation, Amounts of Pyrazines Formed, and Antioxidative Properties of Extracts. *Journal of Agricultural and Food Chemistry*, **53**, pp. 4813-4819.

[28] Hedegaard, R. V., Frandsen, H., Granby, K., Apostolopoulou, A., Skibsted, L. H. (2006). Model Studies on Acrylamide Generation from Glucose/Asparagine in Aqueous Glycerol. *Journal of Agricultural and Food Chemistry*, **55**, pp. 486-492.

[29] Namiki, M., Oka, M., Otsuka, M., Miyazawa, T., Fujimoto, K., Namiki, K. (1993). Weak chemiluminescence at an early stage of the Maillard reaction. *Journal of Agricultural and Food Chemistry*, **41**, pp. 704–1709.

[30] Labuza, (1994). Interpreting the complexity of the kinetics of the Maillard reaction. In: T. P. Labuza, G. A., Reineccius, V. M. Monnier, J. O' Brien, J. W. Baynes, eds., *Maillard reaction in Chemistry, Food and Health*. The Royal Society of Chemistry: Cambridge, pp. 176-181.

[31] Birlouez-Aragon, I., Nicolas, M., Metais, A., Marchond, N., Grenier, J., Calvo, D. (1998). A rapid fluorimetric method to estimate the heat treatment of liquid milk. *International Dairy Journal*, **8**, pp. 771–777.

[32] Birlouez-Aragon, I., Locquet, N., Louvent, E. D., Bouveresse, D. J. R., Stahl, P. (2005). Evaluation of the Maillard reaction in infant formulas by means of front-face fluorescence. *Annals of the New York Academy of Sciences*, **1043**, pp. 308–318.

[33] Birlouez-Aragon, I., Leclere, J., Quedraogo, C. L., Birlouez, E., Grongnet, J. F. (2001). The FAST method, a rapid approach of the nutritional quality of heat-treated foods. *Nahrung/Food*, **45**, pp. 201–205.

[34] Morales, F. J., Romero, C., Jimenez-Perez, S. (1996). Fluorescence associated with Maillard reaction in milk and milk-resembling systems. *Food Chemistry*, **57**, pp. 423–428.

[35] Siegl, T., Schwarzenbolz, U., Henle, T. (2000). Irreversible casein oligomerisation and formation of fluorescent crosslink amino acids in dairy products. *Czech Journal of Food Science*, **18**, pp. 72–73.

[36] Pearce, J. A. (1950). Fluorescence changes in solutions of glucose and glycine and of acetaldehyde and ammonia. *Food Technology*, **4**, pp. 416–419.

[37] Friedman, L., Kline, O. L. (1950). The amino acid-sugar reaction. *Journal of Biological Chemistry*, **184**, p. 599.

[38] Oberby, L. R., Frost, D. V. (1952). The effects of heat on the nutritive value of protein hydrolysates with dextrose. *Journal of Nutrition*, **46**, pp. 539–559.

[39] Baisier, W. M., Labuza, T. P. (1992). Maillard browning kinetics in a liquid model system. *Journal of Agricultural and Food Chemistry*, **40**, pp. 707–713.

[40] Morales, F. J., van Boekel, M. A. J. S. (1997). A study on advanced Maillard reaction in heated casein/sugar solutions: Fluorescence accumulation. *International Dairy Journal*, **7**, pp. 675–683.

[41] Matiacevich, S. B., Pilar Buera, M. (2006). A critical evaluation of fluorescence as a potential marker for the Maillard reaction. *Food Chemistry*, **95**, pp. 423-430.

[42] Taoukis, P., Labuza, T. (1996). Summary: Integrative Concepts. In: Fennema, O. R., ed., *Food Chemistry*, Inc. New York: Marcel Dekker, pp. 1013–1042.

[43] Matiacevich, S. B., Santagapita, P. R., Buera, M. P. (2005). Fluorescence from the Maillard reaction and its potential applications in food science. *Critical reviews in food science and nutrition*, **45**(6), pp. 483-495.

[44] IARC (1994). *Monographs on the Evaluation of Carcinogen Risk to Humans: Some Industrial Chemicals, No. 60*, Lyon: International Agency for Research on Cancer.

[45] Friedman, M. (2003). Chemistry, Biochemistry, and Safety of Acrylamide. A Review. *Journal of Agricultural and Food Chemistry*, **51,** pp. 4504-4526.

[46] Adams, A., Hamdani, S., Lancker, F. V., Mejri, S., De Kimpe, N. (2010). Stability of acrylamide in model systems and its reactivity with selected nucleophiles. *Food Research International*, **43,** pp. 1517-1522.

[47] De Lima, E. F., Carloni, P., (2011). Acrylamide Binding to Its Cellular Targets: Insights from Computational Studies. In: H. Lopes, ed., *Computational Biology and Applied Bioinformatics*. INTECH Open Access Publisher, pp. 431-442.

[48] Sumner, S. C. J., Fennell, T. R., Moore, T. A., Chanas, B., Gonzalez, F., Ghanayem, B. I. (1999). Role of Cytochrome P450 2E1 in the Metabolism of Acrylamide and Acrylonitrile in Mice. *Chemical Research in Toxicology*, **12,** pp. 1110-1116.

[49] Delgado-Andrade, C., Rufián-Henares, J. A., Morales, F. J. (2007a). Lysine availability is diminished in commercial fibre-enriched breakfast cereals. *Food Chemistry*, **100**, pp. 725–731.

[50] Seiquer, I., Díaz-Alguacil, J., Delgado-Andrade, C., López-Frías, M., Hoyos, A. M., Galdó, G., Navarro, M. P. (2006). Diets rich in Maillard reaction products affect protein digestibility in adolescent males aged 11–14 y. *American Journal of Clinical Nutrition*, **8**, pp. 1082– 1088.

[51] Delgado-Andrade, C., Seiquer, I., García, M. M., Galdo, G., Navarro, P. (2011). Increased intake of Maillard reaction products reduces phosphorous digestibility in male adolescents. *Nutrition*, **27**, pp. 86-91.

[52] García, M. M., Seiquer, I., Delgado-Andrade, C., Galdó, G., Navarro, M. P. (2009a). Intake of Maillard reaction products reduces iron bioavailability in male adolescents. *Molecular Nutrition & Food Research*, **53**, pp. 1–10.

[53] Delgado-Andrade, C., Seiquer, I., Navarro, M. P. (2007b). Effects of Consumption of Maillard Reaction Products on Magnesium Digestibility and Tissue Distribution in Rats. *Food Science and Technology International*, **13**, pp. 109–116.

[54] García, M. M., Seiquer, I., Navarro, M. P. (2009b). Influence of Diets Rich in Maillard Reaction Products on Calcium Bioavailability Assays in Male Adolescents and in Caco-2 Cells. *Journal of Agricultural and Food chemistry,* **57**, pp. 9532–9538.

[55] Seifert, S. T., Krause, R., Gloe, K., Henle, T. (2004). Metal complexation by the peptide bound maillard reaction products N^{ε}-fructoselysine and N^{ε}-carboxymethyllysine. *Journal of Agricultural and Food Chemistry*, **52**, pp. 2347-2350.

[56] Furniss, D. E., Vuichoud, J., Finot, P. A., Hurrell, R. F. (1989). The effect of Maillard reaction products on zinc metabolism in the rat. *British Journal of Nutrition*, **62**, pp. 739-749.

[57] Wijewickreme, A. N., Kitts, D. D. (1998). Modulation of metal-induced cytotoxicity by Maillard reaction products isolated from coffee brew. *Journal of Toxicological and Enviromental Health A*, **55**, pp. 151-168.

[58] Friedman, M., Pearce, K. N. (1989). Copper(II) and cobalt(II) affinities of LL- and LD-lysinoalanine diastereomers: implications for food safety and nutrition. *Journal of Agricultural and Food Chemistry,* **37**, pp. 123-127.

[59] Pearce, K. N., Friedman, M. (1988). Binding of copper(II) and other metal ions by lysinoalanine and related compounds and its significance for food safety. *Journal of Agricultural and Food Chemistry,* **36**, pp. 707-717.

[60] Sarwar, G., L'Abbé, M. R., Trick, K., Botting, H. G., Ma, C. Y. (1999). Influence of feeding alkaline/heat processed proteins on growth and protein and mineral status of rats. In: L. S. Jackson, M. G. Knize, J. N. Morgan, eds, *Impact of Processing on Food Safety*. Springer US, pp. 161-177.

[61] Wagner, K. H., Reichhold, S., Koschutnig, K., Chériot, S., Billaud, C. (2007). The potential antimutagenic and antioxidant effects of Maillard reaction products used as "natural antibrowning" agents. *Molecular nutrition & food research*, **51**, pp. 496-504.

[62] Somoza, V. (2005). Five years of research on health risks and benefits of Maillard reaction products: an update. *Molecular Nutrition & Food Research,* **49**, pp. 663-672.

[63] Capuano, E., Fogliano, V. (2011). Acrylamide and 5-hydroxymethylfurfural (HMF): A review on metabolism, toxicity, occurrence in food and mitigation strategies. *LWT-Food Science and Technology*, **44**, pp. 793-810.

[64] Nass, N., Bartling, B., Navarrete Santos, A., Scheubel, R.J., Börgermann, J., Silber, R. E., Simm, A. (2007). Advanced glycation end products, diabetes and ageing. *Zeitschrift für Gerontologie und Geriatrie*, **40**, pp. 349-356.

[65] Barbosa, J. H., Oliveira, S. L., Seara, L. T. (2008). The role of advanced glycation end-products (AGEs) in the development of vascular diabetic complications. *Arquivos Brasileiros de Endocrinologia & Metabologia*, **52**, pp. 940-950.

[66] Kalousova, M., Skrha, J., Zima, T. (2002). Advanced glycation end-products and advanced oxidation protein products in patients with diabetes mellitus. *Physiological Research,* **51**, pp. 597-604.

[67] Mostafa, A. A., Randell, E. W., Vasdev, S. C., Gill, V. D., Han, Y., Gadag, V., Raouf, A. A., El Said, H. (2007). Plasma protein advanced glycation end products, carboxymethyl cysteine, and carboxyethyl cysteine, are elevated and related to nephropathy in patients with diabetes. *Molecular and cellular biochemistry*, **302**, pp. 35-42.

[68] Magalhães, P. M., Appell, H. J., Duarte, J. A. (2008). Involvement of advanced glycation end products in the pathogenesis of diabetic complications: the protective role of regular physical activity. *European Review of Aging and Physical Activity*, **5**, p. 17.

[69] Hartog, J. W., Voors, A. A., Bakker, S. J., Smit, A. J., Veldhuisen, D. J. (2007). Advanced glycation end-products (AGEs) and heart failure: Pathophysiology and clinical implications. *European journal of heart failure*, **9**, pp. 1146-1155.

[70] Grillo, M. A., Colombatto, S. (2008). Advanced glycation end-products (AGEs): involvement in aging and in neurodegenerative diseases. *Amino acids*, **35**, pp. 29-36.

[71] Sato, T., Shimogaito, N., Wu, X., Kikuchi, S., Yamagishi, S. I., Takeuchi, M., (2006). Toxic advanced glycation end products (TAGE) theory in Alzheimer's disease. *American Journal of Alzheimer's Disease & Other Dementias*, **21**, pp. 197-208.

[72] Vytášek, R., Šedová, L., Vilím, V. (2010). Increased concentration of two different advanced glycation end-products detected by enzyme immunoassays with new monoclonal antibodies in sera of patients with rheumatoid arthritis. *BMC musculoskeletal disorders*, **11**, p. 83.

[73] Ding, K. H., Wang, Z. Z., Hamrick, M. W., Deng, Z. B., Zhou, L., Kang, B., Yan, S. L., She, J. X., Stern, D. M., Isales, C. M., Mi, Q. S. (2006). Disordered osteoclast formation in RAGE-deficient mouse establishes an essential role for RAGE in diabetes related bone loss. *Biochemical and biophysical research communications*, **340**, pp. 1091-1097.

[74] Li, Y., Cohenford, M. A., Dutta, U., Dain, J. A. (2008). The structural modification of DNA nucleosides by nonenzymatic glycation: an in vitro study based on the reactions of glyoxal and methylglyoxal with 2′-deoxyguanosine. *Analytical and bioanalytical chemistry*, **390**, pp. 679-688.

[75] Corzo-Martinez, M., Avila, M., Moreno, F. J., Requena, T., Villamiel, M. (2012) Effect of milk protein glycation and gastrointestinal digestion on the growth of bifidobacteria and lactic acid bacteria. *International Journal of Food Microbiology*, **153**, pp. 420-427.

[76] Tuohy, K. M., Hinton, D. J., Davies, S. J., Crabbe, M. J. C., Gibson, G. R., Ames, J. M. (2006). Metabolism of Maillard reaction products by the human gut microbiota–implications for health. *Molecular nutrition & food research*, **50**, pp. 847-857.

[77] Borrelli, R. C., Fogliano, V. (2005). Bread crust melanoidins as potential prebiotic ingredients. *Molecular nutrition & food research*, **49**, pp. 673-678.

[78] Summa, C., McCourt, J., Cämmerer, B., Fiala, A., Probst, M., Kun, S., Anklam, E., Wagner, K. H. (2008). Radical scavenging activity, anti-bacterial and mutagenic effects of cocoa bean Maillard reaction products with degree of roasting. *Molecular nutrition & food research*, **52**, pp. 342-351.

[79] Faist, V., Lindenmeier, M., Geisler, C., Erbersdobler, H. F., Hofmann, T. (2002). Influence of molecular weight fractions isolated from roasted malt on the enzyme activities of NADPH-cytochrome c-reductase and glutathione-S-transferase in Caco-2 Cells. *Journal of agricultural and food chemistry*, **50**, pp. 602-606.

[80] Açar, Ö.Ç., Gökmen, V., Pellegrini, N., Fogliano, V. (2009). Direct evaluation of the total antioxidant capacity of raw and roasted pulses, nuts and seeds. *European Food Research and Technology*, **229**, pp. 961-969.

[81] Chang, H. L., Chen, Y. C., Tan, F. J. (2011). Antioxidative properties of a chitosan-glucose Maillard reaction product and its effect on pork qualities during refrigerated storage. *Food chemistry*, **124**, pp. 589-595.

[82] Chawla, S. P., Chander, R., Sharma, A. (2009). Antioxidant properties of Maillard reaction products obtained by gamma-irradiation of whey proteins. *Food chemistry*, **116**, pp. 122-128.

[83] Rao, M. S., Chawla, S. P., Chander, R., Sharma, A. (2011). Antioxidant potential of Maillard reaction products formed by irradiation of chitosan-glucose solution. *Carbohydrate Polymers*, **83**, pp. 714-719.

[84] Goya, L., Delgado-Andrade, C., Rufián-Henares, J. A., Bravo, L., Morales, F. J. (2007). Effect of coffee Melanoidin on human hepatoma HepG2 cells. Protection against oxidative stress induced by tert-butylhydroperoxide. *Molecular nutrition & food research*, **51**, pp. 536-545.

[85] Martín, M. A., Ramos, S., Mateos, R., Rufián-Henares, J. A., Morales, F. J., Bravo, L., Goya, L. (2009). Biscuit melanoidins of different molecular masses protect human HepG2 cells against oxidative stress. *Journal of agricultural and food chemistry*, **57**, pp. 7250-7258.

[86] Seiquer, I., Ruiz-Roca, B., Mesías, M., Muñoz-Hoyos, A., Galdó, G., Ochoa, J. J., Navarro, M. P. (2008). The antioxidant effect of a diet rich in Maillard reaction products is attenuated after consumption by healthy male adolescents. In vitro and in vivo comparative study. *Journal of the Science of Food and Agriculture*, **88**, pp. 1245-1252.

[87] Bastos, D. M., Monaro, E., Siguemoto, E., Séfora, M. (2012). Maillard reaction products in processed food: Pros and Cons. In: B. Valdez, ed., *Food Industrial Processes - Methods and Equipment*. INTECH Open Access Publisher, pp. 281-300.

[88] Tareke, E., Rydberg, P., Karlsson, P., Eriksson, S., Tornqvist, M. (2000). Acrylamide: A Cooking Carcinogen? *Chemical Research in Toxicology*, **13,** pp. 517-522.

[89] Tareke, E., Rydberg, P., Karlsson, P., Eriksson, S., Tornqvist, M. (2002). Analysis of Acrylamide, a Carcinogen Formed in Heated Foodstuffs. *Journal of Agricultural and Food Chemistry*, **50,** pp. 4998-5006.

2 Research Methodology

2.1 UV-visible spectrophotometry

The energy associated with electromagnetic radiation is defined by the following equation:

$$\mathbf{E = h\nu}$$

where **E** is energy (in joules), **h** is Planck's constant (6.62×10^{-34} Js), and **ν** is frequency (in Hz or sec^{-1}).

Electromagnetic radiation can be considered a combination of alternating electric and magnetic fields that travel through space with a wave motion. Because radiation acts as a wave, it can be classified in terms of either wavelength or frequency, which are related by the following equation:

$$\mathbf{\nu = c/\lambda}$$

where **ν** is frequency (in sec^{-1}), **c** is the speed of light (3×108 ms^{-1}), and **λ** is wavelength (in meters).

In UV-visible spectroscopy, wavelength usually is expressed in nanometers ($1 \text{ nm} = 10^{-9}$ m) [1]. It follows from the above equations that radiation with shorter wavelength has higher energy (**Figure 10**). In UV-visible spectroscopy, the low-wavelength UV light has the highest energy.

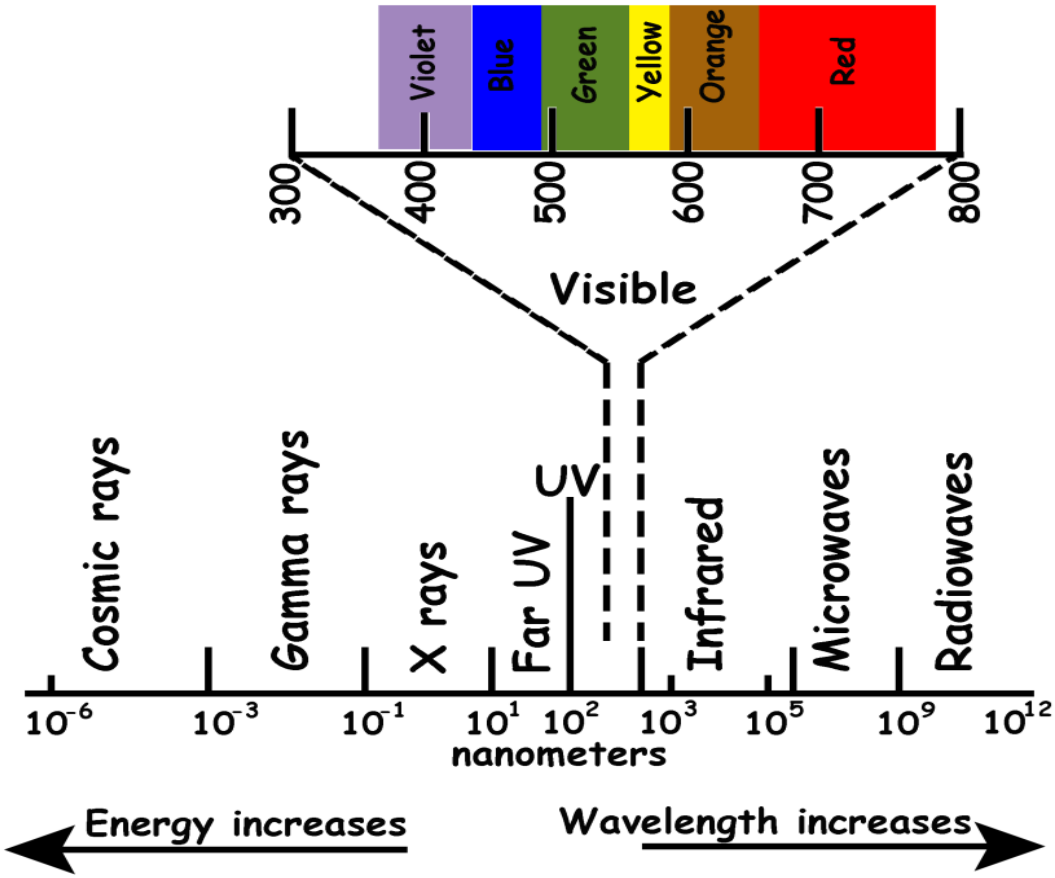

Figure 10. The UV and visible range of the electromagnetic spectrum as a function of energy. Adapted from [1].

When radiation interacts with matter, a number of processes can occur, including reflection, scattering, absorbance, fluorescence/phosphorescence and photochemical reaction. In general, when recording UV-visible spectra, only absorbance is measured. Because light is a form of energy, absorption of light by matter causes the energy content of the molecules (or atoms) to increase. The total potential energy of a molecule is represented as the sum of its electronic, vibrational, and rotational energies [2]. The amount of energy a molecule possesses in each form is a series of discrete levels or states. Absorption of visible and ultraviolet (UV) radiation is associated with excitation of electrons, in both atoms and molecules, from lower to higher energy levels. Since the energy levels of matter are quantized, only light with the precise amount of energy can cause transitions from one level to another will be absorbed. In each case, an electron is excited from a full (low energy, ground state) orbital into an empty (higher energy,

excited state) anti-bonding orbital (**Figure 11**). Each wavelength of light has a particular energy associated with it. If that amount of energy is enough for making one of these electronic transitions, then that particular wavelength will be absorbed. The larger the gap between the energy levels, the larger the energy required to promote the electron to the higher energy level; resulting in light of higher frequency, and therefore shorter wavelength, being absorbed.

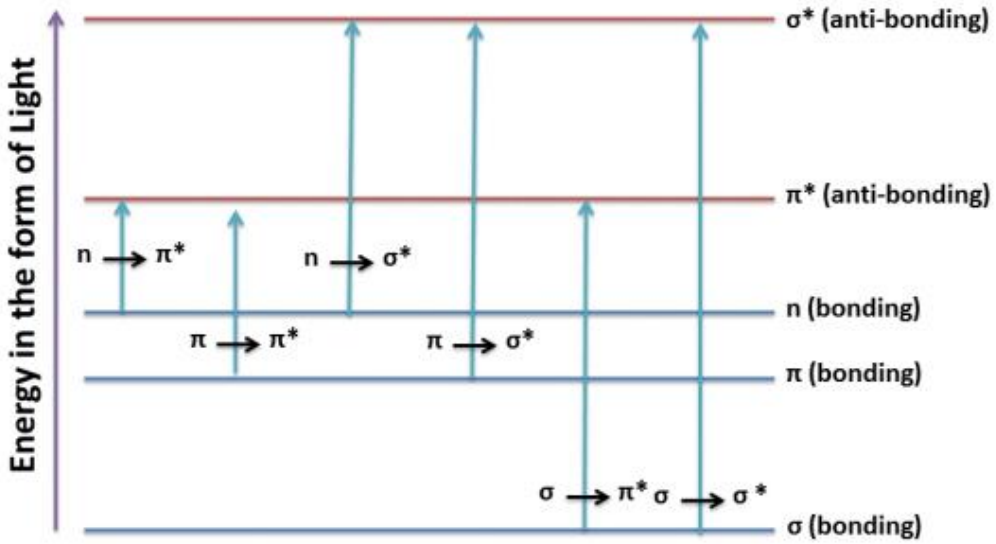

Figure 11. Electronic transitions between the different electronic states when light energy is absorbed. Adapted from [3].

In UV-visible spectroscopy the sample is placed in the UV-visible spectrophotometer to obtain a UV-visible (UV-vis) spectrum. The instrument automatically exposes the sample to all of the wavelengths of light, and measures how much of the light is absorbed by the sample at each wavelength. For each wavelength the intensity of light passing through both a reference cell ($\mathbf{I_0}$) and the sample cell (**I**) is measured. If I is less than Io, then the sample has absorbed some of the light. The absorbance (**A**) of the

sample is related to the transmitted radiation, **I** and the incident radiation, $\mathbf{I_0}$ according to the following equation:

$$\mathbf{A = \log_{10} I_0/I}$$

The instrument detector converts the received light into a current, the higher the current the greater the intensity. Absorption spectra are a plot of the absorbance against wavelength (nm) in the UV and visible range of the electromagnetic spectrum.

The wavelength and amount of light that a compound absorbs depends on its molecular structure and the concentration of the compound used [3]. According to the Beer-Lambert Law the absorbance is proportional to the concentration of the substance in solution:

$$\mathbf{A = \varepsilon cl}$$

where **A** = absorbance **l** = optical path length (cm), **c** = concentration of solution (mol dm^{-3}), **ε** = molar extinction, which is constant for a particular substance at a particular wavelength (dm^3 mol^{-1} cm^{-1}).

2.2 Fourier Transform Infrared spectroscopy (FTIR)

2.2.1 General Principles

2.2.1.1 Vibrations

The simple two-atomic oscillator demonstrates the fundamental principles that govern the relationship between the vibrational spectrum of a molecule and its structure and environment [4]. The frequency, n, of a two-atomic oscillator is given by

$$\mathbf{\nu=(k/m_r)^{0.5}/2\pi},$$

where k is the force constant between the two atoms, and mr the reduced mass ($1/m_r = 1/m_1+1/m_2$).

The frequency increases when the force constant increases, that is when the electron density in the bond between the two atoms increases. Any inter- or intramolecular factor that alters the electron density in the bonds will affect the vibrational spectrum. The

second important influence on the frequency is the mass of vibrating atoms, the larger the mass, the slower the vibration.

Molecular vibrations can range from the simple coupled motion of the two atoms of a diatomic molecule to the much more complex motion of each atom in a large multifunctional molecule. Molecules with N atoms have 3N degrees of freedom, three of which represent translational motion in mutually perpendicular directions (the x, y, and z axes) and three represent rotational motion about the x, y, and z axes. The remaining 3N-6 degrees of freedom give the number of ways that the atoms in a nonlinear molecule can vibrate (i.e., the number of vibrational modes). Each mode involves approximately harmonic displacements of the atoms from their equilibrium positions; for each mode, **i**, all the atoms vibrate at a certain characteristic frequency, $\boldsymbol{\nu_i}$. The potential energy, **V(r)**, of a harmonic oscillator is illustrated as a function of the distance between the atoms, **r (Figure 12)**.

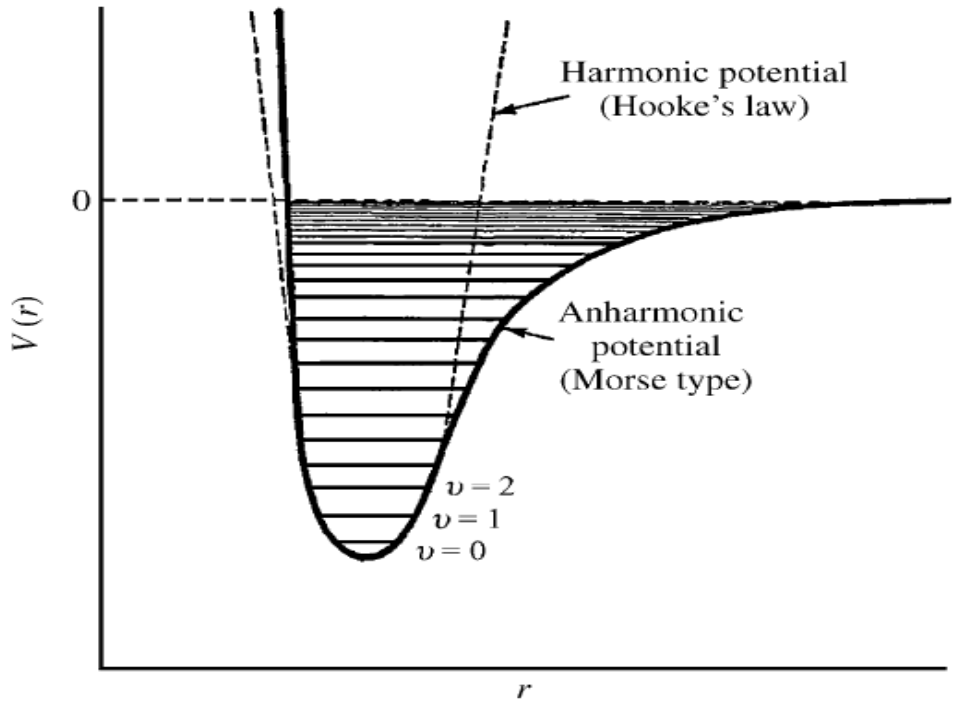

Figure 12. Potential energy of a diatomic molecule as a function of the atomic displacement during a vibration for a harmonic oscillator (dashed line) and an anharmonic oscillator (solid line) [4].

For any mode in which the atoms vibrate with simple harmonic motion (i.e., obeying Hooke's law), the vibrational energy states, $\mathbf{V_{iv}}$, can be described by the equation:

$$\mathbf{V_{iv} = h\nu_i (v_i + 1/2)}$$

where **h** is Planck's constant, $\mathbf{n_i}$ the fundamental frequency of the particular mode, and $\mathbf{v_i}$ the vibrational quantum number of the ith mode: $\mathbf{v_i} = (0, 1, 2,\ldots)$

The energy difference for transitions between the ground state $\mathbf{v_i} = (0)$ and the first excited state $\mathbf{v_i} = (1)$ of most vibrational modes corresponds to the energy of radiation in the mid-infrared spectrum (400 to 4000 cm^{-1}).

2.2.1.2 IR absorption

In basic terms, the infrared spectrum is formed as a consequence of the absorption of electromagnetic radiation at frequencies that correlate to the vibration of specific sets of chemical bonds from within a molecule. The distribution of energy possessed by a molecule at any given moment, defined as the sum of the contributing energy terms:

E total = E electronic + E vibrational + E rotational + E translational

The translational energy relates to the displacement of molecules in space as a function of the normal thermal motions of matter. Rotational energy, which gives rise to its own form of spectroscopy, is observed as the tumbling motion of a molecule, which is the result of the absorption of energy within the microwave region. The vibrational energy component is a higher energy term and corresponds to the absorption of energy by a molecule as the component atoms vibrate about the mean center of their chemical bonds. The electronic component is linked to the energy transitions of electrons as they are distributed throughout the molecule, either localized within specific bonds, or delocalized over structures, such as an aromatic ring. In order to observe such electronic transitions, it is necessary to apply energy in the form of visible and ultraviolet radiation:

E = hv (frequency/energy)

IR absorption is caused by the interaction of electromagnetic waves with molecular vibrations. To be more specific, the electric field vector, E(t), of the electromagnetic wave couples with the dipole moment, m(t), of the molecule. A classic example is that of two vibrating point charges +q and -q connected by a spring. If the frequencies of light and vibration are the same, the electric field will amplify the movement of the partial charges. The vibrational frequency, however, remains unaffected. This simple picture already illustrates two important findings: (i) the frequencies of light and of the vibration have to coincide for absorption to occur and (ii) the larger the point charges +q and -q, the stronger the interaction with the electric field. In quantum mechanical terms, the discrete energy levels of a harmonic oscillator are separated by hν with ν being the vibrational frequency. An IR photon with this energy, hν, can be absorbed by the oscillator which then goes from the ground energy level to the first excited level in a IR measurement. The spacing of energy levels by hν ensures that light can only be absorbed when light frequency and vibrational frequency coincide (this rule strictly applies only to the harmonic oscillator).

The fundamental requirement for infrared activity, leading to absorption of infrared radiation, is that there must be a net change in dipole moment during the vibration for the molecule or the functional group under study. The interaction of the radiation with molecules can be described in terms of a resonance condition where the specific oscillating radiation frequency matches the natural frequency of a particular normal mode of vibration. In order for energy to be transferred from the IR photon to the molecule via absorption, the molecular vibration must cause a change in the dipole moment of the molecule. The dipole moment, **m**, for a molecule is a function of the magnitude of the atomic charges ($\mathbf{e_i}$) and their positions ($\mathbf{r_i}$) and are described by the following relationship:

$$\boldsymbol{\mu} = \boldsymbol{\Sigma}\, \mathbf{e_i}\, \mathbf{r_i}$$

The dipole moments of uncharged molecules derive from partial charges on the atoms, which can be determined from molecular orbital calculations. As a simple approximation, the partial charges can be estimated by comparison of the electronegativities of the atoms.

Typical of an absorption spectroscopy, the relationship between the intensities of the incident and transmitted IR radiation and the analyte concentration is governed by the

Lambert-Beer law. The IR spectrum is obtained by plotting the intensity (absorbance or transmittance) versus the wavenumber, which is proportional to the energy difference between the ground and the excited vibrational states. The IR absorption process involves absorption of energy by the molecule if the vibration causes a change in the dipole moment, resulting in a change in the vibrational energy level.

2.2.1.3 FTIR instrumentation

Infrared spectroscopy has been widely applied to detect the vibrational characteristics of chemical functional groups in a wide range of applications. An FT infrared spectrometer collects an interferogram of a sample signal from an interferometer to obtain an IR spectrum using the Fourier transform system. The FTIR spectrometer is based on the Michelson interferometer (**Figure 13)**. It has a fixed and a movable mirror. The latter generates a variable optical path difference between two beams which gives a detector signal that contains the spectral information. Light emitted from the light source is split by a beam splitter: about half of it is reflected towards the fixed mirror and from there reflected back towards the beamsplitter where about 50% passes to reach the detector. The other half of the initial light intensity passes the beam splitter on its first encounter, is reflected by the movable mirror back to the beamsplitter where 50% of it is reflected towards the detector. When the two beams recombine they interfere and there will be constructive or destructive interference depending on the optical path difference, δ. The instrument measures the light intensity relative to the position of the movable mirror and this is the *interferogram*. A second Fourier transform performed by a computer converts the measured data back into a spectrum [5].

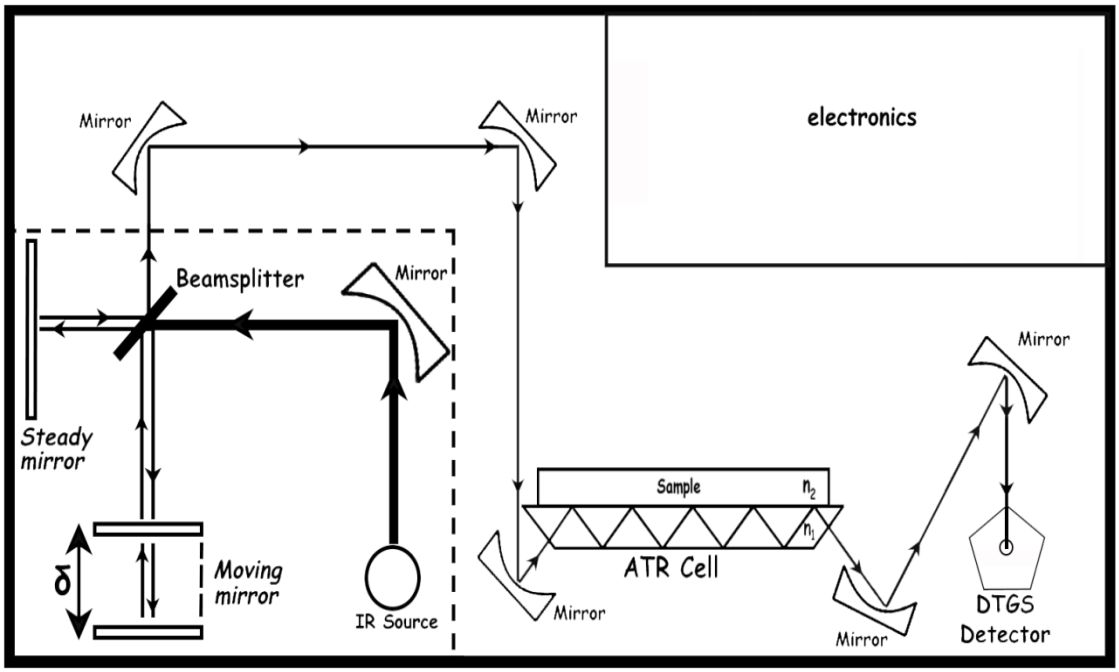

Figure 13. Schematic of the component layout of a typical FTIR spectrophotometer. Adapted from [5].

The Michelson interferometer is a device that divides a beam of radiation into two paths and then recombines the two beams after a path difference has been introduced. A condition is generated under which interference between the beams occurs. The difference of intensity of the beam emerging from the interferometer is measured as a function of path difference by a detector. The simplest form of the Michelson interferometer is shown in **Figure 14**. It comprises of two mutually perpendicular plane mirrors, one of which can move along an axis that is perpendicular to its plane.

Bisecting the fixed mirror and the movable mirror is a beamsplitter, where a collimated beam of radiation from an external source can be partially reflected to the fixed mirror (at point F for the median ray) and partially transmitted to the movable mirror (at point M). When the beams return to the beamsplitter, they interfere and are again partially reflected and partially transmitted. Because of the effect of interference, the intensity of each beam passing to the detector and returning to the source depends on the difference in path of the beams in the two arms of the interferometer. The variation in the intensity of the beams passing to the detector and returning to the source as a function of the path

difference eventually produces the spectral information in a Fourier transform spectrometer [6].

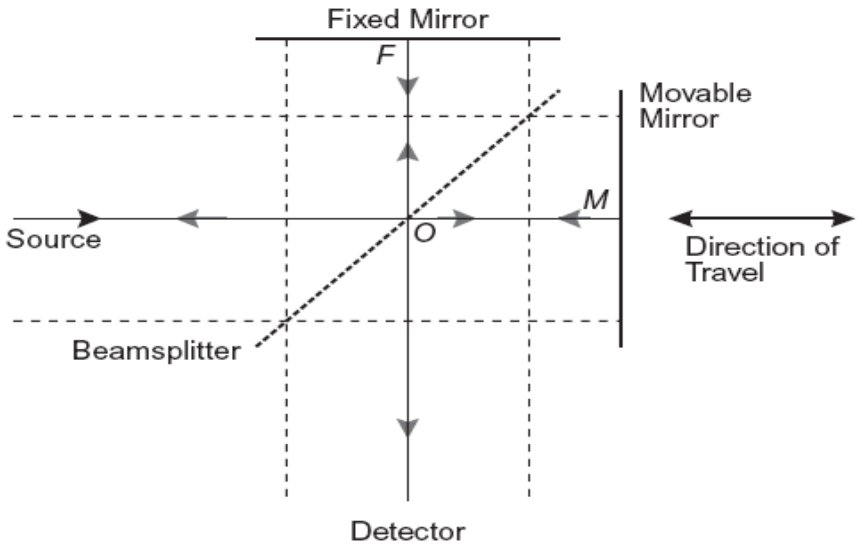

Figure 14. The Michelson interferometer. The median beam is shown by the solid line, and the extremes of the collimated beam are shown by the dashed line [5].

The path difference between the beams which travel to the fixed and movable mirrors and back to the beamsplitter is **2(OM-OF**) (**Figure 15**). This optical path difference (**OPD**) is called the retardation, and is given the symbol **δ**. When the fixed and movable mirrors are halfway between from the beamsplitter i.e., at zero retardation or zero path difference (**ZPD**), the two beams are perfectly in phase on recombination at the beamsplitter (**Figure 15**). At this instant, the beams interfere constructively, and the intensity of the beam passing to the detector is the sum of the intensities of the beams passing to the fixed and movable mirrors. Therefore, all the light from the source reaches the detector at this point and none returns to the source.

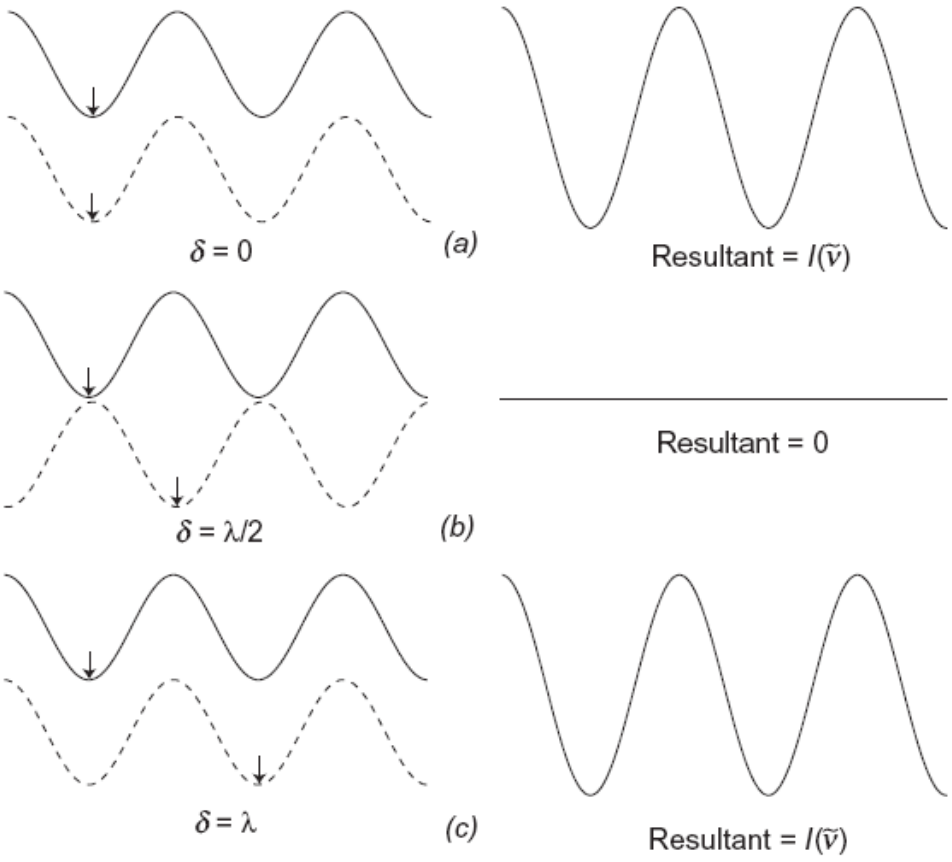

Figure 15. Electromagnetic wave phase from fixed (solid line) and movable (dashed line) mirrors at different values of the optical retardation: (a) zero path difference (b) path difference of one-half wavelength (c) path difference of one wavelength. (Constructive interference occurs for both (a) and (c) and all other retardations of integral numbers of wavelengths) [6].

2.2.2 Attenuated Total Reflection Fourier Transform Infrared spectroscopy (ATR-FTIR)

Attenuated Total Reflectance (ATR) is the most widely used FTIR sampling tool. ATR is a contact sampling method that involves a crystal with a high refractive index and excellent IR transmitting properties [7]. ATR allows qualitative or quantitative analysis of samples with little or no sample preparation, which greatly speeds sample analysis. The main benefit of ATR sampling comes from the very thin sampling path length and depth of penetration of the IR beam into the sample. ATR requires excellent contact

between the sample and the crystal and is therefore an excellent method for analyzing liquid samples.

With ATR sampling the IR beam is directed into a crystal of relatively higher refractive index. The angle of incidence of the beam must be greater than the critical angle so that total internal reflectance occurs [8]. The IR beam reflects from the internal surface of the crystal and creates an evanescent wave, which projects orthogonally into the sample in intimate contact with the ATR crystal. Some of the energy of the evanescent wave is absorbed by the sample and the reflected radiation, some of which is absorbed by the sample is returned to the detector. The reflected light contains spectral information about the sample at the sample-crystal interface. The intensity of the ATR spectrum is related to the penetration depth of the evanescent wave into the sample. This depth is dependent on the refractive index of the crystal and the sample, and upon the wavelength of the IR radiation [9]. The number of internal reflections in the crystal gives a measure of the intensity if the resulting IR spectrum. The number is a function of the effective angle of incidence, and the length and thickness of the crystal. Internal reflectance occurs when the angle of incidence exceeds the "critical" angle. This angle is a function of the real parts of the refractive indices of both the sample and the ATR crystal:

$$\theta_C = \sin^{-1}(\eta_2/\ \eta_1)$$

where θ_C is the critical angle, η_2 is the refractive index of the sample and η_1 is the refractive index of the crystal.

At any angle of incidence greater than or equal to θ_C, the beam will reflect internally with the angle of reflection equal to the angle of incidence. Any material or optic that exhibits internal reflection is known as an internal reflection element (IRE) and should have as high a critical angle as possible when in contact with the sample under investigation. A further useful consideration for ATR analysis is the depth of penetration (d_P) of the IR beam into the sample. Technically, this is defined as the distance required for the electric field amplitude to fall to e^{-1} of its value at the surface and is further defined by:

$$d_P = \lambda / 2\pi(\eta_1^2 \sin^{-1}\theta - \eta_2^2)^{1/2}$$

where **λ** is the wavelength of light and **θ** is the angle of incidence of the IR beam relative to a perpendicular from the surface of the crystal.

As shown in the graphical representation of the ATR phenomenon (**Figure 16**), the strength of the evanescent wave decays rapidly as we progress from the surface of the ATR crystal. We can calculate the volume of the evanescent wave, known as the effective penetration of the IR beam. The effective penetration (**de**) is unique for parallel polarization (**deII**) and perpendicular polarization (**d⊥**). The effective penetration for an unpolarized IR beam is the average of the parallel and perpendicular penetration. When we need to look at minor components of a sample for qualitative or quantitative analysis, then we need to increase the effective path length (**EPL**) by increasing the number of reflections (**N**) within the ATR crystal. The effective path length in ATR is derived by the following equation:

$$EPL = N \times d_e$$

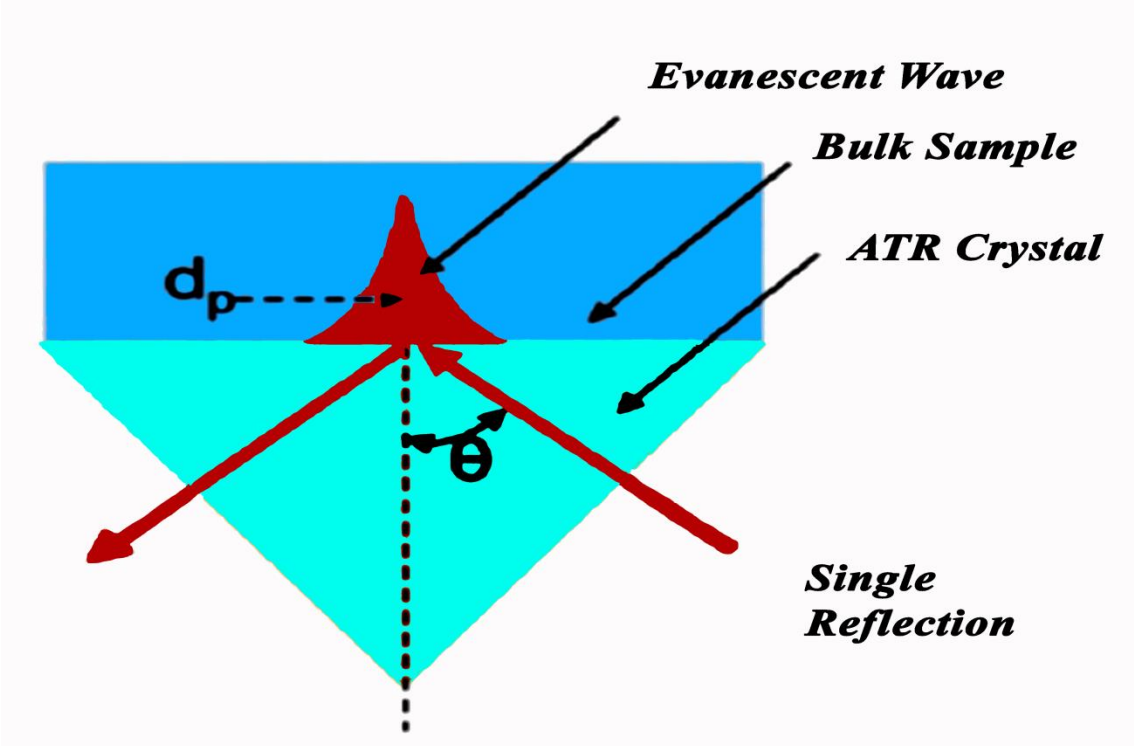

Figure 16. Graphical representation of a single reflection ATR. Adapted from [5].

2.3 High-performance Liquid Chromatography (HPLC)

High-performance liquid chromatography (HPLC) is a chromatographic technique used to separate a mixture of compounds with the purpose of mainly identifying and/or quantifying the individual components of the mixture. The principle of the method is based on the different distribution of components of a mixture between two phases, a stationary phase and a mobile phase [10]. In HPLC, the sample is introduced to the top of the column and, with the aid of the mobile phase, the components are moved in the form of bands and finally eluted one after the other. The analytes are distributed between the static and mobile phases, thus moving at different speeds along the column. Static and mobile phases are selected in such a way that the compounds that we want to separate have a different distribution time in the two phases.

HPLC relies on the pressure of mechanical pumps on a liquid solvent to load a sample onto a separation column, in which the separation occurs. The schematic of an HPLC instrument (**Figure 17**) typically includes a sampler by which the sample mixture is injected into the HPLC, one or more mechanical pumps for pushing liquid through a tubing system, a separation column, a digital analyte detector (e.g. a UV/Vis) for qualitative or quantitative analysis of the separation, and a digital microprocessor for controlling the HPLC components with the aid of a specialized software [11].

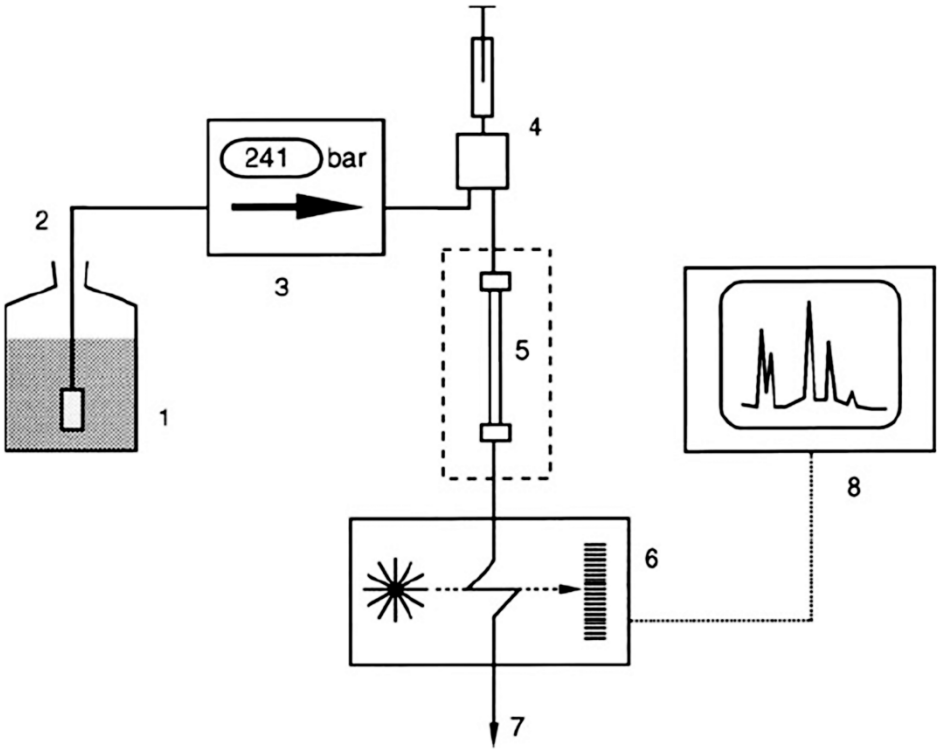

Figure 17. Schematic of an HPLC instrument. 1 = Solvent reservoir; 2 = transfer line with frit; 3 = pump; 4 = sample injection; 5 = column (with thermostat); 6 = detector; 7 = waste; 8 = data acquisition. Adapted from [11].

A HPLC separation column is filled with solid particles (e.g. silica) and the sample mixture is separated into its individual compounds as it interacts with the column particles. The sample (or sample extract) is being dissolved in a mobile phase and the mobile phase is then forced through an immobile, immiscible *stationary phase*. The stationary phase loosely interacts with each analyte based on its chemical structure, resulting in the separation of each analyte as a function of time spent in the separation column. The lesser extent analytes interact with the stationary phase, the faster they are transported through the system. The reverse is true for less mobile analytes that have stronger interactions. Thus, analytes in a sample are identified by retention time in the system for a given set of conditions. HPLC separation is influenced by the liquid solvent's condition (e.g. pressure, temperature), chemical interactions between the sample and the liquid solvent (e.g. hydrophobicity), and chemical interactions between

the sample mixture and the solid particles packed inside of the separation column (e.g. ligand affinity, ion exchange, etc).

When the static phase is less polar than the mobile phase, and the more polar components of the sample are weaker attached to the static phase and hence elute faster than the less polar components, the technique is called Reversed Phase High Performance Liquid Chromatography (RP) -HPLC). In RP-HPLC the elution power is increased by the parallel reduction of the polarity of the solvent, as this reduces the retention of a substance in the static phase. In the case of substances that can undergo ionization, a change in pH may affect their retention and selectivity. Generally, the separation of a particular substance depends on its molecular weight, solubility and chemical structure. The criteria for selecting a solvent suitable for elution depend on the physicochemical properties of the sample and the solvent elution capacity [12].

In column chromatography the separation information is contained in the chromatogram, which is the recording of the amount of the eluted component as a function of the mobile phase movement. This is achieved by using the detector, which responds to the amount (mass or concentration) of the eluted component. Changing the detector signal due to the elution of the component) on the chromatogram is the chromatographic peak.

The chromatogram is the diagram of the detector signal as a function of the elution time of the mobile phase elution component or volume. Information obtained directly from the chromatogram relates to the complexity of the sample (number of peaks), the identity of the components by determining the exact location of the peak, and the amount of ingredients.

When moving along the column the analyte molecules remain part of the time in the mobile phase and the remainder in the static phase. This lasting thermodynamic equilibrium describes the equilibrium constant **K** called the distribution coefficient:

K = CS / CM

Where **CS** is the molar concentration of the substance in the static phase and **CM** is the molar concentration of the substance in the mobile phase. In the case where the K value remains constant over a wide concentration range of the substance, the peak is in the form of the Gaussian curve and the residence time of the substance in the column is

independent of that amount. In any case where **CS** ≠ **CM** the peak is not the symmetrical Gaussian curve but it has a characteristic asymmetric flattened form.

The residence time of the sample molecules in the mobile phase is the same for all components of the sample and is called dead time ($\mathbf{t_m}$). The dead time equals the time it takes for a non-retained by the static phase component to pass through the column. The retention or inhibition time ($\mathbf{t_r}$) is the time between the sample entry and the elution of the component from the column (maximum peak chromatographic peak). Retention is usually measured in units of time (**Figure 18**). Instead of time, however, volume units (mobile phase volume) may be used whenever their measurement is more accurate. In particular, we measure the retention volume ($\mathbf{V_r}$ = Retention Volume) which is the volume of the mobile phase required to elute a particular component from the chromatographic column.

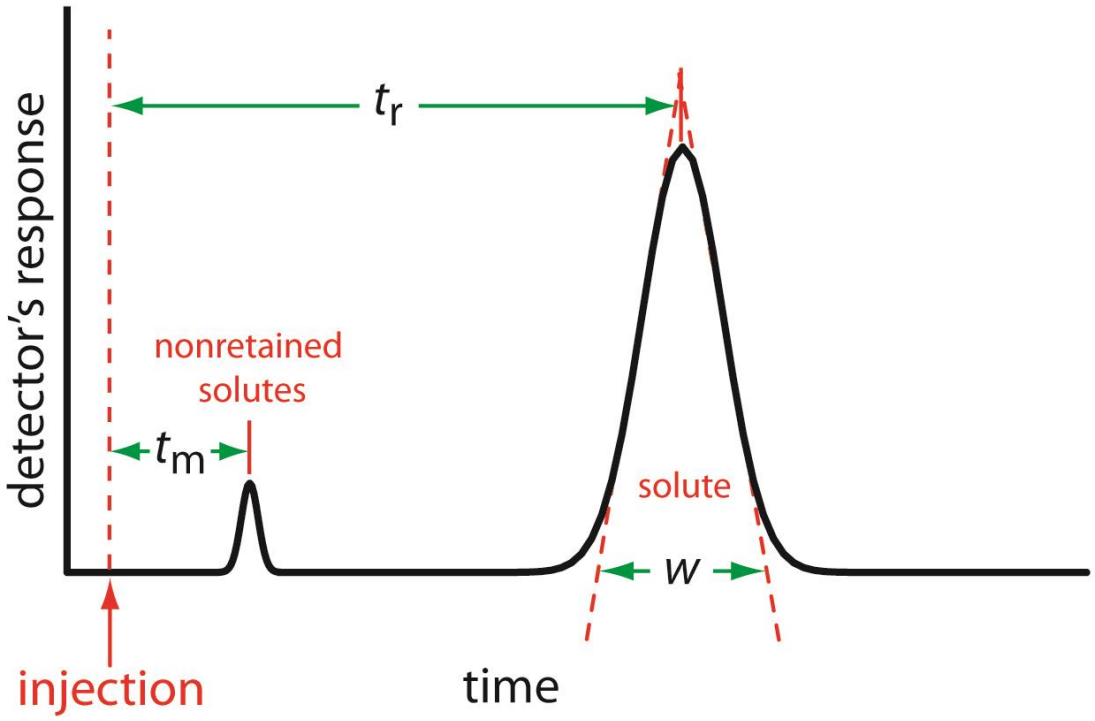

Figure 18 . Illustration of a typical chromatographic elution profile. Adapted from [12].

2.4 HPLC-ATR-FTIR

The coupling of high performance liquid chromatography (HPLC) with Fourier transform infrared (FTIR) spectrometry is a very powerful analytical tool since most compounds absorb in the mid-infrared region. This is of special interest in the case of compounds that exhibit a poor UV absorption like carbohydrates and alcohols [13]. FTIR spectroscopy provides detailed qualitative information on the separated analytes.

The coupling of high performance liquid chromatography (HPLC) with Fourier transform infrared (FTIR) spectrometry may be accomplished by the use either of flow cells or mobile phase elimination techniques [14]. The first method is more straight-forward and it involves the direct on-line sampling of the chromatographic effluent in a flow cell by standard transmission measurements with the solvent compensated for by a ratioing method. In the flow-cell approach, the eluent is led directly through a flow cell where IR spectra are recorded continuously offering fast and relatively easy detection of eluting analytes.

Maximum infrared signal at a particular frequency can be obtained in HPLC-FTIR experiments using the infrared scan taken at the chromatographic peak maximum. FTIR has been shown to be a concentration-dependent detector for chromatography. The combination of liquid chromatography (LC) and FTIR, in principle, can be highly useful when specific detection or identification of separated compounds is required. The high speed and multiplex nature of FTIR allows spectra to be recorded at any point in the chromatogram, and during or after the LC software can be used to calculate a total IR-absorbance based chromatogram or to reconstruct functional-group chromatograms at one or more specific wavelength [15].

The flow cell experimental setup consists of a trough-shaped stainless steel cell body, covered with an IR transparent window**.** The Horizontal ATR employs a pair of transfer optics to direct the infrared beam of the spectrometer to one end of an IR transmitting ATR crystal with a similar pair of optics directing the beam emitted from the other end of the ATR crystal to the spectrometer detector (**Figure 19**). The IR beam is reflected inside the flow cell cavity passing through a high refractive index material in order to maintain total reflection at the crystal boundaries and allow sufficient reflections.

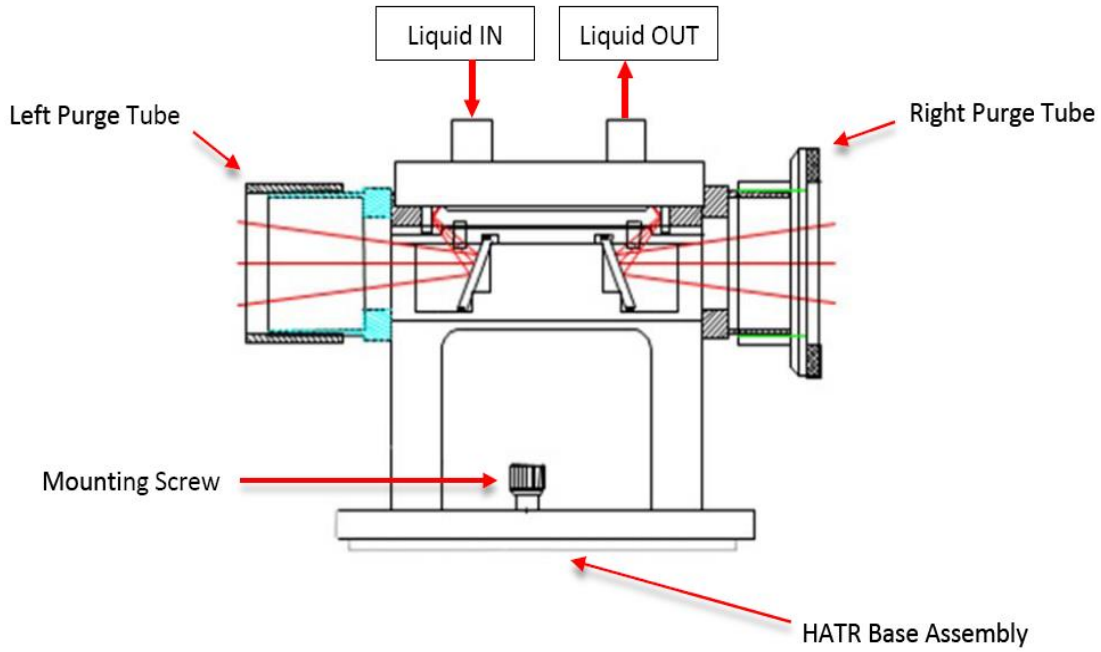

Figure 19. Sectional view of the Horizontal Attenuated Total Refection (HATR) accessory fitting an ATR flow cell [16].

For online FTIR detection, liquid-phase isocratic separation conditions must be used because gradients would result in a significant change that would be extremely difficult to compensate for. This is in agreement with the current HPLC methodology for detection and quantification of highly polar molecules which can be separated and detected using mobile phases that are highly aqueous. Furthermore, other polar substances like Maillard reaction products could be detected by the LC-FTIR interface.

2.5 Fluorescence spectroscopy

Fluorescence spectroscopy measures the intensity of photons emitted from a sample after absorbing photons. Fluorescence is the property of some atoms and the molecules absorb light at a certain wavelength and then emit light at a longer wavelength after a short period of time, called fluorescence lifetime [17]. Most fluorescent molecules are aromatic.

The fluorescence process is governed by three major events, which occur in time scales separated by several orders of magnitude (**Figure 20**). The stimulation of a susceptible

molecule by an incoming photon occurs in femtoseconds ($10E^{-15}$ seconds), while the vibratory relaxation of the electrons in the excited state at the lowest energy level is much slower and can be measured in picoseconds ($10E^{-12}$ seconds). The final process, emitting a longer wavelength photon and returning the molecule to the ground state, takes place over a relatively long period of nanoseconds ($10E^{-9}$ seconds) [18].

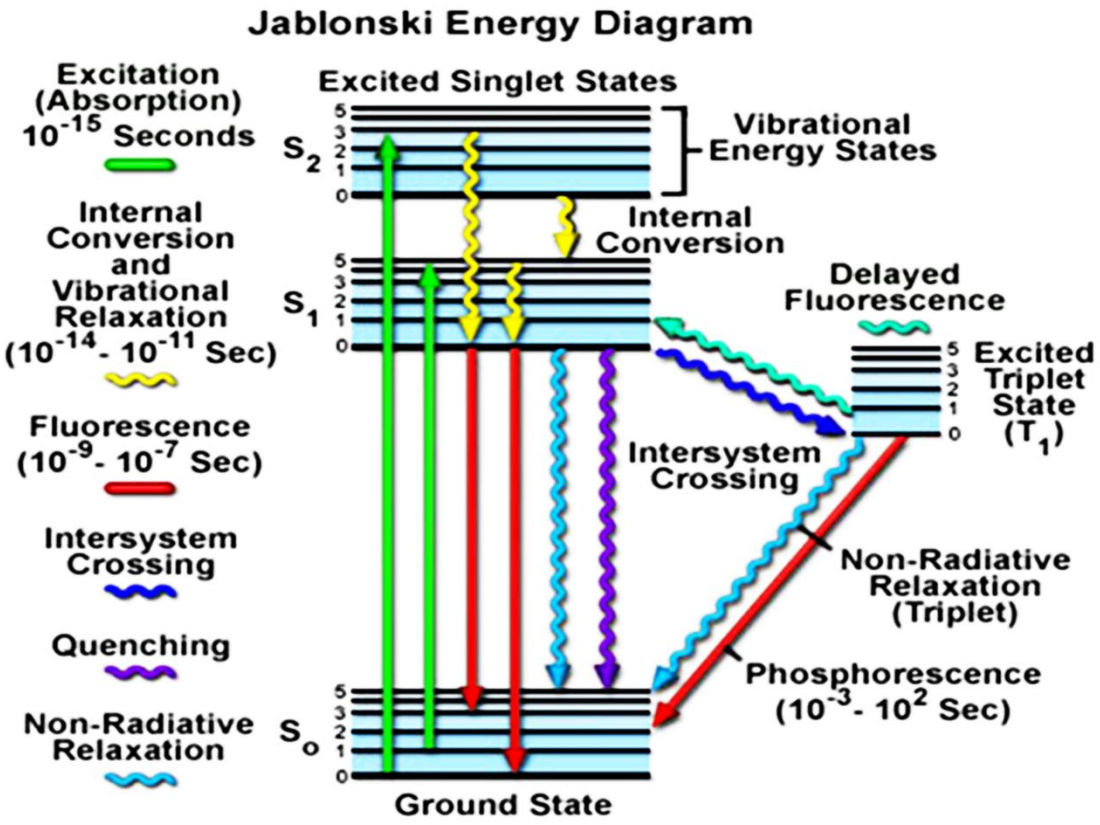

Figure 20. Jablonski energy diagram illustrating the relationship between different processes. Adapted from [19].

For any particular molecule there are several different electronic states (depicted as S(0), S(1), and S(2) in **Figure 20**), depending on the total electron energy and the symmetry of the various electronic spin states [19]. Each electronic state is further subdivided into a number of vibrational and rotational energy levels associated with atomic nuclei and orbits. Transitions between states are represented by straight or wavy arrows, depending on whether the transitions are related to the absorption or emission of a photon (linear arrow) or to the result of molecular internal expansion or non-

irradiating expulsion procedures (thicker arrows). The fundamental condition for most organic molecules is the singlet state, in which all the electrons are in pairs (with the opposite of spin). At room temperature, very few molecules have enough internal energy to exist in a state other than the lower vibrational level of the ground state, and therefore the excitation processes usually come from this level of energy.

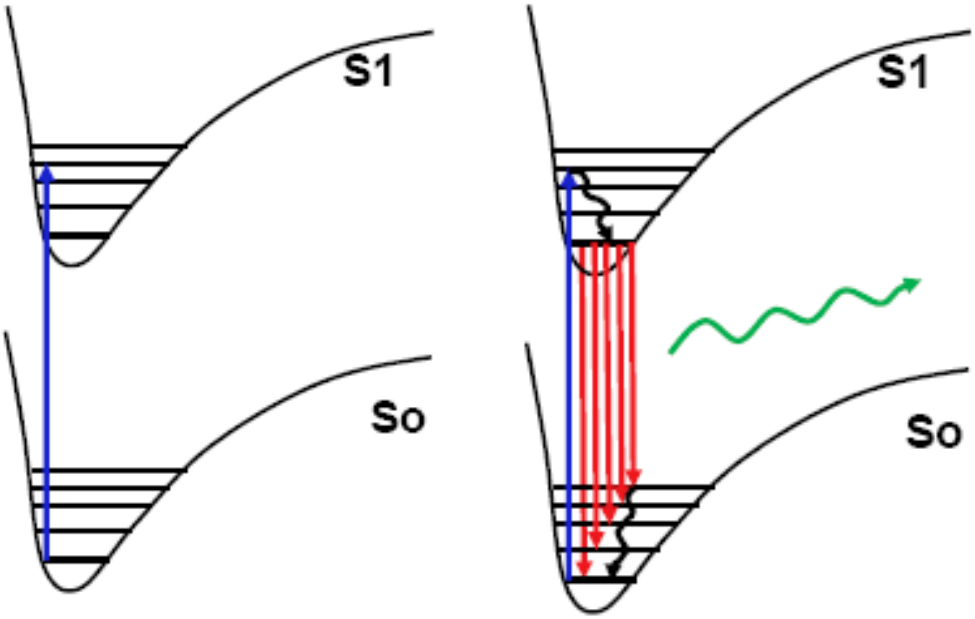

Figure 21. Potential energy diagrams with vertical transitions (Franck-Condon principle). Adapted from [19].

In particular, in fluorescence, the emission of light is caused by the irradiation of a sample with light. The light incident on the sample promotes the atoms, ions or sample molecules at excited levels (due to the absorption of photons), from which they return to their fundamental states by the spontaneous emission of fluorescence photons (**Figure 21**). Thus, in the phenomenon of fluorescence, a molecule absorbs a high energy photon and re-emits it as a lower-energy photon but of longer wavelength. The energy difference between the absorbed and the emitted photons is attributed as molecular excitation or heating. Usually the absorbed photon is in the ultraviolet and the photon emitted is visible, but the emission wavelength depends on the absorption curve and the Stokes displacement of each chromophore. Stoke displacement refers to the difference in wavelength between the peak position of the absorption spectrum and the

fluorescence spectrum of the same electronic transition. Stoke's displacement occurs due to the loss of part of the energy absorbed by the molecule before it is re-transmitted as fluorescence or phosphorescence, depending on the time between absorption and re-transmission. The photons emitted have less energy and are shifted to longer wavelengths [20].

The entire fluorescence process is circular. Unless the fluorescent chromophore is irreversibly destroyed in the excited state (photo bleaching) the same fluorescent chromophore can be stimulated continuously and detected. The fact that a single fluorescent chromophore can produce many hundreds of detectable photons is fundamental to the high sensitivity of detection of fluorescence detection techniques. For polyatomic molecules in solutions, the separate electron transitions represented by hv_{ex} and hv_{em} are replaced by a large energy spectrum called the fluorescence excitation spectrum and fluorescence emission spectrum. The ranges of these spectra are parameters of particular importance for applications where two or more fluorescent chromophores are detected simultaneously.

Apart from a few exceptions, the fluorescence excitation spectrum of a fluorescent chromophore in dilute solution is similar to the absorption spectrum. Under the same conditions, the fluorescence emission spectrum is independent of the excitation wavelength due to the partial loss of excitation energy during the time spent in the excited state. The emission intensity is proportional to the width of the excitation spectrum at the excitation wavelength. The shape of the fluorescence spectrum is independent of the excitation wavelength because the emission always comes from the lowest excited state. The fluorescence spectrum is often a "mirror image" of the absorption spectrum.

The fluorescence spectrometer is an instrument with two separate monochromators which give the ability to select both the excitation and emission wavelengths [21]. The parts necessary for a typical fluorescence spectrometer are a sample holder, an incident photon source (usually a Xe lamp), monochromators used to select specific wavelengths, focusing optics, a photon-collection detector (only, or preferably multiple channel), and a control software unit (**Figure 22**). An emission monochromator or cut-off filters are also commonly used. The detector is set at 90 degrees to the light source.

A quartz cuvette with 4 polished surfaces is used for the sample. Emission is carried out on all sides of the cell and is generally measured perpendicularly to the excitation source to prevent the collection of excitation light.

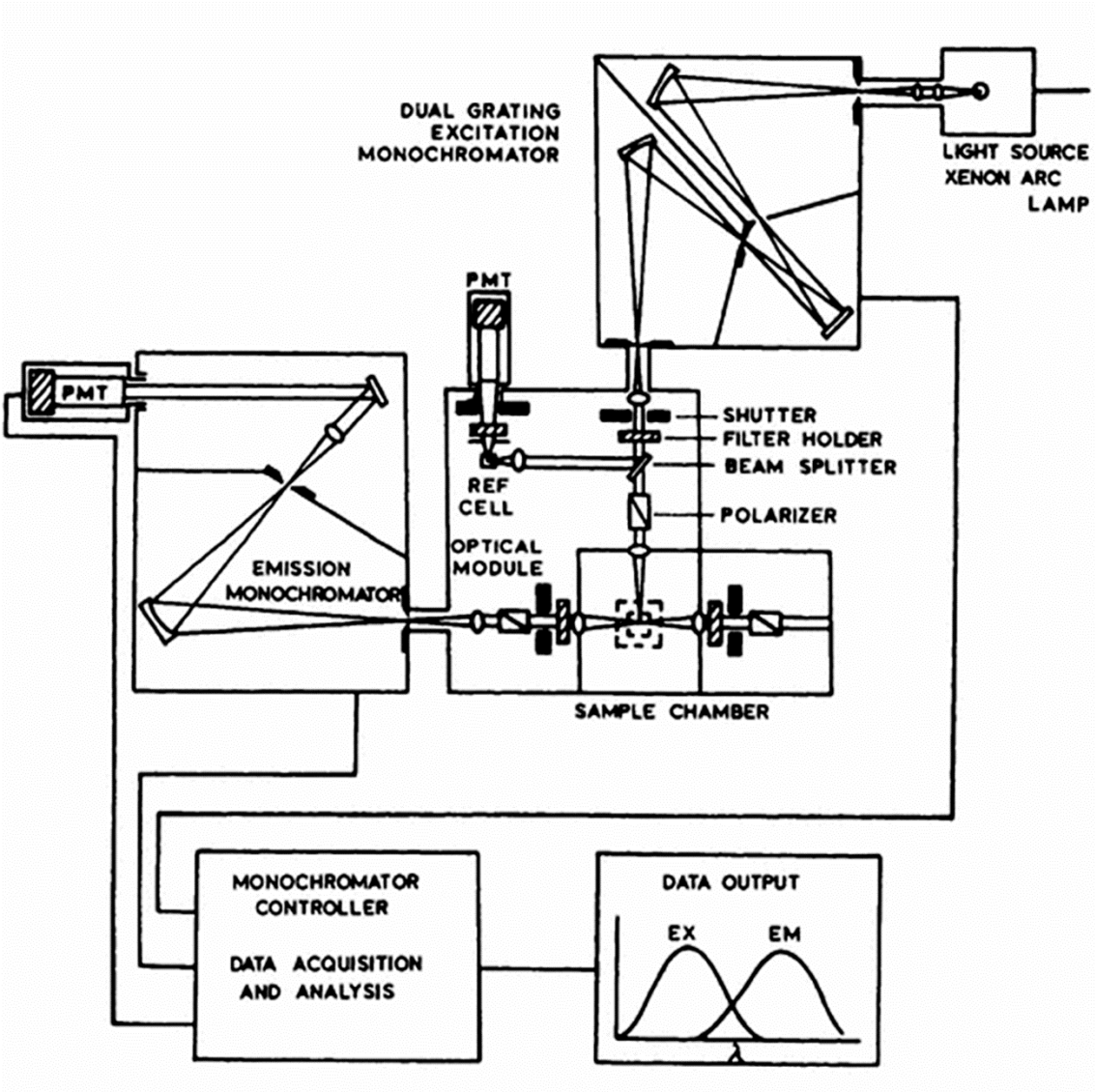

Figure 22. Schematic diagram of a typical fluorescence spectrophotometer [21].

2.6 References

[1] Workman, J. (2014). *The Concise Handbook of Analytical Spectroscopy: Theory, Applications, and Reference Materials*. World Scientific.

[2] Sathyanarayana, D. N. (2015). *Vibrational spectroscopy: theory and applications*. New Age International.

[3] Perkampus, H. H. (2013). *UV-VIS Spectroscopy and Its Applications*. Springer Science & Business Media.

[4] Barth, A., Zscherp, C. (2002). What vibrations tell about proteins. *Quarterly Reviews of Biophysics*, **35**(4), 369-430.

[5] Griffiths, P. R., De Haseth, J. A. (2007). *Fourier transform infrared spectrometry*. 2nd ed. Hoboken, New Jersey: John Wiley & Sons.

[6] Barth, A. (2007). Infrared spectroscopy of proteins. *Biochimica et Biophysica Acta (BBA) - Bioenergetics*, **1767**(9), pp. 1073-1101.

[7] Larkin, P. J. (2011). *Infrared and Raman spectroscopy: principles and spectral interpretation*. Elsevier.

[8] Mirabella, F. M. (1992). *Internal reflection spectroscopy: Theory and applications*. West Palm Beach: CRC Press.

[9] Baker, M. J., Trevisan, J., Bassan, P., Bhargava, R., Butler, H. J., Dorling, K. M., Fielden, P. R., Fogarty, S. W., Fullwood, N. J., Heys, K. A., Hughes, C. (2014). Using Fourier transform IR spectroscopy to analyze biological materials. *Nature protocols*, **9**(8), pp. 1771-1791.

[10] Bird, I. M. (1989). High performance liquid chromatography: principles and clinical applications. *British Medical Journal*, **299**(6702), pp. 783-787.

[11] Meyer, V. R. (2013). *Practical high-performance liquid chromatography*. Hoboken, New Jersey: John Wiley & Sons.

[12] Guillarme, D., Veuthey, J. L. (2017). HPLC Teaching Assistant: A New Tool for Learning and Teaching Liquid Chromatography, Part 1. *LCGC Europe*, **30**(1), pp. 22-29.

[13] Edelmann, A., Diewok, J., Baena, J. R., Lendl, B. (2003). High-performance liquid chromatography with diamond ATR-FTIR detection for the determination of carbohydrates, alcohols and organic acids in red wine. *Analytical and Bioanalytical Chemistry*, **376**(1), pp. 92-97.

[14] Kuligowski, J., Quintas, G., de la Guardia, M., Lendl, B. (2010). Analytical potential of mid-infrared detection in capillary electrophoresis and liquid chromatography: A review. *Analytica Chimica Acta*, **679**, pp. 31-42.

[15] Kok, S. J., Somsen, G. W., Paul, W., Alan, T., Colin, P. (2005). *Liquid Chromatography-Fourier Transform Infrared. Encyclopedia of Analytical Science*. 2nd ed. Oxford: Elsevier.

[16] Pike Technologies (2015, 1 January), *Installation and User Guide*, viewed 1 June 2015, https://www.piketech.com/files/usermanuals/HATRFlowThroughCellManual.pdf

[17] Ashutosh, S., Stephen, G. (1999). *An introduction to Fluorescence spectroscopy*. New York: John Wiley & Sons.

[18] Schulman, S. G. (2013). *Fluorescence and phosphorescence spectroscopy: physicochemical principles and practice*. Elsevier.

[19] Valeur, B. (2012). Introduction: On the Origin of the Terms Fluorescence, Phosphorescence, and Luminescence. In: B. Valeur, J. C. Brochon, eds, *New trends in fluorescence spectroscopy: applications to chemical and life sciences* (Vol. 1). Springer Science & Business Media, pp. 3-6.

[20] Lakowicz, J. R. (1999). Introduction to fluorescence. In: J. R. Lakowicz, ed., *Principles of fluorescence spectroscopy*, 2nd ed. New York: Springer US, pp. 1-23.

[21] Lakowicz, J. R., (1999). Instrumentation for fluorescence spectroscopy. In Principles of fluorescence spectroscopy. In: J. R. Lakowicz, ed., *Principles of fluorescence spectroscopy*, 2nd ed. New York: Springer US, pp. 25-61.

3 Real Time Monitoring the Maillard Reaction Intermediates by HPLC-FTIR

3.1 Abstract

Maillard reaction products in the food-, nutrition- and pharmaceutical related processes are of great interest in cases where the substances involved are chemically reactive or unstable. Detailed data using vibrational FTIR spectroscopy of the Maillard-type reaction products are limited and needs more experimental evidences with explicit mechanisms of the reaction to demonstrate how the reducing sugars be avoided in formulating the amine-containing substances. The combination of high performance liquid chromatography (HPLC) with Fourier transform infrared (FTIR) spectrometry is a powerful instrumental separation-structure sensitive technique that allows characterization in real time of the separated chemical species. In this short review we demonstrate the benefits of the HPLC-FTIR coupling technique in studying the Maillard reaction model Fructose/Asparagine system.

Keywords

Maillard reaction; Asparagine; Fructose; HPLC- ATRFTIR.

3.2 Introduction

The Maillard reaction involves three different stages in which complex reactions take place between reducing sugars and free amino groups of amino acids or peptides. The initial stage involves the formation of the Schiff base and the formation of the Amadori products without the formation of browning compounds. The second stage involves the dehydration of sugar and amino acid degradation. In the final stage, melanoidins are the final heterocyclic nitrogen compounds which are actually nitrogen containing polymeric substances which are difficult to decompose (**Figure 1**). The formation of acrylamide follows a number of possible routes in the frame of Maillard reactions in food products,

in which the asparagine route is the major one. Acrylamide has been shown to originate from the Maillard reaction of the amino acid asparagine with reducing sugars as well as carbonylic compounds deriving from either the Maillard reaction or lipid oxidation processes [1-5] during heating. However, it was demonstrated that the asparagine pathway is the most predominant for the formation of acrylamide through isotope-labelling experiments [1]. This was further supported by model studies showing that the N-glycosyl of asparagine generated twenty times more acrylamide, compared to α-dicarbonyls and the Amadori compound of asparagine concluding that α-hydroxy carbonyl compounds, such as fructose and glucose are more effective than other carbonylic compounds in generating acrylamide [3]. Asparagine alone may form acrylamide through decarboxylation and deamination but the reaction is inefficient giving extremely low yields. Nevertheless, asparagine in the presence of the hydroxycarbonyl moiety of reducing sugars can produce acrylamide in the range of 1 mol percent in model systems [3].

There are only few studies utilizing the monitoring ability of the FTIR technique to elucidate the reaction network in the acrylamide formation pathway [6,7]. The decarboxylated Schiff base (azomethine ylide) and decarboxylated Amadori product are both key intermediates contributing to the formation of acrylamide (**Figure 1**). Their relative importance was determined when both of the intermediates were synthesized and their relative abilities to generate acrylamide under dry and wet heating conditions were investigated [6]. One of these intermediates is oxazolidin-5-one which was recently monitored by FTIR in a dry model reaction system [7]. Imines formed subsequent to carbonyl-amine reactions were characterized by FTIR spectroscopy. Recently, a DSC-FTIR microspectroscopy method was applied to detect continuous pathways in the solid state asparagine/glucose reaction [8]. In this work, we demonstrate the feasibility of applying the coupled HPLC-FTIR separation-structure sensitive technique to Maillard-type reaction of the fructose-Asparagine products in real time.

3.3 Materials and Methods

3.3.1 Chemicals

Acrylamide (>99.5%) was purchased from Panreac Quimica SA (Barcelona, Spain). L-Asparagine monohydrate (>99%) and fructose (>99.5%) were purchased from Sigma-Aldrich (St. Louis, MO, USA). The water used was Milli-Q grade water (Millipore, Ireland). Acrylamide stock solutions and calibration standards were prepared in water and kept at -20°C until use. All samples were filtered with disposable syringe filters (45-μm pore size, PTFE, Millex, Millipore, Ireland) prior to analysis.

3.3.2 Sample preparation

Equimolar solutions of fructose and asparagine (0.2 M) were prepared in phosphate buffer (0.1 M) and the pH was adjusted to the desired value (pH 8). Samples (10 ml) were heated in closed screwcapped tubes at 100, 120, and 140°C in a heating oven (Memmert, Germany). At predetermined heating times (30, 60, 90 and 120 mins), samples were taken and immediately cooled on ice and stored at -20°C prior to analysis.

3.3.3 Experimental setup

HPLC: Maillard reaction product (MPRs) formation was monitored on a Shimadzu Prominence 20A HPLC system consisting of a quaternary pump with online degasser, a temperature-controlled column oven and a UV-SPD detector. A 1 μl aliquot of sample was injected for LC separation whilst a 100 μl aliquot of the same sample was injected to acquire the FTIR measurements. HPLC analysis was performed on a 4.6 × 250 mm, 5 μm particle size, Zorbax SB-Aq analytical column (Agilent Technologies). Water at a flow rate of 0.5 ml/min was used isocratically as the mobile phase at room temperature. Maillard reaction products (MPRs) and acrylamide were detected at 200 nm.

FTIR: A Bruker Tensor 27 FTIR spectrometer equipped with a triglycine sulfate (TGS) detector was used for spectra acquisition (**Figure 1**). For controlling the spectrometer the software package OPUS 7.0/IR/3D (Bruker) was used. The OPUS CHROM Version 7 (Bruker) software package was used to acquire time-dependent spectra in the coupled HPLC-FTIR process. The result of the measurement performed with the OPUS CHROM package was a number of spectra taken at defined, constant time intervals. During the measurement, the acquired spectra and generated traces were displayed in

real time. A horizontal ATR (HATR) accessory (Pike Technologies, Inc., Madison, USA) was employed fitting a Germanium flow-through liquid ATR cell with ten internal reflections. This enabled the pumping through of solutions over the ATR Germanium surface with minimal dead volume. The Horizontal ATR is designed with a pair of transfer optics to direct the infrared beam of the spectrometer to one end of the IR transmitting ATR crystal. A similar pair of optics directs the beam emitted from the other end of the ATR crystal to the spectrometer detector. The Germanium crystal is trapezoid shape with a thickness of 4 mm (**Figure 23**). This feature maximizes the signal to noise of the resulting spectra. Spectra were collected in the 900-1800 cm-1 range with 8 cm^{-1} resolution and 16 co-added scans each (apodisation function: Blackman-Harris- 3-term). A time resolution of 8 spectra per minute was achieved. The scanner velocity was 20 kHz (HeNe frequency). A background spectrum was collected before each sample measurement with only water flowing thought the ATR cell. This was used to calculate the absorption spectra during the CHROM measurement. The single pure substances were injected and a chromatographic run was performed. These were used as reference spectra for the identification asparagine and sugars. The intensity changes of the spectra as a function of time were stored as traces in a 3D file for all FTIR measurements. Data extraction and processing was carried out using the OPUS 7.0/IR/3D (Bruker) software. The spectra were extracted from the 3D data set of the chromatographic peak maximum and were graphically plotted using Origin Pro v8.0 software.

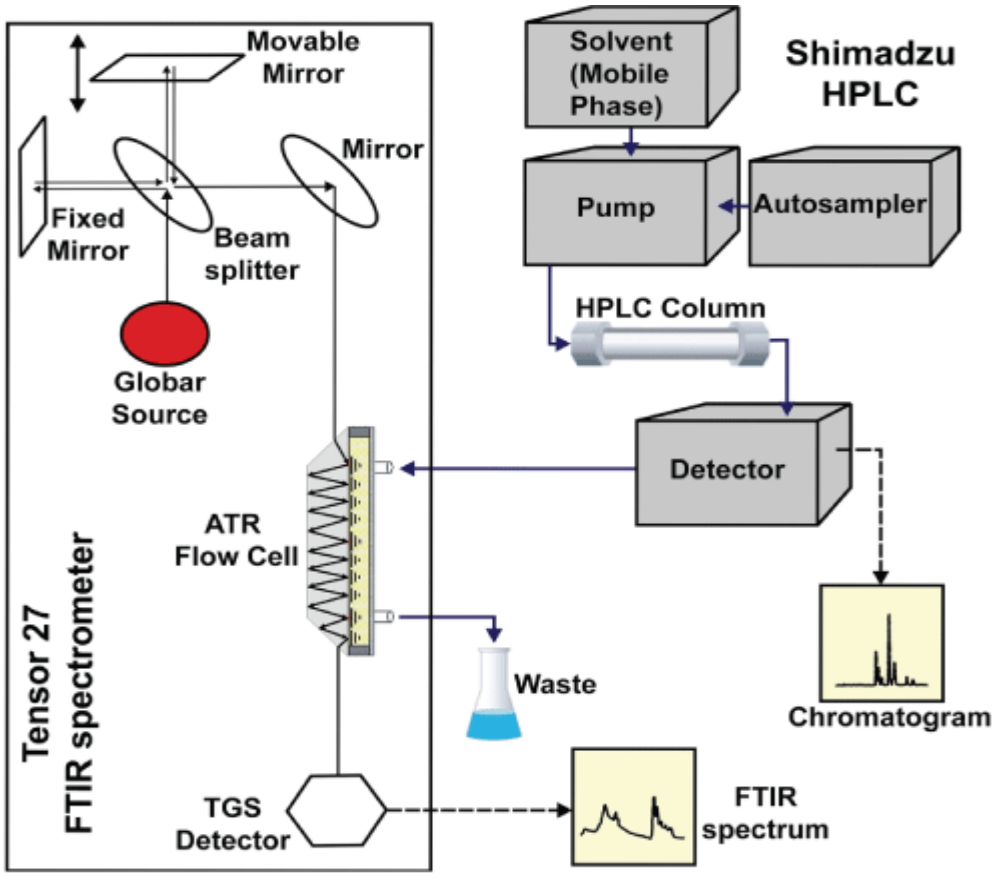

Figure 23. Schematic of the experimental layout of the coupled HPLC-FTIR technique. Chromatographic separations were performed by HPLC system using the Zorbax SB-Aq column. The mobile phase is then directed through a dedicated flow cell comprising a germanium ATR cell which was used for on-line FTIR detection.

3.4 Results and Discussion

A new analytical setup allowing the concurrent identification of precursors and products of the Maillard reaction is described. It is based on high-performance liquid chromatography (HPLC) with UV-vis detector and a FTIR-ATR flow cell coupled in series. Separation and qualitative determination of individual Maillard species have been achieved using various chromatographic techniques including GC-MS and High-Performance Anion Exchange Chromatography (HPAEC) [9]. The main advantage of HPLC over GC in the MR analysis context is that non-volatile water-soluble

compounds can be analyzed directly without the need for prior derivatization. However, high-performance liquid chromatography (HPLC) on its own has limited ability to adequately resolve and give structure sensitive information when analyzing Maillard reaction compounds. The collected fractions were then analyzed by the ATR-FTIR technique.

Glycoconjugates, such as N-glycosides and related compounds formed in the early phase of the Maillard reaction have been proposed as key intermediates leading to acrylamide formation [10]. This hypothesis was supported by the work of Yaylayan et al. and Zyzak et al. [1,11]. Both groups provided evidence of the importance of Schiff base of asparagine which is formed after a dehydration step. The Schiff base is formed early in the Maillard reaction as the result of elimination of water from the conjugate of glucose and asparagine [1,3].

The next step is the transformation of the Schiff base intermediate to an Amadori product through an Amadori rearrangement. Following this, there is a decarboxylation reaction of the Amadori product to the decarboxylated Amadori product. It is therefore considered that the key mechanistic step is the decarboxylation of the Schiff base leading to other intermediates that can directly release acrylamide (**Figure 24**). With respect to structure, asparagine alone is in theory capable of being converted thermally to acrylamide through decarboxylation and deamination reactions, however experimentally this was not the case with maleimide being the main reaction product [11].

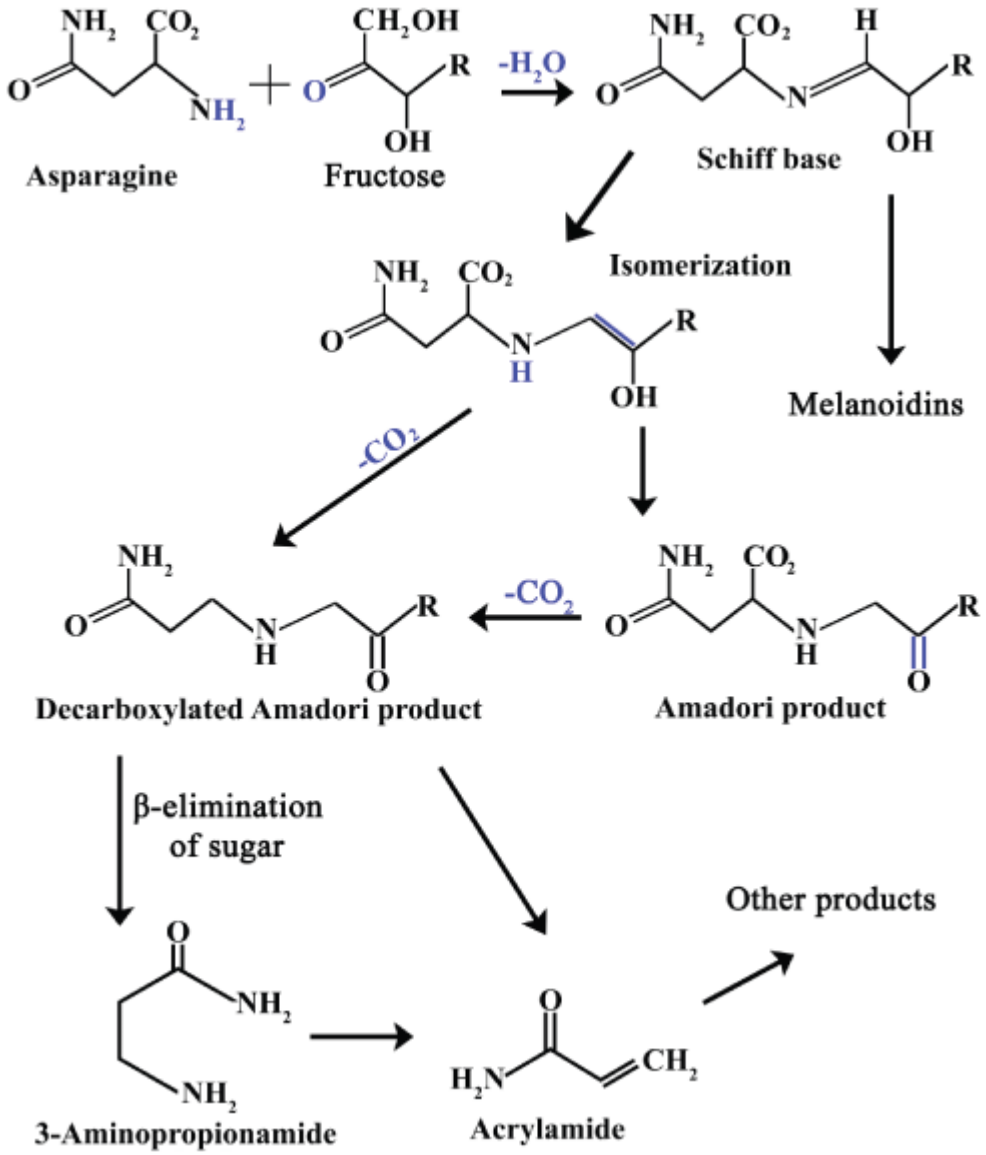

Figure 24: Overall mechanistic pathway of the reaction between asparagine and fructose (R_1 = CH_2OH, R_2 = CH_2O).

When asparagine and fructose react at high temperatures it is evident mainly from the HPLC data that there is a mixture of reactants and multiple products in the reaction vessel (**Figure 25**). Time and temperature-dependent evolution of Maillard reaction products (MRPs), including that of acrylamide were monitored on the Zorbax column which is highly selective for polar molecules in aqueous phases. Despite the fact that there was only partial separation of the two reactants we notice that at 140°C there is

degradation of asparagine and fructose as we can observe from the absorption peaks at Reaction time (Rt) 5.4 and Rt 6.0 mins respectively (Figure 3). It is also apparent that

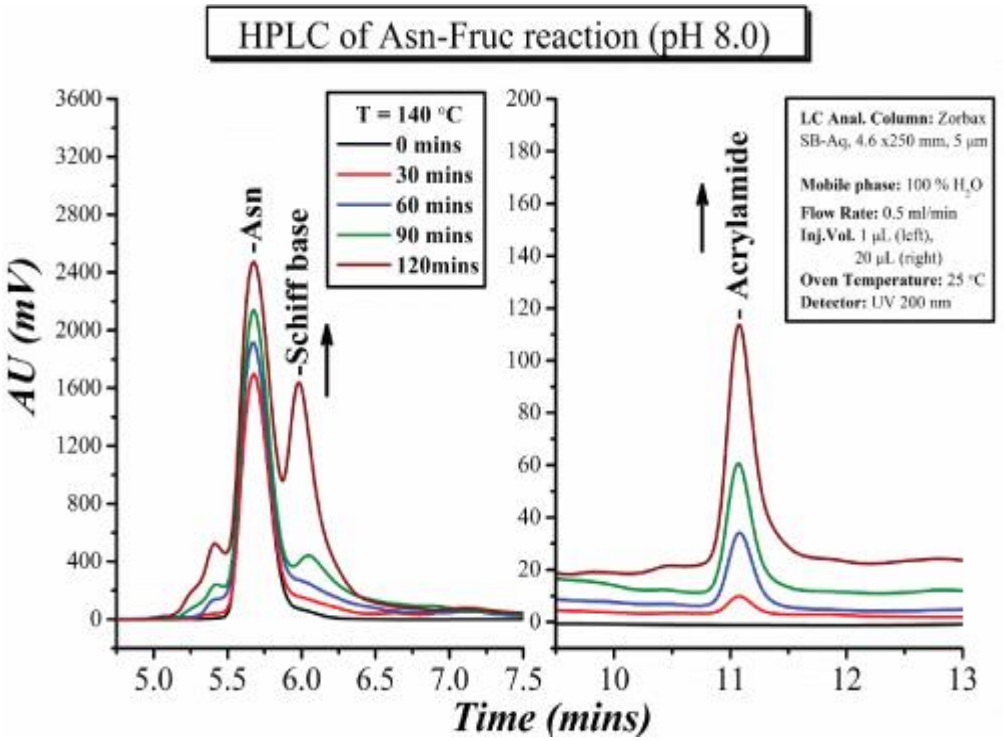

Figure 25: HPLC chromatograms of the time and temperature (T=25-140°C) - dependent evolution of Maillard reaction products (MRPs) at pH 8.0.

the peak at Rt 5.7 mins corresponding to asparagine increases with time at 140 °C (**Figure 25**). In the FTIR spectra, the spectral range between 1200 and 1800 cm-1 is shown where the majority of the asparagine FTIR absorptions are found [12-30].

In Figure 4a-c we show the coupled HPLC-FTIR spectra at room temperature (**Figure 26a**) and T=140°C (**Figure 26b**), in the Rt 5.5-6.5 min and 1200-1700 cm^{-1} spectral region. All traces in **Figure 26a** are the unheated, room temperature reactants. All traces in **Figure 26b** are those of the reaction products at T=140°C. All traces in **Figure 26c** are the difference spectra of the heated asparagine-fructose reaction product in the Rt=5.5-6.5 min range at pH 8 and T=140°C (**Figure 26b**) minus the unheated spectra shown in **Figure 26a**. The spectra in **Figure 26b** reveals intensity changes in the region of the C=O band of Asn at 1675 cm^{-1} as well large broadening in the region of the Asn

$\delta(NH_2)$ at 1621 cm^{-1}. However, from the absolute FTIR data due to the overlapping vibrations with the unreacted species and since in the newly formed species the ν(C=O) and δ(NH2) are expected to retain similar frequencies with those of the unreacted, it is not possible to assign the vibrations of the new species with certainty. The FTIR difference spectra in **Figure 26c** reveal features at 1660, 1575, and 1387 cm^{-1}. Based on our HPLC data at Rt=5.5-6.5 we expect that the FTIR spectra have contributions from the formation of the Schiff base Imine group, the enaminol group stretching frequency and/or from the Amadori and decarboxylated Amadori products with distinct C=O vibrations in the 1700 cm^{-1} region. For the Schiff base, the carbonyl (C=O) and NH_3 groups have very similar frequency with that of the unreacted Asn and thus they are spectators in the reaction without any contributions to the bands observed in the difference spectra. Imines under Maillard reactions have been characterized, and as the first step in the carbonyl-amine interaction have been proposed to play a crucial role in the formation of the Schiff base and degradation of the Amadori products towards the formation of the 3-Aminopropionamide and Acrylamide (**Figure 24**). The main feature in the FTIR spectrum of the imine (Schiff base) species is the vibration of ν(-C=N) at 1660 cm^{-1}. Given that the 1660 cm^{-1} mode originates from the Schiff base we assign the other vibrations at 1569 cm^{-1} to HN-C and that at 1388 cm^{-1} to ν(CFru-N=CHAsn). We have excluded the possibility that the species we have observed originate from either the Amadori or the decarboxylated Amadori product due the lack of a C=O vibration in the 1700 cm^{-1} region. However, we can't exclude the possibility that the species we have observed originate from the isomerization of the Schiff base only, forming the enaminol moiety CFru-NH=CHAsn (1660 cm^{-1}). In this case, the 1589 and 1388 cm^{-1} modes originate from the N-H and C–N stretching vibrations of the enaminol moiety CFru-NH=CHAsn, respectively. It should be noted that the concentration of the imine intermediate is increased at elevated temperatures and under alkaline conditions without being converted to an Amadori product. Our data find also support from the results of the model systems where it was shown that imines are converted to Amadori products only under strong acidic conditions and raising temperatures [12]. This suggests that the initial deprotonated amine attack is favored by a protonated form of the imine in order to proceed to the Amadori products and beyond. Another feature that is clearly evident is the loss of the 1502 cm^{-1} asparagine band corresponding to the backbone amino

and/or carboxylate group. This further supports the hypothesis that there is loss of the backbone amino group and successive decarboxylation reaction occurring.

The new approach of the HPLC-FTIR application to the Maillard reaction has applications to other similar chemical reaction in food, nutrition and pharmaceutical industries without the need to isolate the species and characterize them separately. This is the major advantage of this coupling technique. It can be concluded that the real time monitoring of the imine bonds it is reported for the first time in the Fructose-Asparagine system under physiological conditions. In addition, the formation of acrylamide at T=140°C raises major concerns about the safety in using fructose with asparagine in such temperatures.

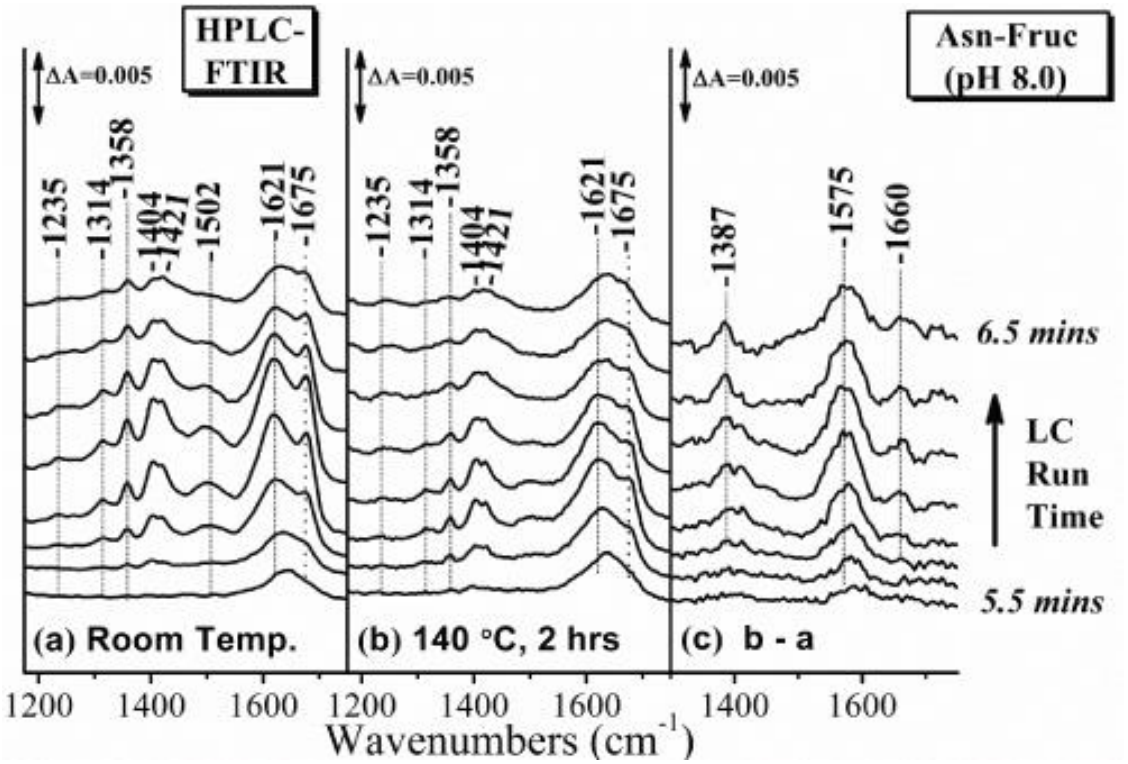

Figure 26: HPLC-FTIR spectra of the reaction mixture of asparagine and fructose (pH 8.0) at 140°C. (a) Room temperature (b) Heated (c) Difference spectra.

3.5 References

[1] Zyzak, D. V., Sanders, R. A., Stojanovic, M., Tallmadge, D. H., Eberhart, B. L., Ewald, D. K., Gruber, D. C., Morsch, T. R., Strothers, M. A., Rizzi, G. P., Villagran, M. D. (2003). Acrylamide formation mechanism in heated foods. *Journal of Agricultural and Food Chemistry*, **51**, pp.4782-4787.

[2] Amrein, T. M., Andres, L., Manzardo, G. G., Amado, R. (2006). Investigations on the promoting effect of ammonium hydrogencarbonate on the formation of acrylamide in model systems. *Journal of Agricultural and Food Chemistry*, **54**, pp. 10253-10261.

[3] Stadler, R. H., Robert, F., Riediker, S., Varga, N., Davidek, T., Devaud, S., Goldmann, T., Hau, J., Blank, I. (2004). In-Depth Mechanistic Study on the Formation of Acrylamide and Other Vinylogous Compounds by the Maillard Reaction. *Journal of Agricultural and Food Chemistry*, **52**, pp. 5550-5558.

[4] Hidalgo, F. J., Delgado, R. M., Navarro, J. L., Zamora, R. (2010). Asparagine decarboxylation by lipid oxidation products in model systems. *Journal of Agricultural and Food Chemistry*, **58**, pp. 10512-10517.

[5] Hidalgo, F. J., Delgado, R. M., Zamora, R. (2009). Degradation of asparagine to acrylamide by carbonyl-amine reactions initiated by alkadienals. *Food Chemistry*, **116**, pp. 779-784.

[6] Perez-Locas, C., Yaylayan, V. A. (2008). Further insight into thermally and pH-induced generation of acrylamide from glucose/asparagine model systems. *Journal of Agricultural and Food Chemistry*, **56**, pp. 6069-6074.

[7] Chu, F. L., Yaylayan, V. A. (2009). FTIR monitoring of oxazolidin-5-one formation and decomposition in a glycolaldehyde-phenylalanine model system by isotope labeling techniques. *Carbohydrate Research*, **344**, pp. 229-236.

[8] Hwang, D. F., Hsieh, T. F., Lin, S. Y. (2013). One-Step Simultaneous Differential Scanning Calorimetry-FTIR Microspectroscopy to Quickly Detect Continuous Pathways in the Solid-State Glucose/Asparagine Maillard Reaction. *Journal of AOAC International*, **96**, pp. 1362-1364.

[9] Davidek T, Clety N, Devaud S, Robert F, Blank I (2003) Simultaneous Quantitative Analysis of Maillard Reaction Precursors and Products by High-Performance Anion

Exchange Chromatography. *Journal of Agricultural and Food Chemistry*, **51**, pp. 7259-7265.

[10] Stadler, R. H., Blank, I., Varga, N., Robert, F., Hau, J., et al. (2002) Acrylamide from Maillard reaction products. *Nature*, **419**, pp. 449-450.

[11] Yaylayan, V. A., Wnorowski, A., Perez-Locas, C. (2003). Why asparagine needs carbohydrates to generate acrylamide. *Journal of Agricultural and Food Chemistry*, **51**, pp. 1753-1757.

[12] Wnorowski, A., Yaylayan, V. A. (2003). Monitoring carbonyl-amine reaction between pyruvic acid and alpha-amino alcohols by FTIR spectroscopy--a possible route to Amadori products. *Journal of Agricultural and Food Chemistry*, **51**, pp. 6537-6543.

[13] Bellamy, L. J., Williams, R. L. (1957). The NH stretching frequencies of primary amines. *Spectrochimica Acta*, **9**, pp. 341-345.

[14] Biemel, K. M., Buhler, H. P., Reihl, O., Lederer, M. O. (2001). Identification and quantitative evaluation of the lysine-arginine crosslinks GODIC, MODIC, DODIC, and glucosepan in foods. *Nahrung*, **45**, pp. 210-214.

[15] Boeckx, B., Maes, G. (2012). The conformational behavior and H-bond structure of asparagine: a theoretical and experimental matrix-isolation FT-IR study. *Biophysical Chemistry*, **165-166**, pp. 62-73.

[16] Borrelli, R. C., Visconti, A., Mennella, C., Anese, M., Fogliano, V. (2002). Chemical characterization and antioxidant properties of coffee melanoidins. *Journal of Agricultural and Food Chemistry*, **50**, pp. 6527-6533.

[17] Chu, F. L., Yaylayan, V. A. (2008). Post-schiff base chemistry of the Maillard reaction: mechanism of imine isomerization. *Annals of the New York Academy of Sciences*, **1126**, pp. 30-37.

[18] Davidek, T., Clety, N., Aubin, S., Blank, I. (2002). Degradation of the Amadori compound N-(1-deoxy-D-fructos-1-yl)glycine in aqueous model systems. *Journal of Agricultural and Food Chemistry*, **50**, pp. 5472-5479.

[19] Edelmann, A., Diewok, J., Baena, J. R., Lendl, B. (2003). High-performance liquid chromatography with diamond ATR-FTIR detection for the determination of

carbohydrates, alcohols and organic acids in red wine. *Analytical and Bioanalytical Chemistry*, **376**, pp. 92-97.

[20] Hartkopf, J., Pahlke, C., Ludemann, G., Erbersdobler, H. F. (1994). Determination of Ne-carboxymethyllysine by a reversed-phase high-performance liquid chromatography method. *Journal of Chromatography A*, **672**, pp. 242-246.

[21] Hodge, J. E. (1953). Dehydrated Foods, Chemistry of Browning Reactions in Model Systems. *Journal of Agricultural and Food Chemistry*, **1**, pp. 928-943.

[22] Hofmann, T. (1998). Studies on melanoidin-type colorants generated from the Maillard reaction of protein-bound lysine and furan-2-carboxaldehyde - chemical characterisation of a red coloured domaine. *Zeitschrift fur Lebensmitteluntersuchung und -Forschung A*, **206**, pp. 251-258.

[23] Kok, S. J., Somsen, G. W., Paul, W., Alan, T., Colin, P. (2005). Liquid Chromatography-Fourier Transform Infrared. In: Townshend, A., Poole, C. F., Worsfold, P. J., Eds. *Encyclopedia of Analytical Science*, 2nd ed., Oxford, Elsevier.

[24] Kuntcheva, M., Obretenov, T. (1996). Isolation and characterization of melanoidins from beer. *Zeitschrift fur Lebensmittel-Untersuchung und Forschung*, **202**, pp. 238-243.

[25] López-Navarrete, J. T., Casado, J., Hernández, V., Ramírez, F. J. (1997). Experimental and theoretical vibrational studies of the amino acid l-asparagine in solution. *Journal of Raman Spectroscopy*, **28**, pp. 501-509.

[26] Martins, S. I. F. S., Jongen, W. M. F., Van Boekel, M. A. J. S. (2000). A review of Maillard reaction in food and implications to kinetic modelling. *Trends in Food Science & Technology*, **11**, pp. 364-373.

[27] Mc Kittrick, P. T., Danielson, N. D., Katon, J. E. (1991). A Comparison Between a Micro and an Ultramicro Circle Cell for on-Line Ft-Ir Detection in a Reverse Phase HPLC System. *Journal of Liquid Chromatography*, **14**, pp. 377-393.

[28] Moreno, F. J., Lopez-Fandino, R., Olano, A. (2002). Characterization and functional properties of lactosyl caseinomacropeptide conjugates. *Journal of Agricultural and Food Chemistry*, **50**, pp. 5179-5184.

[29] Motai, H. (1976). Viscosity of Melanoidins Formed by Oxidative Browning Validity of the Equation for a Relationship between Color Intensity and Molecular Weight of Melanoidin. *Agricultural and Biological Chemistry*, **40**, pp. 1-7.

[30] Pischetsrieder, M., Grob, U., Schoetter, C. (1999). Detection of Maillard products of lactose in heated or processed milk by HPLC/DAD. *Zeitschrift fur Lebensmitteluntersuchung und -Forschung A*, **208**, pp. 172-177.

[31] Robb, C. S., Geldart, S. E., Seelenbinder, J. A., Brown, P. R. (2002). Analysis of green tea constituents by HPLC-FTIR. *Journal of Liquid Chromatography & Related Technologies*, **25**, pp. 787-801.

[32] Rufian-Henares, J. G. N., Guerra-Hernandez, E., Garcia-Villanova, B. N. (2004). Pyrraline content in enteral formula processing and storage and model systems. *European Food Research and Technology*, **219**, pp. 42-47.

[33] Sabo, M., Gross, J., Wang, J. S., Rosenberg, I. E. (1985). On-line high-performance liquid chromatography/Fourier tranform infrared spectrometry with normal and reverse phases using an attenuated total reflectance flow cell. *Analytical Chemistry*, **57**, pp. 1822-1826.

[34] Silvan, J. M., van de Lagemaat, J., Olano, A., Del Castillo, M. D. (2006). Analysis and biological properties of amino acid derivates formed by Maillard reaction in foods. *Journal of Pharmaceutical and Biomedical Analysis*, **41**, pp. 1543-1551.

[35] Somoza, V., Lindenmeier, M., Wenzel, E., Frank, O., Erbersdobler, H. F., Hofmann, T. (2003). Activity-guided identification of a chemopreventive compound in coffee beverage using in vitro and in vivo techniques. *Journal of Agricultural and Food Chemistry*, **51**, pp. 6861-6869.

[36] Sylvestre, S., Sebastian, S., Edwin, S., Amalanathan, M., Ayyapan, S., Jayavarthanan, T., Oudayakumar, K., Solomon, S. (2014). Vibrational spectra (FT-IR and FT-Raman), molecular structure, natural bond orbital, and TD-DFT analysis of l-Asparagine Monohydrate by Density Functional Theory approach. *Spectrochimica Acta Part A: Molecular and Biomolecular Spectroscopy*, **133**, pp. 190-200.

[37] Tareke, E., Rydberg, P., Karlsson, P., Eriksson, S., Tornqvist, M. (2000). Acrylamide: a cooking carcinogen? *Chemical Research in Toxicology*, **13**, pp. 517-522.

[38] Tauer, A., Hasenkopf, K., Kislinger, T., Frey, I., Pischetsrieder, M. (1999). Determination of Ne-carboxymethyllysine in heated milk products by immunochemical methods. *European Food Research and Technology*, **209**, pp. 72-76.

[39] Vinale, F., Monti, S. M., Panunzi, B., Fogliano, V. (1999). Convenient synthesis of lactuloselysine and its use for LC-MS analysis in milk-like model systems. *Journal of Agricultural and Food Chemistry*, **47**, pp. 4700-4706.

[40] Wolpert, M., Hellwig, P. (2006). Infrared spectra and molar absorption coefficients of the 20 alpha amino acids in aqueous solutions in the spectral range from 1800 to 500 cm^{-1}. *Spectrochimica Acta Part A: Molecular and Biomolecular Spectroscopy*, **64**, pp. 987-1001.

[41] Yaylayan, V. A. (1997). Classification of the Maillard reaction: A conceptual approach. *Trends in Food Science & Technology*, **8**, pp. 13-18.

4 Detection of the Amadori products of the Glucose/Asparagine reaction by a SPE-ATR-FTIR technique

4.1 Abstract

The early phase Maillard reaction products of the reaction between asparagine and sugars are most significant in the progress of the Maillard reaction chemical network. We have investigated the formation of Amadori products by employing a combined analytical technique of Solid Phase Extraction (SPE) and Attenuated Total Reflection-Fourier Transform Infrared Spectroscopy (ATR-FTIR). We have identified the vibrational marker bands primarily of the C=O group of the Amadori compounds in the FTIR spectra after methanolic SPE elution. The present study clearly indicates that this unique SPE-ATR-FTIR technique not only enhances detection of the Amadori compounds but also offers separation of these products from their initial reactants.

Key words: Maillard reaction; Asparagine; Glucose; Amadori; SPE; ATR-FTIR.

4.2 Introduction

The Maillard reaction (MR) which is one of the most important chemical reactions in food processing consists of the early, the advanced and final stages [1, 2]. The early stage involves the condensation of a free amino group with a reducing sugar to form the Amadori products whilst the advanced stage is characterized by their degradation. The final stage is characterized by the formation of brown nitrogenous polymers and co-polymers like melanoidins. The progress of MR is dependent upon the concentrations of reactants and the reactant types, pH, time, temperature, and finally the water activity. The later has a significant catalytic effect because it can act as either a proton donor or proton acceptor and thus affect the reaction pathway(s) that leads to the formation of Amadori species and acrylamide [3]. The MR can cause both enhancement and deterioration of food quality owing to anti-oxidant, anti-allergenic, anti-microbial and

the cytotoxic properties of the reaction products (MRPs) and also formation of mutagens and carcinogens due to the discovery of acrylamide in foods [4-5].

Acrylamide is produced from the Maillard reaction of the amino acid asparagine with reducing sugars and from carbonylic compounds derived from either the Maillard reaction or lipid oxidation during heating [6-9]. The asparagine pathway is the most predominant for the formation of acrylamide and model studies have demonstrated that the N-glycosyl of asparagine generates twenty times more acrylamide than the α-dicarbonyls and the Amadori compound of asparagine [6,10]. Furthermore, fructose and glucose are more effective than other carbonylic compounds in generating acrylamide [6] which follows a number of possible routes in the frame of Maillard reactions in food products.

Although it has been reported that the primary step in the reaction leads to the formation of the Schiff base [11] and subsequently to the Amadori compounds, the detection of these species under aqueous conditions remains difficult. In this study, we have used Solid Phase Extraction, Fourier transform infrared spectroscopy (FTIR) and accomplished the combination of a solid phase extraction technique with FTIR spectrometry by the use of an ATR germanium plate to enhance the detection of intermediate species of the reaction of asparagine with glucose at pH 8. The ultimate goal was to identify the vibrational marker bands primarily of the C=O group of the Amadori compounds in the FTIR spectrum. This involved the direct sampling of the methanolic SPE elution fractions in a germanium ATR plate. We have identified the structure sensitive FTIR marker bands at 1732 and 1740 cm^{-1} which have allowed us to characterize the structure of the primary Amadori compound in the reaction of Asn-Gluc at T=140 $^{\circ}$C. We report the conditions under which Maillard reaction products of a complex reaction mixture can be identified without the need to chemically synthesize these compounds.

4.3 Materials and methods

4.3.1 Sample preparation

L-Asparagine monohydrate (>99%) and glucose (>99.5%) were purchased from Sigma-Aldrich (St. Louis, MO, USA). Asparagine and glucose solutions (0.2M, pH 8.0) were

prepared in phosphate buffer (50 mM). Samples were heated in sealed tubes in a heating oven (Memmert, Germany) at a temperature of 140 °C for 2 hours. The sample heated for 2 hours was used for SPE-ATR-FTIR analysis.

4.3.2 Solid phase extraction

The reaction mixture was loaded onto a pre-conditioned Oasis HLB SPE cartridge and successively eluted with methanol. Each eluted SPE methanolic fraction was dried onto the surface of the germanium ATR crystal creating films for FTIR analysis.

4.3.3 ATR-FTIR spectroscopy

FTIR analysis was performed on a Bruker Tensor 27 FTIR spectrometer equipped with a deuterated triglycine sulfate (dTGS) detector. A horizontal ATR (HATR) accessory was accommodated in the spectrometer sample compartment hosting a germanium ATR plate (Pike Technologies, Inc, Madison, USA). A pair of transfer optics on the HATR directed the spectrometer infrared beam to one end of the germanium crystal. The ten internal reflections of the ATR cell enabled maximization of signal to noise ratio. A similar pair of optics directed the beam emitted from the other end of the germanium crystal to the spectrometer detector. OPUS 7.0/IR (Bruker) software package was used for spectral acquisition. Spectra were collected in the 900-1850 cm^{-1} range. The spectral resolution was 4 cm^{-1} with 100 co-added scans each.

4.4 Results and Discussion

When collecting absolute FTIR data of a reaction mixture, there is strong overlap of the vibrations of different intermediates with the reactants. The SPE method aims firstly to retain largely hydrophilic species yielding the highest recovery of these analytes and secondly provides a selective separation of these analytes from their reaction matrix. Due to the large excess in concentration of reactants compared to products, it is expected that when eluting the mixture from the SPE cartridges, the reactants will elute first. In the FTIR spectra, the spectral range between 1200 and 1800 cm^{-1} is shown where the major band of asparagine is the carbonyl group (C=O) of the side chain at 1672 cm^{-1}

[12]. The other major band largely corresponds to the deformation vibration of the NH_2 side chain group can be found at 1621 cm^{-1}, but there might be also coupling of $\nu_a(COO^-)$, $\delta(NH_2)$ and $\nu(C=O)$ vibrations for asparagine [13]. The main vibrational frequencies of asparagine, glucose and related reaction species are summarized in **Table I**.

In the side chain of Asn, the NH_2 group allows the formation of additional H-bonds affecting the frequencies of the NH_2 group. Intramolecular H-bonds such as NH_2…O=C, NH_2…(O)H, and OH…N result in altered conformations in the amino acid backbone structure [14]. The downshifting of the 1621 cm^{-1} asparagine absorption band to 1575 cm^{-1} as illustrated in the FTIR Spectra (**Figure 27**) may actually be a result of these conformational alterations of the asparagine amino groups.

It should be noted however, that in an amide group the side chain proton-acceptor capabilities are only located in the C=O group. Therefore, we assign the 1732 cm^{-1} mode we have observed in the ATR-FTIR spectra (**Figure 27**) to a carbonyl (C=O) group of the Amadori products which is distinct from that of asparagine. The appearance of an additional frequency mode at 1740 cm^{-1} may originate from either the Amadori or the decarboxylated Amadori product. The two species may be both present in the reaction mixture. It was previously discussed that the formation of the Amadori product in model systems features absorption bands near 1700 cm^{-1} [15]. Consequently, our findings are in agreement with previous observations identifying the appearance of newly formed absorption peaks at 1711 cm^{-1} and 1724 cm^{-1} relating to the νC=O of COOH in a dry, high temperature, model system [16].

Table I. Frequencies of vibrational modes of asparagine, glucose and their related reaction species.

Species	**Experim. FTIR (cm^{-1})**	**Assignment**	**Reference**
L-Asparagine monohydrate	1681	ν_s (C=O)	Wolpert and Hellwig, 2006
	1618	ν_{as} COO^-, δ_{as} NH_2, δ NH2, ν (C=O)	Boeckx and Maes, 2012
	1502	δ_s NH_3^+, ν COO^-	
	1421	ν C-NH2, δ CH2, ω CH2, ν CC	
	1404	δ CH, ν_s COO^-, ν CC, δ COO^-	
	1358	δ CH, ν CC, δ COO^-	
	1328	δ CH, ν COO^-, ν CC, δ COO^-	
	1314	ω CH_2, ν C-NH_2, ν COO^-	
Glucose	993, 1035, 1081, 1108	νCO νCO + νCC	Ibrahim et al., 2006
Schiff base	1388	δ(C-N=C)	Ioannou and Varotsis, 2016
	1569	ν(-C=NH-)	
	1660	ν(C=O..H)	
Amadori	1732	ν(C=O)	
	1740	ν(C=O)	

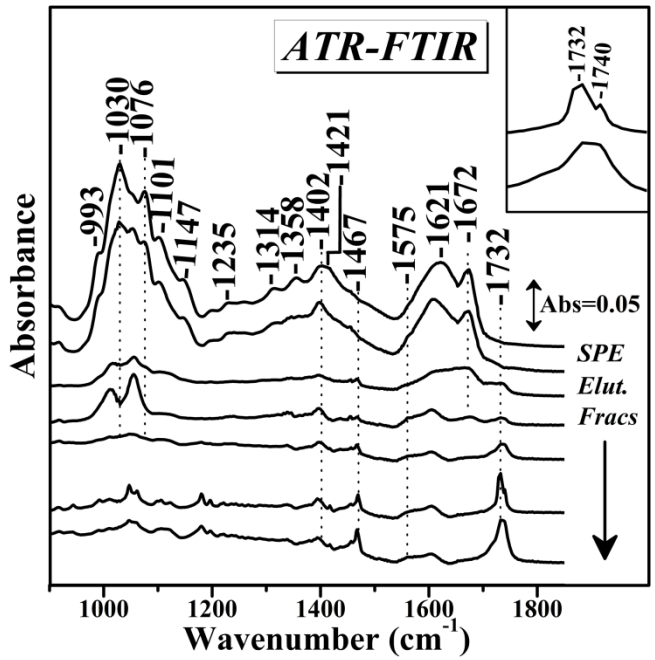

Figure 27. SPE elution fractions of the asparagine and glucose reaction mixture analyzed by ATR-FTIR.

4.5 References

[1] Hodge, J. E. (1953). Dehydrated foods, chemistry of browning reactions in model systems. *Journal of Agricultural and Food Chemistry*, **15**, pp. 928-943.

[2] Yaylayan, V. A. (1997). Classification of the Maillard reaction: A conceptual approach. *Trends in Food Science and Technology*, **8**(1), pp. 13-18.

[3] Robert, F., Vuataz, G., Pollien, P., Saucy, F., Alonso, M.I., Bauwens, I., Blank, I. (2005). Acrylamide formation from asparagine under low moisture Maillard reaction conditions. 2. Crystalline vs Amorphous Model Systems. *Journal of Agricultural and Food Chemistry*, **53**, pp. 4628-4632.

[4] Martins, S.I.F.S., Jongen, W.M.F., Van Boekel, M.A.J.S. (2000). A review of Maillard reaction in food and implications to kinetic modelling, *Trends in Food Science and Technology*, **11**, pp. 364-373.

[5] Tareke, E., Rydberg, P., Karlsson, P., Eriksson, S., Tornqvist, M. (2000). Acrylamide: A cooking carcinogen? *Chemical Research in Toxicology*, **13**, pp. 517-522.

[6] Stadler, R.H., Robert, F., Riediker, S., Varga, N., Davidek, T., Devaud, S.P., Goldmann, T., Hau, J.R., Blank, I. (2004). In-depth mechanistic study on the formation

of acrylamide and other vinylogous compounds by the Maillard reaction, *Journal of Agricultural and Food Chemistry,* **52**, pp. 5550-5558.

[7] Amrein, T.M., Andres, I., Manzardo, G.G.G., Amado, R. (2006). Investigations on the promoting effect of ammonium hydrogencarbonate on the formation of acrylamide in model systems, *Journal of Agricultural and Food Chemistry,* **54**(26), pp. 10253-10261.

[8] Hidalgo, F.J., Delgado, R.M., Zamora, R. (2009). Degradation of asparagine to acrylamide by carbonyl-amine reactions initiated by alkadienals. *Food Chemistry*, **116**, pp. 779-784.

[9] Hidalgo, F.J., Delgado, R.M., Navarro, J.L., Zamora, R. (2010). Asparagine decarboxylation by lipid oxidation products in model systems. *Journal of Agricultural and Food Chemistry*, **58**, pp. 10512-10517.

[10] Zyzak, D.V., Sanders, R.A., Stojanovic, M., Tallmadge, D.H., Eberhart, B.L., Ewald, D.K., Gruber, D.C., Morsch, T.R., Strothers, M.A., Rizzi, G.P., Villagran, M.D. (2003). Acrylamide formation mechanism in heated foods. *Journal of Agricultural and Food Chemistry*, **51**, pp. 4782-4787.

[11] Wnorowski, A., Yaylayan, V.A. (2003). Monitoring carbonyl-amine reaction between pyruvic acid and α-amino alcohols by FTIR spectroscopy - A possible route to Amadori products. *Journal of Agricultural and Food Chemistry,* **51**, pp. 6537-6543.

[12] Wolpert, M., Hellwig, P. (2006). Infrared spectra and molar absorption coefficients of the 20 alpha amino acids in aqueous solutions in the spectral range from 1800 to 500 cm^{-1}. *Spectrochimica Acta Part A: Molecular and Biomolecular Spectroscopy*, **64** pp. 987-1001.

[13] López Navarrete, J.T., Casado, J., Hernández, V., Ramírez, F.J. (1997). Experimental and theoretical vibrational studies of the amino acid l-asparagine in solution. *Journal of Raman Spectroscopy,* **28**, pp. 501-509.

[14] Boeckx, B., Maes, G. (2012). The conformational behavior and H-bond structure of asparagine: A theoretical and experimental matrix-isolation FT-IR study, *Biophysical Chemistry,* **165**, pp. 62-73.

[15] Wnorowski, A., Yaylayan, V.A. (2003). Monitoring Carbonyl-Amine Reaction between Pyruvic Acid and α-Amino Alcohols by FTIR Spectroscopy－A Possible Route To Amadori Products. *Journal of Agricultural and Food Chemistry,* **51**, pp. 6537–6543.

[16] Hwang, D.F., Hsieh, T.F., Lin, S.Y. (2013). One-Step Simultaneous Differential Scanning Calorimetry-FTIR Microspectroscopy to Quickly Detect Continuous Pathways in the Solid-State Glucose/Asparagine Maillard Reaction. *Journal of AOAC International*, **96**(6), pp. 1362-1364.

5 Detection of Maillard reaction products by a coupled HPLC Fraction collector technique and FTIR characterization of Cu(II)-complexation with the isolated species

5.1 Abstract

The isolation of reaction products of asparagine with reducing sugars at alkaline pH and high temperature has been probed by a combination of high performance liquid chromatography (HPLC) coupled with a Fraction Collector. The UV-vis and FTIR spectra of the isolated Maillard reaction products showed structure-sensitive changes as depicted by deamination events and formation of asparagine-saccharide conjugates. The initial reaction species of the Asn-Gluc reaction were also characterized by Density Functional Theory (DFT) methods. Evidence for Cu (II) metal ion complexation with the Maillard reaction products is supported by UV-vis and FTIR spectroscopy.

Keywords: Maillard reaction; Asparagine; HPLC; Fraction collector; UV-vis; ATR-FTIR.

5.2 Introduction

The Maillard reaction (MR) is one of the most important chemical reactions in foods occurring wherever non-enzymatic browning is induced by heat-treatment during food processing [1-3]. Most unprocessed foods contain the necessary starter reactants which are amino acids/proteins and reducing sugar. The Maillard reaction is a series of subsequent and parallel reactions and it typically consists of three major stages: the early, the advanced, and the final stage [1]. The early stage involves the condensation of a free amino group from free amino acids and/or proteins with a reducing sugar to form Amadori or Heyns rearrangement products via an N-substituted glycosylamine. The advanced stage is the degradation of the Amadori or Heyns rearrangement products via different alternative routes which involve four possible routes including deoxyosones,

fission or Strecker degradation. Complex series of reactions including dehydration, elimination, cyclization, fission and fragmentation result in a pool of flavour intermediates and flavour compounds [2]. The final stage is characterized by the formation of brown nitrogenous polymers and co-polymers. The color compounds can be grouped into two general classes: a) low molecular weight compounds which comprise between two and four linked rings of heterocyclic compounds, and b) the melanoidins, which have much higher molecular weights.

One important Maillard reaction intermediate is acrylamide, the formation of which follows a number of possible routes in concurrence with the Maillard reactions system in food products. The asparagine route is the major one for formation of acrylamide (**Figure 28**). Acrylamide has been shown to originate from the Maillard reaction of the amino acid asparagine with reducing sugars as well as carbonylic compounds deriving from either the Maillard reaction or lipid oxidation processes during heating [3-6]. Glycoconjugates, such as N-glycosides and related compounds formed in the early phase of the Maillard reaction have been proposed as key intermediates leading to acrylamide formation [7]. The first critical step is the amino-carbonyl reaction between asparagine and a carbonyl substance, preferably reducing sugars, resulting in N-glycosyl conjugation and forming the Schiff base as a key intermediate after dehydration under elevated temperatures. This hypothesis was supported by two groups that provided evidence of the importance of Schiff base of asparagine which is formed after a dehydration step [3, 8]. The Schiff base is formed early in the Maillard reaction as the result of elimination of water from the conjugate of glucose and asparagine [3, 5]. The key mechanistic step seems to be the decarboxylation of the Schiff base leading to intermediates that can directly release acrylamide. However, some researchers have discussed the fact that at high temperature conditions, formation of the Schiff base is accordingly rate determining, while at lower temperatures, decarboxylation becomes rate determining [9]. Imines or Schiff bases formed through the interaction of reducing sugars with amino acids are known to play a critical role not only in initiating the Maillard reaction but also in its propagation through isomerization reactions. Imines formed subsequent to carbonyl–amine reactions between amino acids and reducing sugars tend to undergo various chemical transformations depending on the nature of the

carbonyl moiety such as Amadori rearrangement, the Strecker reaction, or cyclizations to generate N-containing heterocyclic compounds.

Separation and qualitative determination of individual Maillard species have been achieved using various chromatographic techniques including GC-MS [10] and High-Performance Anion Exchange Chromatography (HPAEC) [11]. The main advantage of HPLC over GC in the MR analysis context is that non-volatile water-soluble compounds can be analyzed directly without the need for prior derivatization. An important aspect of opting for a highly aqueous mobile phase is the ability to study Maillard reactions in their native aqueous environment without incorporating organic solvents to the reaction mixtures. This is in agreement with a recent HPLC analytical procedure for real-time detection and characterization of intermediate species in the Maillard reaction network many of which are highly polar.

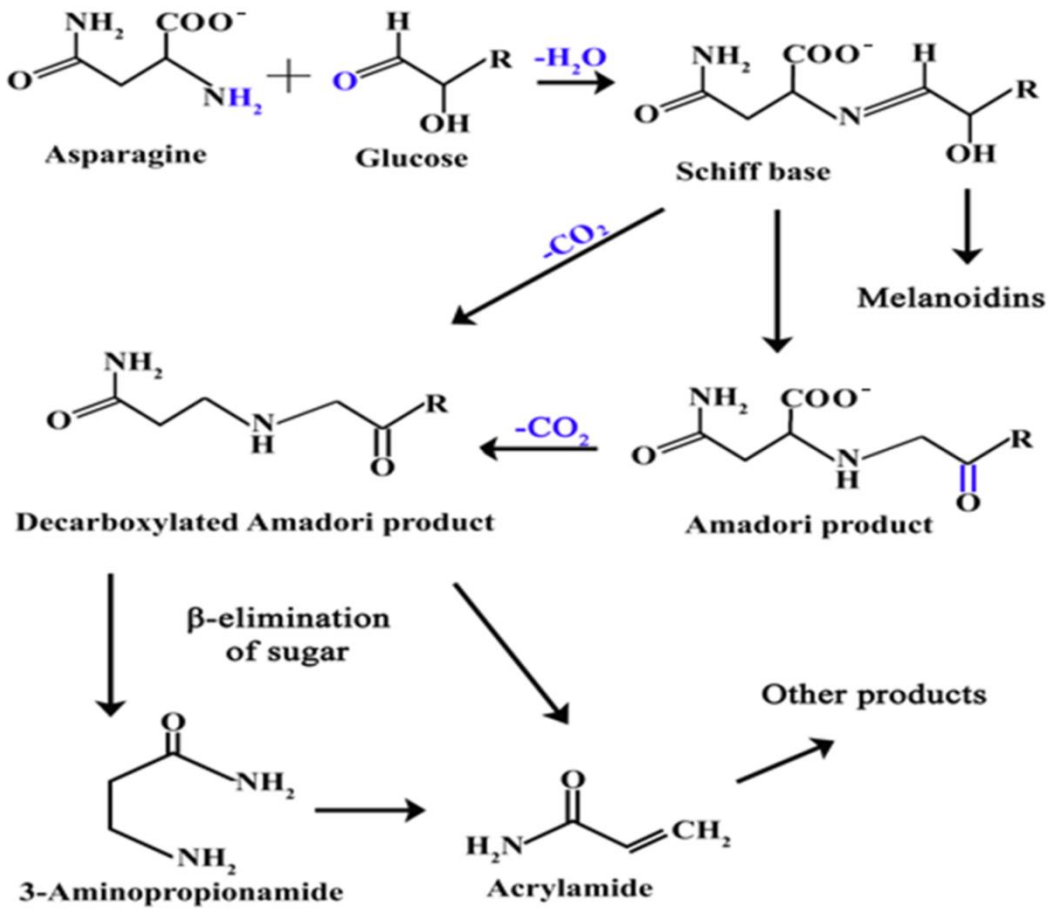

Figure 28. Overview of the Maillard reaction product (MRP) chemical reaction network starting from asparagine and glucose.

This facilitates chromatographic separation and detection using highly aqueous mobile phases and stationary phases suitable for small polar molecules such as being the asparagine glycoconjugates that are examined in this study. A procedure was described previously in the literature consisting of a multidetector HPLC system for the analysis of Amadori and other fluorescent products employing a fraction collector to their system [12]. The authors argued that many of the important intermediates that form during Maillard reactions are fluorescent species so they have opted for a fluorescent and an electrochemical detector in their online system. Although a multitude of products are being formed in Maillard reaction there is no up to date a combined analytical system to simultaneously resolve and characterize the products being formed in these complex mixtures.

Oxidative degradation reactions of amino acids are of particular significance factors in the overall Maillard reaction, and metal ions can function as redox catalysts. Metal ions, such Cu(II) and Fe(III) can be involved in oxidative pathways in both *in vivo* and *in vitro* Maillard reaction and there is a significant loss of antioxidant activity by MRP/copper complexes [13]. Furthermore, glycated amino acids, peptides and proteins possess metal-binding properties different from those of their non-glycated analogous. Although Cu(II) can be involved in the oxidative pathways, little is known about the Cu(II) complexes.

In this study, a new analytical setup allowing the concurrent identification of precursors and products of the Maillard reaction is described. It is based on high-performance liquid chromatography (HPLC) with UV-vis detector and a fraction collector coupled in series (**Figure 29**). During the early stages of the Maillard reaction, the products formed are polar water-soluble compounds mainly consisting of reducing sugars and Amadori products and amino acids. High-performance liquid chromatography (HPLC) on its own has limited ability to adequately resolve and give structure sensitive information when analyzing Maillard reaction compounds. A fraction collector was interfaced to the system and connected to the effluent, exiting the UV-vis detector to collect fractions for further analysis. The collected fractions and their Cu (II) metal ion complexations were then analyzed by the UV-vis and ATR-FTIR techniques. The ultimate goal was to identify the vibrational marker bands of the C_{Asn}-N=C_{Gluc} moiety of the Schiff base in the FTIR spectrum and that of the Amadori products, and thus, in conjunction with

Density functional theory (DFT) calculations, to establish vibrational marker bands for monitoring the formation of MR products.

5.3 Materials and methods

5.3.1 Sample preparation

Equimolar solutions of glucose and asparagine (0.2 M) were prepared in phosphate buffer (50 mM) and the pH was adjusted to 8.0. Samples (10 ml) were heated in closed screw-capped tubes at 180 °C in a heating oven (Memmert, Germany) for 2 hours. For HPLC analysis, the samples were diluted hundred-fold. Isolated HPLC fractions from the reacted asparagine and sugars mixtures with added copper (II) chloride in excess (approx. 1 mM $CuCl_2$) were prepared for FTIR analysis. For FTIR spectroscopy, the individual fractions were dried onto the surface of the germanium crystal creating films. The dried films were placed on the FTIR sample compartment for the FTIR measurements.

5.3.2 HPLC

The HPLC experimental setup (**Figure 29**) consisted of a Varian 218 Prepstar Solvent Delivery Module, an Agilent Manual FL-Injection Valve, an Agilent 1260 Infinity Variable Wavelength Detector (VWD) and an Agilent 440 LC Fraction Collector. HPLC analysis was performed on a 4.6 x 250 mm, 5 µm particle size, Zorbax SB-Aq analytical column (Agilent Technologies, California, USA). Water at a flow rate of 0.5 ml/min was used isocratically as the mobile phase at room temperature. Maillard reaction products (MPRs) were detected at 200 nm.

5.3.3 Fraction Collector

An Agilent Technologies 440 Fraction Collector which is a single probe, automated sample collector, was coupled to the chromatographic system (**Figure 29**). The fraction collector uses the Agilent OpenLAB Software real-time peak detection algorithms to achieve accurate and reproducible chromatographic detection of fractions eluting from the analytical column. It has the capacity of collecting the individual resolved elements of a multi-component sample. A time-slice method was employed to collect discrete fractions. During the chromatographic run the fraction collector allows for collection at defined time intervals. Fractions were collected in time slices thus creating a time frame

window for each chromatographic peak. This is achieved by means of a diverter valve which is switched from the waste to the collect position. The time frames for each eluting peak and the system delay time were incorporated to a time program table generated by the Agilent OpenLAB Software. Mobile phase during equilibration between chromatographic runs was sent to the waste position since the valve was switched back to this position after the finish of each run. Pooling of identical fractions between runs was also performed to enhance FTIR detection.

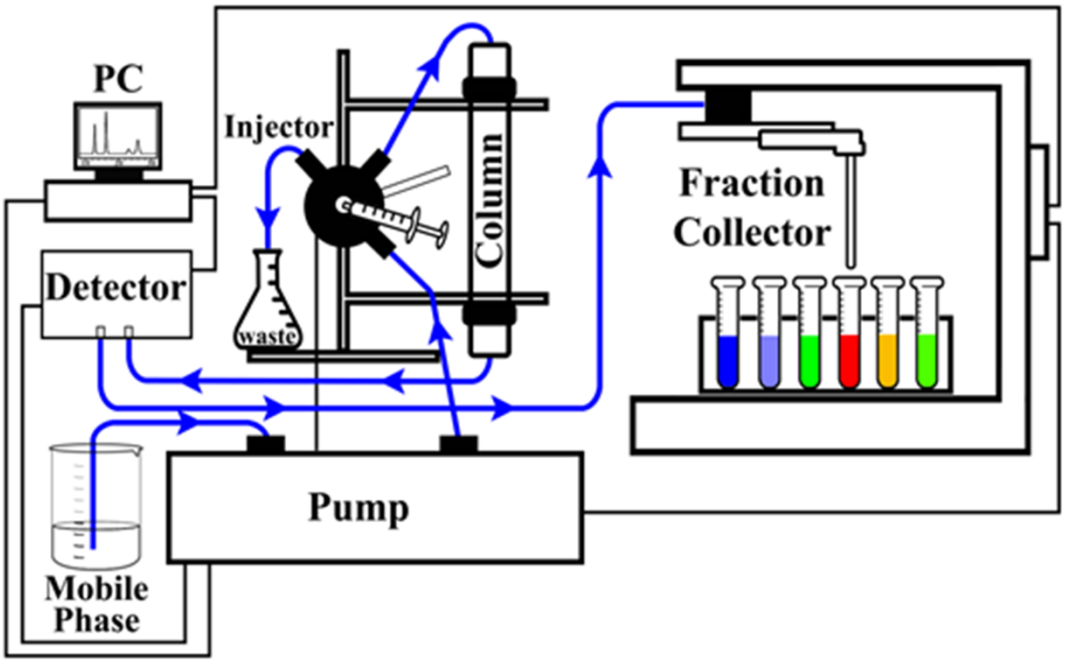

Figure 29. Experimental layout of the customized High Performance Liquid Chromatography (HPLC) apparatus combined with a fraction collector. The different colors illustrated on the sample tube rack of the fraction collector represent different species collected as individual fractions.

5.3.4 UV-vis spectrophotometry

Fractions of individual Maillard reaction products (MRPs) were assessed by recording UV-visible spectra against the buffer using a UV–Visible Lambda 25 (Perkin Elmer, Beaconsfield, United Kingdom) spectrophotometer.

5.3.5 Attenuated Total Reflection-Fourier Transform Infrared (ATR-FTIR) spectrophotometry

A horizontal ATR (HATR) accessory (Pike Technologies, Inc, Madison, USA) was employed fitting a germanium ATR plate with ten internal reflections. The Horizontal ATR is designed with a pair of transfer optics to direct the infrared beam of the spectrometer to one end of the IR transmitting ATR crystal. Another pair of optics directs the beam emitted from the other end of the ATR crystal to the spectrometer detector. A Tensor 27 FTIR spectrometer (Bruker, Karlsruhe, Germany) equipped with a deuterated triglycine sulfate (DTGS) detector was used for spectral acquisition. Spectra were collected in the range 1,800–800 cm^{-1} with 4 cm^{-1} spectral resolution and 100 co-added scans each. A background spectrum was collected before each sample measurement.

5.3.6 Density Functional Theory Geometry (DFT)

Optimization and subsequent vibrational frequency analysis was performed by Density Functional Theory at the B3LYP/6-311g**++ level for all compounds, employing the Schrödinger Jaguar Software [14]. The results are shown in **Table II**.

5.4 Results and Discussion

5.4.1 Isolation of MRPs by HPLC-Fraction collector

Glycoconjugates, such as N-glycosides and related compounds formed in the early phase of the Maillard reaction have been proposed as key intermediates leading to acrylamide formation [7]. When asparagine and glucose (**Figure 30**, **left panel**) or fructose (**Figure 30, right panel**) react at high temperatures it is evident mainly from the HPLC chromatograms that there is a mixture of reactants and multiple products in the reaction vessel (**Figure 30**). Maillard reaction products (MRPs) were monitored on the Zorbax column which is highly selective for polar molecules in aqueous phases [15]. Fraction 1 is a combined fraction encompassing a major signal at Rt=5.7 mins which corresponds to the excess unreacted asparagine as well as three other smaller signals arising from the heated reaction mixture. Fractions 2-5 corresponding to discrete MRPs were collected separately.

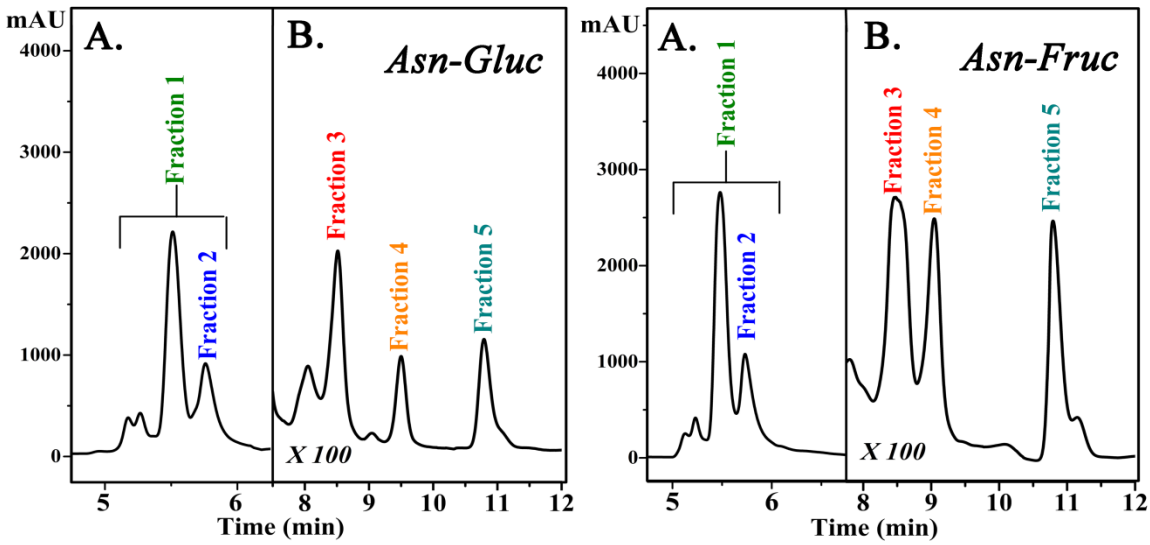

Figure 30. High performance liquid chromatography (HPLC) chromatogram of the reaction mixtures of asparagine and sugars (pH 8.0, 180 °C). **A.** Combined fraction comprising of excess reactants and products. **B.** Fractions collected comprising of discrete MRPs. **Left:** Reaction of asparagine with glucose. **Right**: Reaction of asparagine with fructose.

5.4.2 Detection of MRPs and MRP-complexes by spectroscopic methods

5.4.2.1 UV-vis spectroscopy of Maillard reaction products (MRPs)

The UV-vis spectra of the collected fractions show discrete absorption spectra. Absorption maxima at 234, 277, 294, and 307 nm were observed in the different fractions in the asparagine-fructose model system (**Figure 31**). MRPs from fructose - amino acid models were reported to have similar UV–Vis spectra with MRPs from glucose-amino acid models [16]. Changes in absorbance at 294 nm were detected as a measurement of intermediate products of the Maillard reaction [15-17]. It reflects the amount of uncolored intermediate products (UIPs) and these compounds relate to the glycosylation process as being aldehydes and small molecule ketones [17-19]. The advance stage soluble pre-melanoidins are detected in the range 320-350 nm while high molecular weight melanoidins are detected in the range 420-450 nm. This is clearly not the case here, since we lack the melanoidin spectral fingerprint. The strategy of many researchers was to use this generic assignment at 294 nm to measure overall increase in

these products thought to be precursors to browning pigments. Absorbance in the range of 270-300 nm is characteristic for molecules containing carbonyl groups. The 277 nm assignment may correspond to a (n->π*) transition. A similar absorption was observed close to 265 nm in UV-vis spectra of heated asparagine and sugars except that the heating temperature was lower [16]. These absorbances tend to be weaker relative to (π->π*) transitions located in the low UV region. Simple unconjugated chromophores such as C=O and C=N typically show (n->π*) transitions at approximately 300 nm. Conjugation in aliphatic ketones lowers the energy of the (n->π*) transition close to 280 nm but this has low intensity as its symmetry is forbidden. The 234 nm absorption seems to be linked with the 307 nm absorption center, and it may be related to the corresponding bathochromic π->π* transition. It is generally accepted that fructose has a higher reactivity than glucose and this is also in agreement with the UV-vis profile in the asparagine-glucose compared to the asparagine-fructose model system where more subtle changes appear in the absorption maxima (**Figure 31**). This may relate to the higher proportion of open-chain form for fructose compared to glucose and the properties and nature of the reaction products themselves [20].

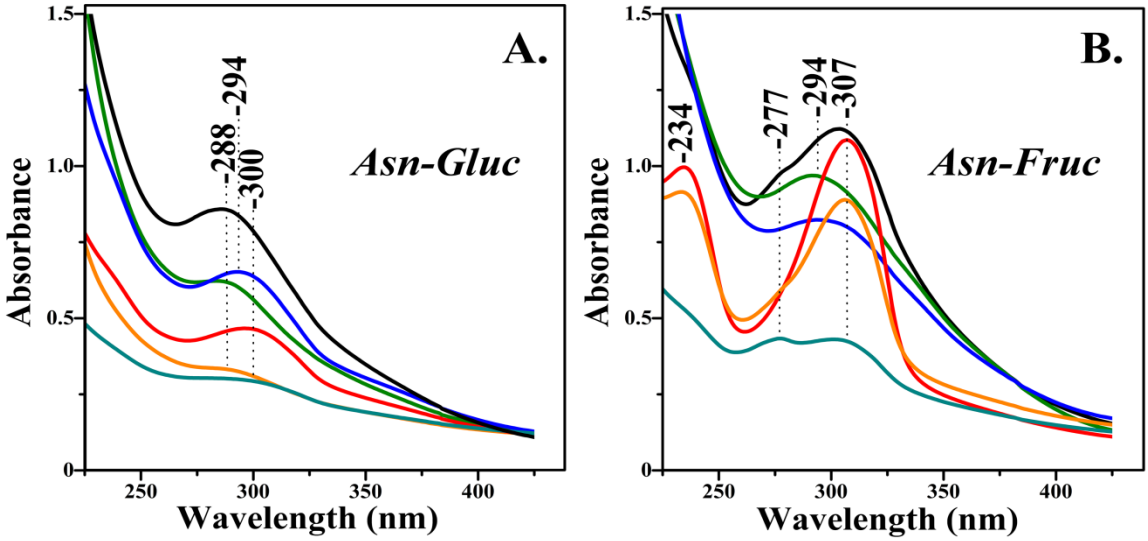

Figure 31. UV-vis spectra of the reaction mixtures and individual LC fractions of asparagine and sugars (pH 8.0) at 180 °C. **A.** Reaction with glucose. **B.** Reaction with fructose. (Black: Reaction mixture, Green: LC Fraction 1, Blue: LC Fraction 2, Red: LC Fraction 3, Orange: LC Fraction 4, Cyan: LC Fraction 5).

5.4.2.2 UV-vis spectroscopy of Copper(II)-MRP complexes

The UV-vis spectra of the individual fractions 2 and 3 (**Figure 32A-B**), show that when excess of Cu^{2+} were added the broad absorption band at 294 nm was shifted to 260 nm. This indicates that Cu(II)-MRP complexation is initiated upon immediate addition of the metal solution. The electronic rearrangement resulting from metal binding to MRPs from various model systems was previously observed spectrophotometrically by monitoring mainly hypsochromic shifts of absorption bands [13, 21-22]. In **Figure 32A-B** there is also a hypochromic effect which is in accordance with a previously reported disappearance of a 284 nm absorption band in a Glucose–Lysine model system [21]. For fractions 4 and 5 there is only a decrease in the absorption bands upon addition of Cu(II) (**Figure 32C-D**). This may be attributed to ligand to metal charge transfer, involving lone pairs in oxygen or nitrogen atoms of amino/carboxylate groups.

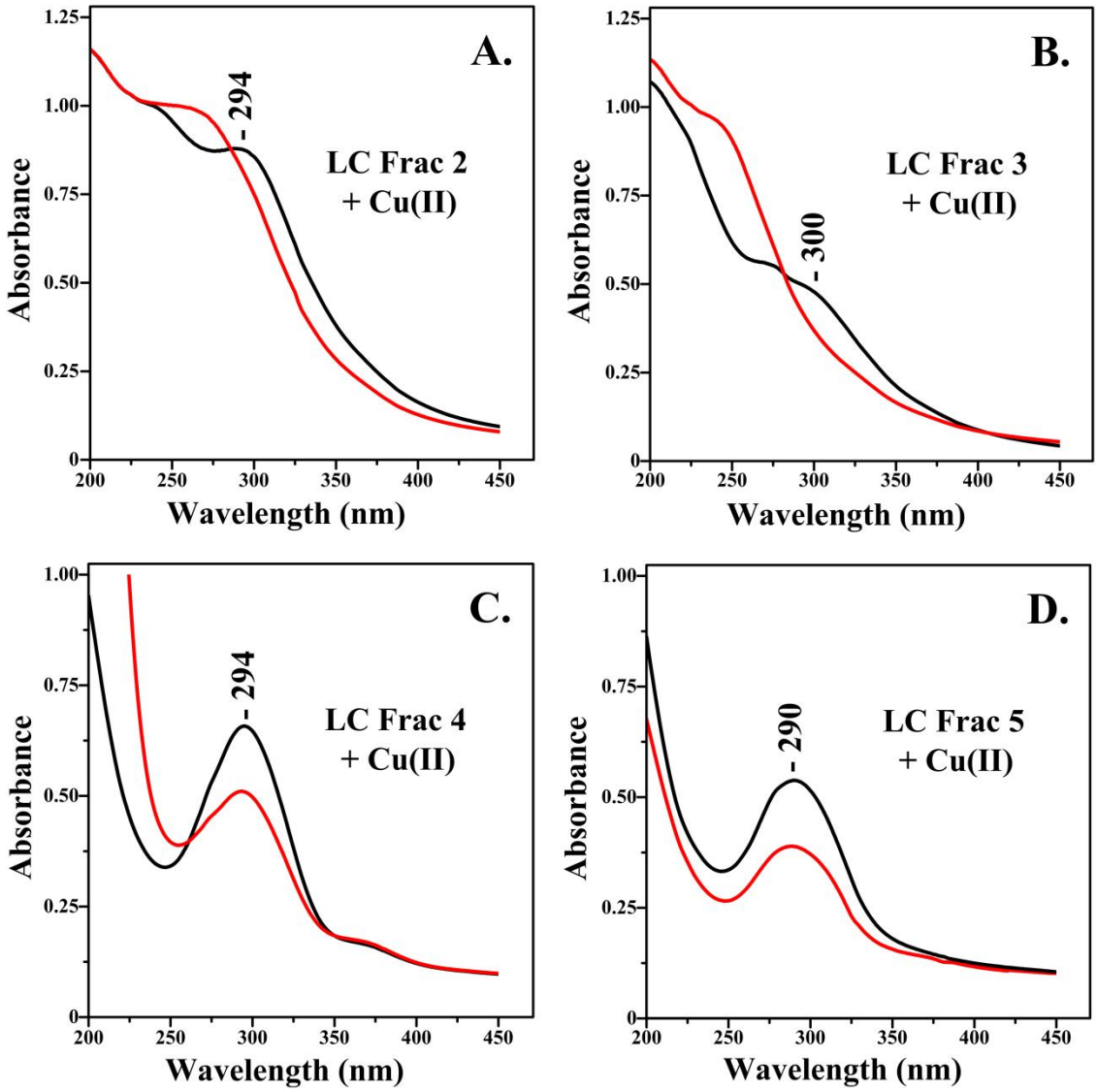

Figure 32. UV-vis spectra of collected fractions with (red) and without (black) Cu (II) ions from the reaction mixture of asparagine and glucose (pH 8.0) at 180 °C. **A.** LC Fraction 2. **B.** LC Fraction 3. **C.** LC Fraction 4. **D.** LC Fraction 5.

5.4.3 ATR-FTIR spectroscopy of MRPs

The first major band in the case of asparagine is the carbonyl group which is present as a strong band observed due to the C=O stretching vibration at around 1681 cm^{-1}. This has been attributed to the carbonyl of the side chain of asparagine [23]. This band is not involved in the initial conjugation between asparagine and glucose since the backbone amino group is involved in this first step. It is well established that extensive coupling

occurs among the $\nu_a(COO^-)$, $\delta(NH_2)$ and $\nu(C=O)$ vibrations for asparagine in the region between 1700 and 1620 cm^{-1} and also for $\delta(OH)$ and $\nu_s(CO_2)$ between 1390 and 1310 cm^{-1} [24]. The L-asparagine monohydrate molecule possesses two NH_2 groups (side chain and backbone). The second major band largely corresponds to the deformation (scissoring) vibration of the NH_2 side chain group can be found at around 1618 cm^{-1} but there might be also contribution from the backbone amino group [23, 25]. Some authors have predicted the backbone NH_2 scissoring mode at 1598, 1595 cm^{-1} by a DFT method [26] which is in good correlation with the observed 1621 cm^{-1} in our FTIR experimental data. Additionally, $\delta(NH_2)$ modes were observed at 1593 and 1575 cm^{-1} in another recent study concerning the conformational behavior of asparagine [25]. Looking at the FTIR spectra of the collected HPLC fractions, we notice several features when asparagine and monosaccharides are heated at T=180 °C. The first observed feature is that the 1621 cm^{-1} absorption center is downshifted with respect to the other major band of 1672 cm^{-1} corresponding to the side chain C=O stretching vibration. Thus, the spectra in **Figure 6** reveal intensity changes in the region of the C=O band of Asn at 1672 cm^{-1} as well as frequency changes due to broadening in the region of the Asn $\nu(NH_2)$ at 1621 cm^{-1}. The first critical step in the amino-carbonyl reaction between asparagine and a carbonyl substance results in the relative N-glycosyl conjugation which is thought to occur in the backbone NH_2 group of asparagine. The feature from the FTIR spectra related to this event is the downshifting of the 1621 cm^{-1} absorption center to approximately 1605 cm^{-1} in fractions 3-5. This might correspond to different hydrogen-bonded asparagine backbone NH_2 modes as a result of conformational changes that set apart different species in the reaction mixture.

Nevertheless, a limitation when examining absolute FTIR data is that due to overlapping vibrations with unreacted species, the newly formed species the $\nu(C=O)$ and $\nu(NH_2)$ are expected to retain very similar frequencies with those of the unreacted, so it is not possible to assign the vibrations of the new species with certainty. When separating species with a fraction collector these changes in the infrared frequencies are somewhat more evident. Looking at the carboxylate vibrations of the L-asparagine monohydrate molecule, it is suggested that the O–H in-plane and out of bending vibrations fall between 1440–1395 cm^{-1} and 970–875 cm^{-1} [26]. Moreover, the $\delta(OH)$ modes involved in an intramolecular OH…N backbone hydrogen-bond in two separate

asparagine conformers were predicted at 1393 and 1390 cm^{-1} [24]. We observe that the 1402 cm^{-1} asparagine band is downshifted in fractions 3-5 towards the reported 1393 cm^{-1} band corresponding to a distinct hydrogen-bonded asparagine conformer with contributions of δOH and νC-O. The absorption band at 1421 cm^{-1} is coupled with the 1402 cm^{-1} asparagine band and is considered to have mixed contributions from several asparagine backbone modes, namely C–C stretching, O–H–O bending and H–O–C bending vibrations [26]. We observe that the 1421 cm^{-1} band disappears specifically in fractions 4-5 (**Figure 33**). This observation indicates the formation of new asparagine conjugate species.

Further evidence is provided by the fact that there is lack of the lower wavenumber bands of glucose at 993, 1030, 1076, 1147 cm^{-1} and fructose at 867, 920, 978, 1058, 1147 cm^{-1} in fraction 5 (**Figure 33**). The lack of sugar FTIR absorption bands observed in fraction 5 which may suggest cleavage of the sugar moiety from the conjugate species in order to form a smaller species like acrylamide. Only the small 915 cm^{-1} asparagine monohydrate backbone vibration remains, which is mainly torsion H-O-C-O backbone vibration. This is not likely to be involved in the initial conjugation between asparagine and sugar. Appearance of the small band at 1339 cm^{-1} band in fractions 3-5 (**Figure 33**) is likely to correspond to δCCH and δOCH of the sugars [27]. Moreover, there is concomitant disappearance of the 1358 cm^{-1} and 1314 cm^{-1} asparagine bands which are more likely to correspond to the backbone bending H-N-C and H-C-N vibrations and torsion C-C-N-H, respectively [26]. Another feature that is clearly evident is the loss of the 1502 cm^{-1} band [23] in all the fractions except the first combined fraction (**Figure 33A**). This occurs only in the reaction of asparagine and glucose (**Figure 33A**) but not in the reaction of asparagine and fructose (**Figure 33B**) due to the fact that the latter reaction is faster. This mode relates to the backbone amino and/or carboxylate group of asparagine. In Fraction 1 there is excess asparagine a fact that justifies the appearance of this band in the first combined fraction. This further supports the hypothesis that there is loss of the backbone amino group and successive decarboxylation event occurring in the overall reaction mechanism.

Based on the FTIR data of the collected fractions 1 and 2 we expect the spectra to have contributions from the formation of the Schiff base and/or from the Amadori and decarboxylated Amadori products (**Figure 28**) with distinct asymmetric vibration C_{Asn}-

N-C_{Gluc} in the 1350-1450 cm^{-1} region, as predicted by the DFT calculations (**Table I**). For the Schiff base, the carbonyl (C=O) and NH_2 groups are likely to have similar frequencies with those of the unreacted Asn, assuming that there is no H-bonding interactions with the (C=O) and NH_2 groups.

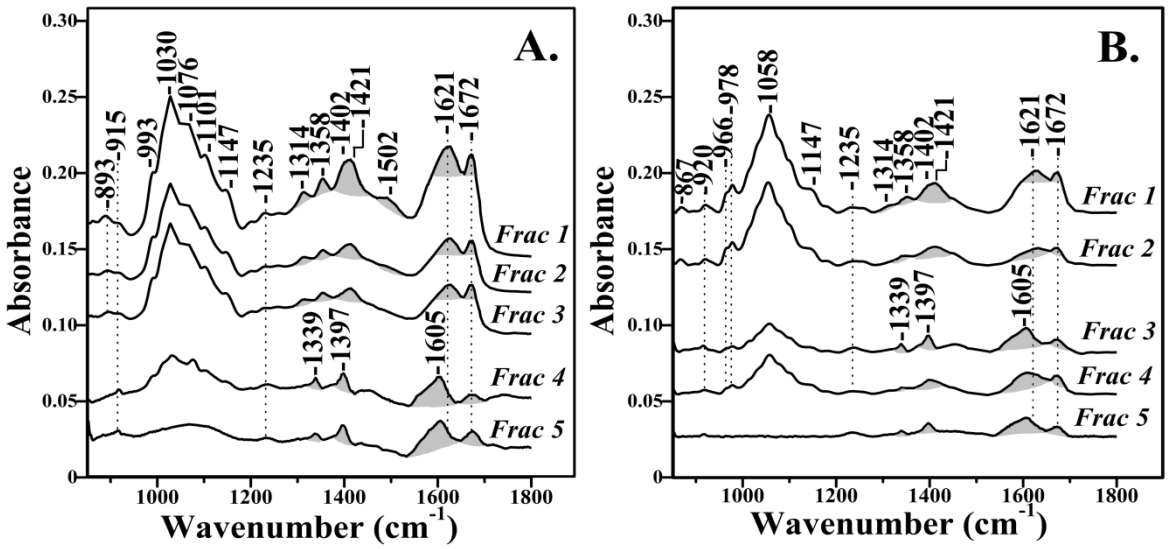

Figure 33. Attenuated Total Reflection-Fourier Transform Infrared (ATR-FTIR) spectra of collected fractions from the reaction mixture of asparagine and sugars (pH 8.0) at 180 °C. **A.** Reaction with glucose. **B.** Reaction with fructose.

Imines under Maillard reactions have been characterized, and as the first step in the carbonyl-amine interaction have been proposed to play a crucial role in the formation of the Schiff base and degradation of the Amadori products towards the formation of the 3-Aminopropionamide and Acrylamide (**Figure 28**). The presence of feature between 1358-1421 cm^{-1} in the FTIR spectrum strongly resembles those of the $\nu(C_{Asn}\text{-}N\text{=}C_{Cluc})$ of the imine (Schiff base) species we have calculated by DFT. In the side chain of Asn, the NH_2 group allows the formation of additional H-bonds affecting the frequencies of the NH_2 group. It should be noted however, that in an amide group the side chain proton-acceptor capabilities are only located in the C=O group. The presence of a feature at 1502 cm^{-1} strongly resembles the $\nu(C_{Asn}\text{-}N\text{-}C_{Gluc})$ either of the Amadori or the decarboxylated Amadori species, as predicted by DFT.

Table II. Theoretical Vibrational Frequency analysis for the compounds at the B3LYP/6-311g**++ level of theory (the calculated frequencies were in resonance with other modes).

Substance	$\nu(C_{Asn}\text{-}\mathbf{N_{Asn}}\text{-}\mathbf{C_{Gluc}})$ cm^{-1}	$\nu(\mathbf{C_{Asn}}\text{-}\mathbf{N_{Asn}}\text{-}C_{Gluc})$	$\delta(\mathbf{C_{Asn}}\text{-}\mathbf{N_{Asn}}\text{-}\mathbf{C_{Gluc}})$
Schiff base	**1377***	**1377***	**1440**
Amadori	**1506***	**1506***	**1113,1380**
Decarboxylated Amadori	**1504***	**1504***	**1112,1386**
*** asymmetric**			
Substance	ν(N-**CO**-**C**)	ν(**N-CO**-C)	ν(**C=O**) cm^{-1}
3-Aminopropionate	**1368***	**1368***	**1755**

***asymmetric N-CO-C**

5.4.4 ATR-FTIR spectroscopy of Copper(II)-MRP complexes

Copper (II) ion is a biologically active essential ion, creating ability and positive redox potential that allows participation in biological transport reactions. Copper (II) ion is an essential component of several enzymes and can be involved in the reactions producing active radicals, which affect the structure of all types of biomolecules. Simple sugars and their derivatives can form metal ion complexes of variable composition and stability [28]. Of particular interest is the fact that metal complexes with oligo- and poly-saccharides and their derivatives are of growing importance in medicine and pharmacy. Nevertheless, to date no detailed structural information about the exact binding and conformational changes of the formed complexes with individual MRPs are available. The correlation of spectral and structural information of the metal complexes can be performed by using modern spectroscopic techniques like ATR-FTIR. We have performed the separation experiment with the fraction collector and added an excess amount of Cu (II) ions to each fraction. The first key observation from the FTIR spectra is the downshift of the 1672 cm^{-1} asparagine band to 1658 cm^{-1} (**Figure 34**) which can

be explained by the notion that there is coordination of the carbonyl group with the metal copper ion. Free amino acids can also form stable chelating complexes with metal ions giving a coordination function. It was recently demonstrated that $CuCl_2$ can form stable complexes with alanine and the resulting complex can undergo thermal decomposition [29]. In our study, this is confirmed by the fact that Fraction 1 containing excess asparagine also exhibits this coordination function with the Cu metal as the IR shift suggests. A previous study relating metal complexation by the peptide-bound Maillard reaction products discussed the hypothesis that the coordinated Cu(II) is assumed to bind to the N-donor atom of the amino group and in the case of the synthesized lysine derivative with one O-atom of the neighboring carboxylate group whilst in the case of the sugar derivative the authors presume that an O-donor of the sugar ring is involved [30]. However, this was not confirmed by a structure-sensitive spectroscopic method. Previous studies concerning synthesis and characterization of Schiff bases with Cu(II) complexes have proposed that the resulting complexes were found to have tetragonal geometry involving two ligand molecules [31, 32]. Our results indicate that there is metal coordination with the asparagine carboxylate moiety but there is evidence that the amino group is involved, as the large bending NH_2 vibration of free asparagine around 1615 cm^{-1} is significantly altered in Fraction 1 as it is downshifted to 1608 cm^{-1}. In the case of the glycoconjugate fractions there is progressive loss in the intensity of the 1658 cm^{-1} band. A second feature from the FTIR spectra is the absence of the sugar bands in fractions 4 and 5 (**Figure 34**). Moreover, the small band at 1339 cm^{-1} band which is more likely to correspond to the δOCH of the sugars in fractions 4-5 also disappears (**Figure 34**). These events may be explained by the hypothesis that the O-donor on the sugar and the carboxylate O-donor are progressively lost and the initially formed Cu complex with these fractions is becoming less stable. The loss of the sugar band intensity may indicate that a degradation reaction is occurring due to the presence of the metal ions. It was previously discussed that chelation of metal ions by amino and carboxyl groups in amino acids or hydroxyl groups in saccharides can delay the progress of the Maillard reaction in mixtures with excess concentrations of metal ions [33]. Thus, the inhibiting effect of higher concentrations of Cu^{2+} with respect to MRPs can be justified in this manner.

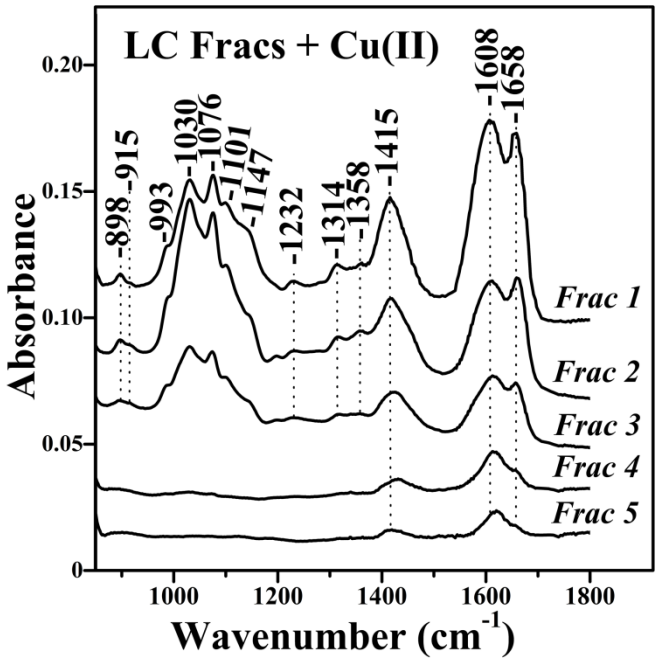

Figure 34. Attenuated Total Reflection-Fourier Transform Infrared (ATR-FTIR) spectra of collected fractions with added Cu (II) ions from the reaction mixture of asparagine and glucose (pH 8.0) at 180 °C.

5.5 Conclusions

In this study, we have demonstrated the application of high performance liquid chromatography (HPLC) for separation and of UV-vis spectrometry and ATR germanium plate for FTIR detection. We have accomplished the coupling of HPLC with a fraction collector to isolate both reactants and products of the reaction of asparagine with fructose and glucose at pH 8 at high temperature. The FTIR experimental evidence revealed structure-related changes as related with a deamination event and subsequent formation of asparagine glycoconjugates. Furthermore, we have devised a new analytical procedure which provides spectroscopic evidence of Cu (II) metal ion complexation with Maillard reaction products from the reaction products of asparagine and monosaccharides.

5.6 References

[1] Hodge, J. E. (1953). Dehydrated foods, chemistry of browning reactions in model systems. *Journal of Agricultural and Food Chemistry*, **1**, pp. 928-943.

[2] Yaylayan, V. A. (1997). Classification of the Maillard reaction: A conceptual approach *Trends Food Science and Technology*, **8**, pp. 13-18.

[3] Zyzak, D. V., Sanders, R. A., Stojanovic, M., Tallmadge, D. H. Eberhart, B. L. Ewald, D. K., Gruber, D.C., Morsch, T. R., Strothers, M. A., Rizzi, G. P., Villagran, M. D. (2003). Acrylamide formation mechanism in heated foods. *Journal of Agricultural and Food Chemistry*, **51**, pp. 4782-4787.

[4] Amrein, T. M., Andres, I., Manzardo, G. G. G., Amado, R. (**2006**). Investigations on the promoting effect of ammonium hydrogencarbonate on the formation of acrylamide in model systems. *Journal of Agricultural and Food Chemistry*, **54**, pp. 10253-10261.

[5] Stadler, R. H., Robert, F., Riediker, S., Varga, N., Davidek, T., Devaud, S. P., Goldmann, T., Hau, J.R., Blank, I. (2004). In-depth mechanistic study on the formation of acrylamide and other vinylogous compounds by the Maillard reaction. *Journal of Agricultural and Food Chemistry*, **52**, pp. 5550-5558.

[6] Hidalgo, F. J., Delgado, R. M., Navarro, J. L., Zamora, R. (2010). Asparagine decarboxylation by lipid oxidation products in model systems. *Journal of Agricultural and Food Chemistry*, **58**, pp. 10512-10517.

[7] Stadler, R. H., Blank, I., Varga, N., Robert, F., Hau, J., Guy, P. A., Robert, M.C., Riediker, S. (2002). Food chemistry: Acrylamide from Maillard reaction products. *Nature*, **419,** pp. 449-450.

[8] Yaylayan, V. A., Wnorowski, A., Perez-Locas, C. (2003). Why Asparagine Needs Carbohydrates To Generate Acrylamide. *Journal of Agricultural and Food Chemistry*, **51,** pp. 1753-1757.

[9] Hedegaard, R. V., Frandsen, H., Skibsted, L. H. (2008). Kinetics of formation of acrylamide and Schiff base intermediates from asparagine and glucose. *Food Chemistry*, **108,** pp. 917-925.

[10] Koutsidis, G., De La Fuente, A., Dimitriou, C., Kakoulli, A., Wedzicha, B.L., Mottram, D.S. (2008). Acrylamide and pyrazine formation in model systems containing asparagine. *Journal of Agricultural and Food Chemistry*, **56**, pp. 6105-12.

[11] Davidek, T., Clety, N., Devaud, S. P., Robert, F., Blank, I. (2003). Simultaneous quantitative analysis of Maillard reaction precursors and products by high-performance anion exchange chromatography. *Journal of Agricultural and Food Chemistry*, **51**, pp. 7259-7265.

[12] Huyghues-Despointes, A., Yaylayan, V.A. (1994). A multidetector HPLC system for the analysis of Amadori and other Maillard reaction intermediates. *Food Chemistry*, **51**, pp. 109-117.

[13] Bersuder, P., Hole, M., Smith, G. (2001). Antioxidants from a heated histidine-glucose model system. Investigation of the copper(II) binding ability. *Journal of the American Oil Chemists' Society*, **78**, pp. 1079-1082.

[14] ö Bochevarov A. D., Harder, E., Hughes, T. F., Greenwood, J. R., Braden, D. A., Philipp, D. M., Rinaldo, D., Halls, M. D., Zhang, J., Friesner, R. A. (2013). Jaguar: A high-performance quantum chemistry software program with strengths in life and materials sciences, *International Journal of Quantum Chemistry*, **113**, pp. 2110-2142.

[15] Ioannou, A., Varotsis, C. (2016). Real Time Monitoring the Maillard Reaction Intermediates by HPLC- FTIR. *Journal of Physical Chemistry and Biophysics***, 6**, p. 210.

[16] Yu, X., Zhao, M., Hu, J., Zeng, S., Bai, X. (2012). Correspondence analysis of antioxidant activity and UV-Vis absorbance of Maillard reaction products as related to reactants. *Food Science and Technology*, **46**, pp. 1-9.

[17] Ajandouz, E. H., Tchiakpe, L. S., Ore, F. D., Benajiba, A., Puigserver, A. (2001). Effects of pH on Caramelization and Maillard Reaction Kinetics in Fructose-Lysine Model Systems. *Journal of Food Science*, **66**, pp. 926-931.

[18] Benjakul, S., Lertittikul, W., Bauer, F. (2005). Antioxidant activity of Maillard reaction products from a porcine plasma protein-sugar model system. *Food Chemistry*, **93**, pp. 189-196.

[19] Lertittikul, W., Benjakul, S., Tanaka, M. (2007). Characteristics and antioxidative activity of Maillard reaction products from a porcine plasma protein-glucose model system as influenced by pH. *Food Chemistry*, **100**, pp. 669-677.

[20] Laroque, D., Inisan, C., Berger, C. L., Vouland, E., Dufosse, L., Guerard, F. (2008). Kinetic study on the Maillard reaction. Consideration of sugar reactivity. *Food Chemistry*, **111**, pp. 1032-1042.

[21] Maillard, M. N., Billaud, C., Chow, Y. N., Ordonaud, C., Nicolas, J. (2007). Free radical scavenging, inhibition of polyphenoloxidase activity and copper chelating properties of model Maillard systems. *LWT - Food Science and Technology*, **40**, pp. 1434-1444.

[22] Zhuang, Y., Sun, L. (2011). Antioxidant activity of maillard reaction products from lysine-glucose model system as related to optical property and copper (II) binding ability. *African Journal of Biotechnology*, **10**, pp. 6784-6793.

[23] Wolpert, M., Hellwig, P. (2006). Infrared spectra and molar absorption coefficients of the 20 alpha amino acids in aqueous solutions in the spectral range from 1800 to 500 cm^{-1}. *Spectrochimica Acta Part A: Molecular and Biomolecular Spectroscopy*, **64**, pp. 987-1001.

[24] López-Navarrete, J. T., Casado, J., Hernández, V., Ramírez, F. J. (1997). Experimental and theoretical vibrational studies of the amino acid l-asparagine in solution. *Journal of Raman Spectroscopy*, **28**, pp. 501-509.

[25] Boeckx, B., Maes, G. (2012). The conformational behavior and H-bond structure of asparagine: A theoretical and experimental matrix-isolation FT-IR study. *Biophysical Chemistry*, **165-166**, pp. 62-73.

[26] Sylvestre, S., Sebastian, S., Edwin, S., Amalanathan, M., Ayyapan, S., Jayavarthanan, T., Oudayakumar, K., Solomon, S. (2014). Vibrational spectra (FT-IR and FT-Raman), molecular structure, natural bond orbital, and TD-DFT analysis of l-Asparagine monohydrate by density functional theory approach. *Spectrochimica Acta Part A: Molecular and Biomolecular Spectroscopy*, **133**, pp. 190-200.

[27] Ibrahim, M., Alaam, M., El-Haes, H., Jalbout, A. F., Leon, A. D. (2006). Analysis of the structure and vibrational spectra of glucose and fructose. *Ecletica quimica*, **31**, pp. 15-21.

[28] Nikolić, G. S., Cakic, M. D. (2011). Analysis of Bioactive Olygosaccharide-Metal Complexes by Modern FTIR Spectroscopy: Copper Complexes. In: Nikolić, G. S. Ed., *Fourier Transforms - New Analytical Approaches and FTIR Strategies*, InTech, pp.15-44.

[29] Nashalian, O., Yaylayan, V. A. (2014). Thermally induced oxidative decarboxylation of copper complexes of amino acids and formation of Strecker aldehyde. *Journal of Agricultural and Food Chemistry*, **62**, pp. 8518-8523.

[30] Seifert, S. T., Krause, R., Gloe, K., Henle, T. (2004). Metal complexation by the peptide-bound Maillard reaction products N^{ε}-Fructoselysine and N^{ε}-Carboxymethyllysine. *Journal of Agricultural and Food Chemistry*, **52**, pp. 2347-2350.

[31] Rosu, T., Pahontu, E., Ilies, D. C., Georgescu, R., Mocanu, M., Leabu, M., Shova, S., Gulea, A. (2012). Synthesis and characterization of some new complexes of Cu(II), Ni(II) and V(IV) with Schiff base derived from indole-3-carboxaldehyde. Biological activity on prokaryotes and eukaryotes. *European Journal of Medicinal Chemistry*, **53**, pp. 380-389.

[32] Tyagi, M., Chandra, S., Tyagi, P. (2013). Mn(II) and Cu(II) complexes of a bidentate Schiff's base ligand: Spectral, thermal, molecular modelling and mycological studies. *Spectrochimica Acta Part A: Molecular and Biomolecular Spectroscopy*, **117**, pp. 1-8.

[33] Ramonaityte, D. T., Kersiene, M., Adams, A., Tehrani, K. A., Kimpe, N. D. (2009). The interaction of metal ions with Maillard reaction products in a lactose-glycine model system. *Food Research International*, **42**, pp. 331-336.

6 Modifications of Hemoglobin and Myoglobin by Maillard reaction products (MRPs)

6.1 Abstract

High performance liquid chromatography (HPLC) coupled with a Fraction Collector was employed to isolate Maillard reaction products (MRPs) formed in model systems comprising of asparagine and monosaccharides in the 60-120 °C range. The primary MRP which is detected at 60 °C is important for Acrylamide content and color/aroma development in foods and also in the field of food biotechnology for controlling the extent of the Maillard reaction with temperature. The discrete fractions of the reaction products were reacted with Hemoglobin (Hb) and Myoglobin (Mb) at physiological conditions and the reaction adducts were monitored by UV-vis and Attenuated Total Reflection-Fourier transform infrared (FTIR) spectrophotometry. The UV-vis kinetic profiles revealed the formation of a Soret transition characteristic of a low-spin six-coordinated species and the ATR-FTIR spectrum of the Hb-MRP and Mb-MRP fractions showed modifications in the protein Amide I and II vibrations. The UV-vis and the FTIR spectra of the Hb-MRPs indicate that the six-coordinated species is a hemichrome in which the distal E7 Histidine is coordinated to the heme Fe and blocks irreversibly the ligand binding site. Although the Mb-MRPs complex is a six-coordinated species, the 1608 cm^{-1} FTIR band characteristic of a hemichrome was not observed.

Key words: Maillard reaction products; Hemoglobin; Myoglobin; HPLC; Fraction Collector; UV-vis difference spectroscopy; ATR-FTIR.

6.2 Introduction

The glycation process as illustrated by Maillard reactions and its health consequences have gained considerable attention and have been studied extensively in recent years [1-9]. Glycation processes cause the pathology in diabetes principally by the non-enzymatic modification of proteins by glucose and other products of glucose

metabolism. The glycation reaction's kinetics are heightened by elevated and prolonged exposure to glucose and other glycated species, which in turn leads to the chronic health problems. The classical example is that of the post-translational modification of hemoglobin occurring from the covalently bound intermediate arising from the interaction of the electrophilic glucose groups with the nucleophilic primary amino-groups of protein amino-acid residues. Hemoglobin advanced glycation end products (Hb-AGEs) are formed when the initial Schiff bases typically undergoes an Amadori rearrangement resulting in the formation a fructosamin (ketosamin) [10] (**Figure 35**).

Glycated hemoglobin (Hb) is an effective index of long-term blood glucose level and has been widely used in the diagnosis of diabetes mellitus. Glycated Hb comprises HbA1 (Amadori product) and other Hb variants and adducts [11]. HbA1c which is the major component of HbA1 is formed by a non-enzymatic irreversible process in which the aldehyde group of glucose combines with the amino-terminal valine of the β-chain of Hb [12]. More broadly, the terms glycated hemoglobin or glycohemoglobin (GHb, GlcHb) refer to the full range of glycated hemoglobins, including those containing glycated valine and/or lysine residues. The major hemoglobin glycosylation sites *in vitro* and *in vivo* include β-Lys-66 and β-Lys-120 [13]. The exact mechanisms are not clear as to which MRP/AGE components are present in the blood stream. The presence of an AGE-modification alters or destroys enzymatic activity, one example being methylglyoxal-modified serum albumin [14].

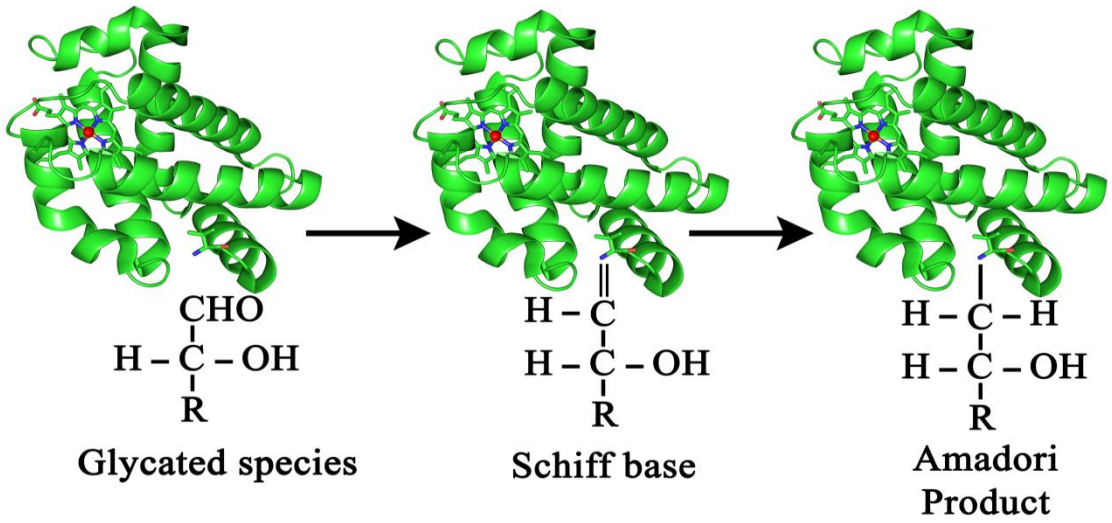

Figure 35. The glycation process in hemoglobin as related to protein structural modifications by glycated species.

Hemichromes are formed when hemoglobin undergoes conformational changes resulting in the formation of a six-coordinated Fe^{3+} low-spin His-Fe-His species [15]. Hemoglobin A in humans can form hemichromes even under physiological conditions as a result of pH and temperature alterations, and ιn the autoxidation of oxyHb [15]. Hemichromes are mainly produced by partially denatured hemoglobin and thought to be precursors of Hb denaturation processes, such as unfolding, precipitation, and heme dissociation. In tetrameric α2β2 Hb it is always thought that oxidized forms adopt either aquo-met or hydroxy-met states, according on the pH of their medium. However, it was recently shown that alternate forms like bis-histidyl hemichrome states could be compatible with folded structures [16]. The crystal structure of Hb in which a partial hemichrome was formed has been reported [17].

In the Maillard reactions a cascade of events each with a discrete role can affect the product composition and generate distinct colors and aromas. One of the factors with instructive significance is temperature and for this reason we have investigate the reaction in the 60-180 ^{0}C range. Many of the studies on protein glycation lack details dealing with the glycation process such as the identification of the glycated sites and spectroscopic assessment of protein structural changes. In this work, we have monitored the reactions of the isolated MRPs products which are originated from the reactions of 1) asparagine with glucose and 2) asparagine with fructose and were separated and isolated by an HPLC component system coupled to a fraction collector in the 60-180 ^{o}C range and found that the primary reaction product is formed at 60 ^{o}C. Because the Maillard reaction is a cascade of consecutive and parallel reaction steps, it is important for the food biotechnology industry to be able to control the extent of the Maillard reaction with temperature. All reaction products were reacted with Hb and Mb. Our results demonstrate the formation of hemichromes in the reactions of the individual MRPs products originated from the Asn/Gluc and Asn/Fruc reactions with Hb, as indicated by 1) the UV-vis data for the formation of a six-coordinate species and 2) the observation of the 1608 cm^{-1} protein Hb FTIR band. On the other hand, although Mb has a number of ε-amino groups which could be glycosylated as similarly occurring in Hb and the UV-vis difference spectra show peaks/troughs at 425/407 nm with a zero-crossing at 420 nm which is characteristic of a six-coordinated species, the 1608 cm^{-1} FTIR band was not observed in none of the Mb-MRPs. Of note is a 6 cm^{-1} downshift in

both the Amide I and II bands that demonstrate conformational changes in all of the Mb-MRPs.

6.3 Experimental Procedures

6.3.1 Sample preparation

Equimolar solutions of glucose or fructose and asparagine (0.2 M) were prepared in phosphate buffer (50 mM) and the pH was adjusted to 8.0. Samples (10 ml) were heated in closed screw-capped tubes at 60, 80, 100 and 180 °C in a heating oven (Memmert, Germany) for 2 hours. For HPLC analysis the samples were diluted hundred-fold.

6.3.2 Spectroscopic monitoring of hemoglobin with added MRPs

Hemoglobin and myoglobin from bovine blood (Sigma) at pH 8.0 and approximately 1 mM concentration was diluted hundred-fold and immediately mixed with each individual LC fraction (2:1 v/v) from the reaction between asparagine and glucose or fructose at 180 °C. For the ATR-FTIR analysis, the protein samples remained undiluted and mixed with each individual LC fraction with the protein concentration being in excess. The ATR-FTIR spectra of the mixtures were collected after 1 day incubation.

6.3.3 HPLC-Fraction collector analysis

The customized HPLC experimental setup consisted of a Varian 218 Prepstar Solvent Delivery Module, an Agilent Manual FL-Injection Valve, an Agilent 1260 Infinity Variable Wavelength Detector (VWD) and an Agilent 440 LC Fraction Collector. The instrumental setup and the separation of individual fractions were described in detail earlier [20]. HPLC analysis was performed on a 4.6 x 250 mm, 5 μm particle size, Zorbax SB-Aq analytical column (Agilent Technologies). Maillard reaction products (MPRs) were analyzed under aqueous conditions using a previously reported method [19].

6.3.4 UV-vis spectrophotometry

Difference UV-vis spectra of hemoglobin and myoglobin with added fractions corresponding to individual MRPs were recorded using a UV–Visible Lambda 25 Perkin Elmer spectrophotometer. A time cycle program was employed which allowed recording a scan spectrum every 5 minutes.

6.3.5 ATR-FTIR spectrophotometry

A horizontal ATR (HATR) accessory (Pike Technologies, Inc, Madison, USA) was employed fitting a Germanium ATR plate with ten internal reflections. The Horizontal ATR employs a pair of transfer optics to direct the infrared beam of the spectrometer to one end of the IR transmitting ATR crystal. A similar pair of optics directs the beam emitted from the other end of the ATR crystal to the spectrometer detector. A Bruker Tensor 27 FTIR spectrometer equipped with a deuterated triglycine sulfate (DTGS) detector was used for spectral acquisition. Spectra were collected in the range 1,800–800 cm^{-1} with 4 cm^{-1} resolution and 100 co-added scans each. A background spectrum was collected before each sample measurement. The software package OPUS 7.0/IR (Bruker) was used to acquire and process the FTIR spectra.

6.4 Results and discussion

6.4.1 Isolation and characterization of MRPs by HPLC-Fraction collector

Glycoconjugates, such as N-glycosides and related compounds are recognized as key Maillard reaction intermediates [18]. When asparagine and glucose (**Figure 36A-B**) or fructose (**Figure 36C-D**) reacts in a 60-180 ^{0}C range it is evident from the HPLC chromatograms that there is elution of several individual products in the reaction mixture (**Figure 36**). These are even formed at lower temperatures but their yield is affectedly increased at higher temperatures. Maillard reaction products (MRPs) were eluted on the Zorbax column which can retain a high selectivity for polar molecules in aqueous phases [19]. Fraction 1 was a combined fraction encompassing a major signal at Rt=5.7 min corresponding to the excess unreacted asparagine arising from the heated reaction mixture [20]. Fractions 2-5 corresponding to discrete MRPs were collected separately. Fractions 2, 3 and 5 have been characterized to originate from the Schiff base, the Amadori product and acrylamide, respectively [20].

All fractions displayed characteristic absorbance bands around 294 nm [20] which was previously reported as a generic marker band of Maillard reaction intermediate products [21-23]. These compounds relate to the glycosylation process as being aldehydes and small molecule ketones arising from the glycosylation of the asparagine molecule. UV

absorbance in the range of 270-300 nm is characteristic for molecules containing carbonyl groups (n->π* transitions).

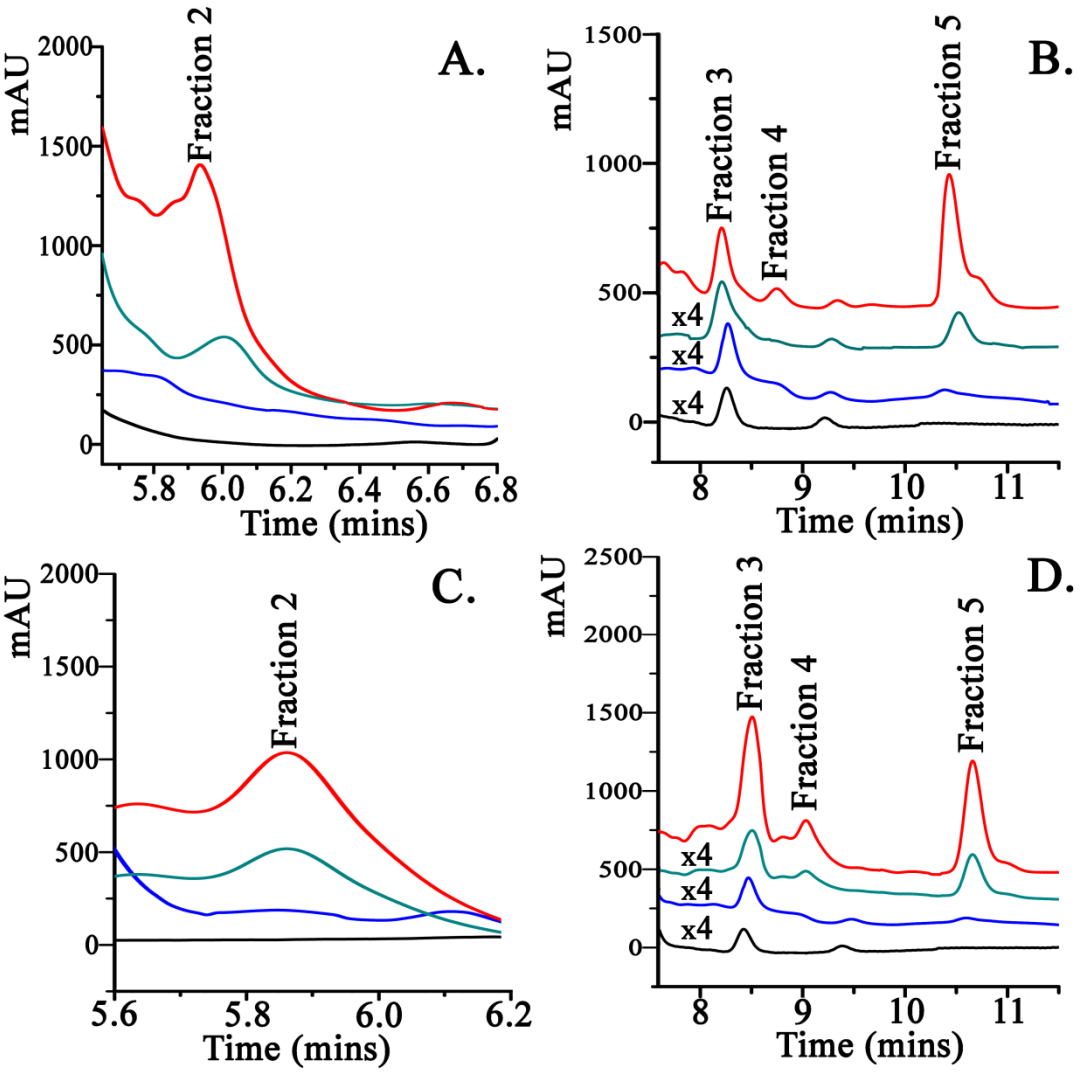

Figure 36. High performance liquid chromatography (HPLC) chromatogram of the reaction mixtures of asparagine and sugars (black: 60 °C, blue: 80 °C, cyan: 100 °C, red: 180 °C). **A:** Fraction 2from the reaction of asparagine with glucose. **B:** Fractions 3-5 collected as discrete MRPs in the reaction of asparagine with glucose. **C**: Fraction 2 from the reaction of asparagine with fructose. **D:** Fractions 3-5 collected as discrete MRPs in the reaction of asparagine with fructose.

6.4.2 Modifications of Hemoglobin and Myoglobin by MRPs

Figure 37A depicts the time evolution of the difference absorption spectrum of the reaction product of Hb which is formed upon the addition of the Schiff base LC fraction 2 from the reaction of asparagine and glucose at pH 8 *minus* oxidized Hb. The difference spectrum shows maxima at 423 nm and minima at 406 nm. The 423 nm transition is attributed to the formation of a six-coordinate species. It has been shown that the selection of a wavelength close to 423 nm is possible a precise measurement for the concentration of glycated hemoglobin [24]. Similar observations have been reported where the spectral difference between hemoglobin and hemichrome was monitored by the difference spectrum with a minimum at 405 nm and a maximum at 423 nm in a fatty acid-hemoglobin system [25].

The UV-vis difference spectra of Hemoglobin with added LC fraction 2 of the reaction mixture of asparagine and fructose, show a 426 nm band that resembles that at 423 nm shown in panel A and an additional transition at 402 nm (**Figure 37B**). Obviously, the Hb-MRPs originated from the Asn/Glu and Asn/Fruc reactions differ significantly. On the other hand, the analogous Mb-MRPs show strong similarities as indicated by the observation of a peak/trough at 425/410 nm, in both the reactions with the isolated compounds from the Asn/Glu and Asn/Fruc reactions (**Figure 37C-D**).

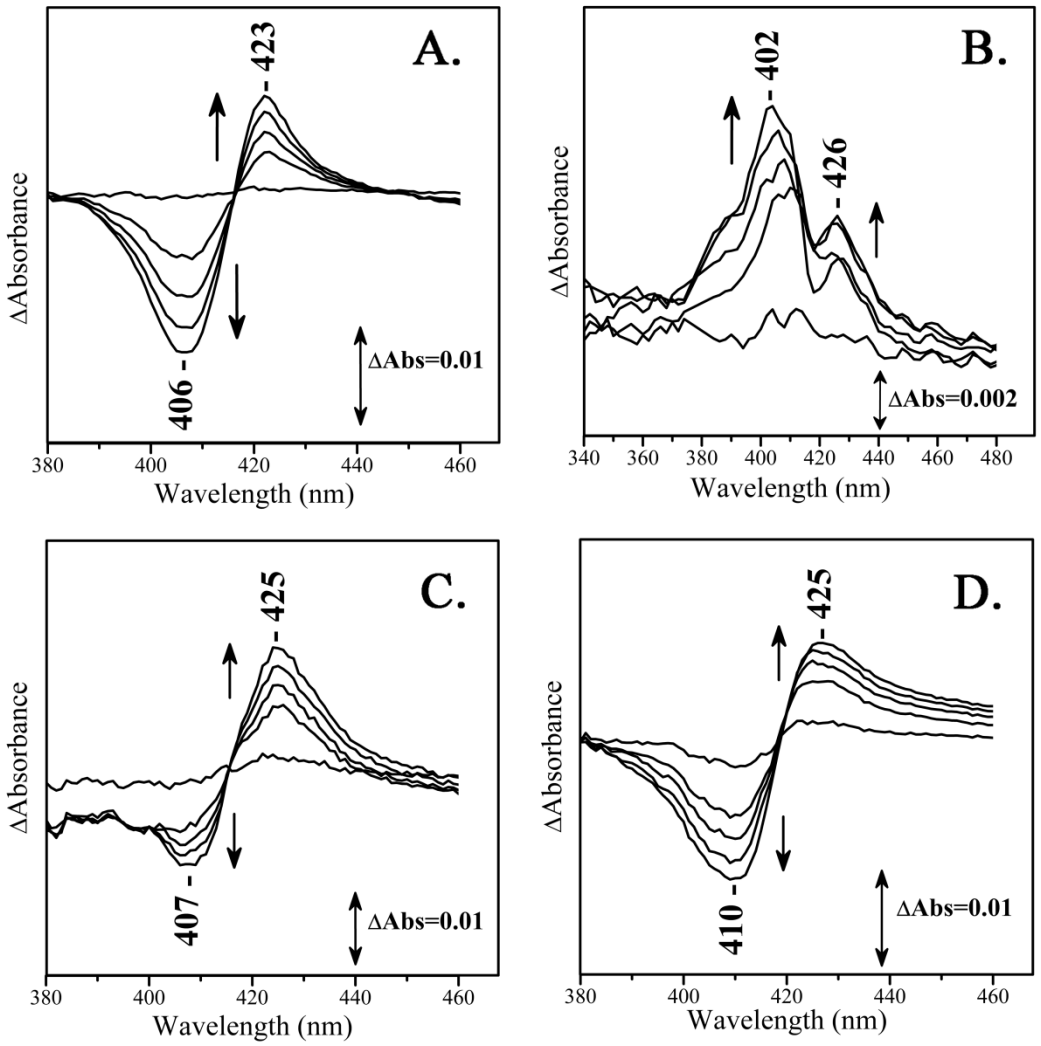

Figure 37. UV-vis difference spectra (protein Hb & Mb adducts *minus* oxidized) of Hb (panel A and B) and Mb (panel C and D) with added Schiff base fraction (LC fraction 2) of the reaction mixture of: **A.** Asn/Gluc + Hb; **B.** Asn/Fruc + Hb; **C.** Asn/Gluc + Mb; **D.** Asn/Fruc + Mb; (Time course: 0-120mins; Spectra displayed every 30 minutes).

Figure 38A-D shows the FTIR spectra of the Hb-adducts at pH 8.0 formed from the reactions of Hb with the compounds from the LC Fractions 2-5. In Figure 38A are the FTIR spectra of the Hb-adducts formed from the reactions of Hb with the compounds from the LC fractions 2-5 from the reaction of Asparagine with Glucose and in Figure 38B those from the reactions of LC fractions 2-5 of Asparagine with Fructose. Figure 38C shows the second derivative spectra of the spectra shown in Figure 38A and in

Figure 38D are the second derivative spectra of the spectra shown in Figure 38B. Amides I and II are the major bands in the IR spectrum of a protein. Amide I absorption originates from the C=O stretching vibration (70-85%) of the amide group (coupled to in-phase bending of the N–H bond and stretching of the C–N bond), which gives rise to IR band(s) in the region between ~1600 and 1700 cm^{-1} [25-28]. Amide II originates from the N–H bending (40–60%) and C–N stretching vibrations (18–40%) [26-29]. From the ATR-FTIR spectra, the ratio of the Amide I to Amide II is slightly lower in the Hb-LC Fractions spectra compared to the initial Hb **(Figure 38A-B)** suggesting conformational changes. Another evident feature from the ATR-FTIR spectra is the observation of a new band at 1608 cm^{-1} in all spectra of the Hb-adducts. We attribute the appearance of the new 1608 cm^{-1} band to the formation of strong beta-sheet structures [30]. In a recent study probing the α-helix to β-sheet transition in fibrin, a band at 1612–1614 cm^{-1} was assigned as a marker band of nascent inter-chain β-sheets, consistent with protein aggregation [31]. An additional spectral feature is the increase in intensity of the 1396 cm^{-1}Hb band which corresponds to the symmetric C=O stretching vibration of COO^- groups. This absorption band is related to aspartic acid residues which function as important subunit contact sites. The Tyrα42⋯Aspβ99 H-bond is in the "switch" region of the $\alpha_1\beta_2$ interface [32] involving the interface residues between the αC helix and the βFG corner experience large dislocations during R to T transition. An equally important hydrogen bonded pair is the Trpβ37⋯Aspα94 which comprises of the "hinge" region, in which the R–T shift is restricted to a change in orientation [32]. The above mentioned feature is particularly evident and it seems to be coupled to the appearance of the 1608 cm^{-1} band in the Hb-LC Fractions 2-4. Fraction 5 forms a very low yield compared to fractions 2-4 of the newly formed 1608 cm^{-1} band and the 1396 cm^{-1} band does not exhibit any intensity change. Similar results are obtained in the reactions of Hb with the reactions products of Asn/ Fruc (LC fractions 2-5) shown in Figure 38B. The second derivative spectra of the Hb-adducts formed from the reactions of both the Asn/Gluc and Asn/Fruc reactions shown in Figure 38C and Figure 38D, respectively, show that the amide I vibration remains constant and small frequency changes in the amide II vibration. The presence of the 1608 cm^{-1} band is evident in both cases.

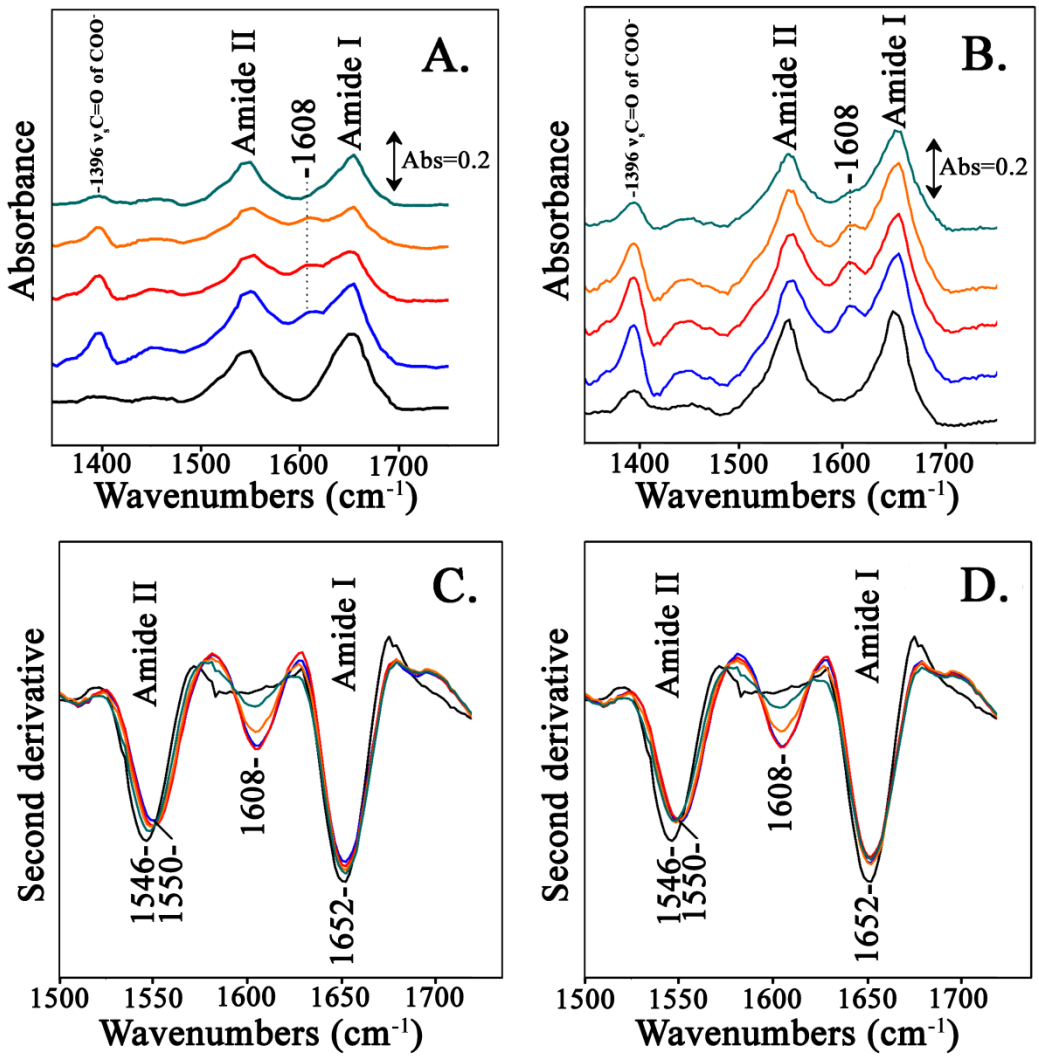

Figure 38. ATR-FTIR spectra of hemoglobin (pH8.0) with added LC Fractions 2-5. **A.** Reaction of asparagine with glucose. **B.** Reaction of asparagine with fructose. **C.** Corresponding second derivative spectra of A. **D.** Corresponding second derivative spectra of B. (Black: Hb, Blue: Hb + Fraction 2, Red: Hb + Fraction 3, Orange: Hb + Fraction 4, Cyan: Hb + Fraction 5).

In the case of Mb-LC Fractions spectra **(Figure 39A-B)**, we do not observe the presence of any new bands but it is evident that there is broadening in both Amide I and Amide II FTIR bands. The broadening of the Amide I band may result from the formation of a more β-sheet-like structure since at the tails of the Amide I band lie the β-sheet band subcomponents [30]. Likewise, the minimum between Amide I and Amide II shows

significant changes, and more evidently, there is also loss in the intensity of the Amide II band. This is confirmed by the second derivative spectra that reveal also a downshift of 6 cm^{-1} in the Amide II region **(Figure 39C-D)**. This observation suggests that there is also modification of the protein Amide II band. There is also a similar downshift of 5 cm^{-1} in the Amide I frequency. Amide I and II frequencies are often affected by the strength of hydrogen bonds involving amide C=O and N-H groups. In contrast with hemoglobin, there is also no significant change in the 1396 cm^{-1} band. This may relate to the fact that there are no subunit contact sites in myoglobin and therefore no alteration in the subunit organization of the protein.

The different behavior of myoglobin versus hemoglobin glycation is interesting to note since it was previously highlighted by a comparative study on the structural stability of myoglobin and glycomyoglobin [33]. The molecular dynamics simulation study revealed an increased stability in the glycomyoglobin molecule as a consequence of increased contacts with water molecules. Moreover, another study has shown that glycation of apomyoglobin with glucose would not effect in fibril formation [34]. This stresses out the importance of the heme component in the whole glycation process. A recent molecular dynamics simulation investigation has pointed out that glucose molecules can interact with heme via the two propionate groups and aspartic and glutamic acid residues by hydrogen bonds, as well as with surrounding water molecules [35].

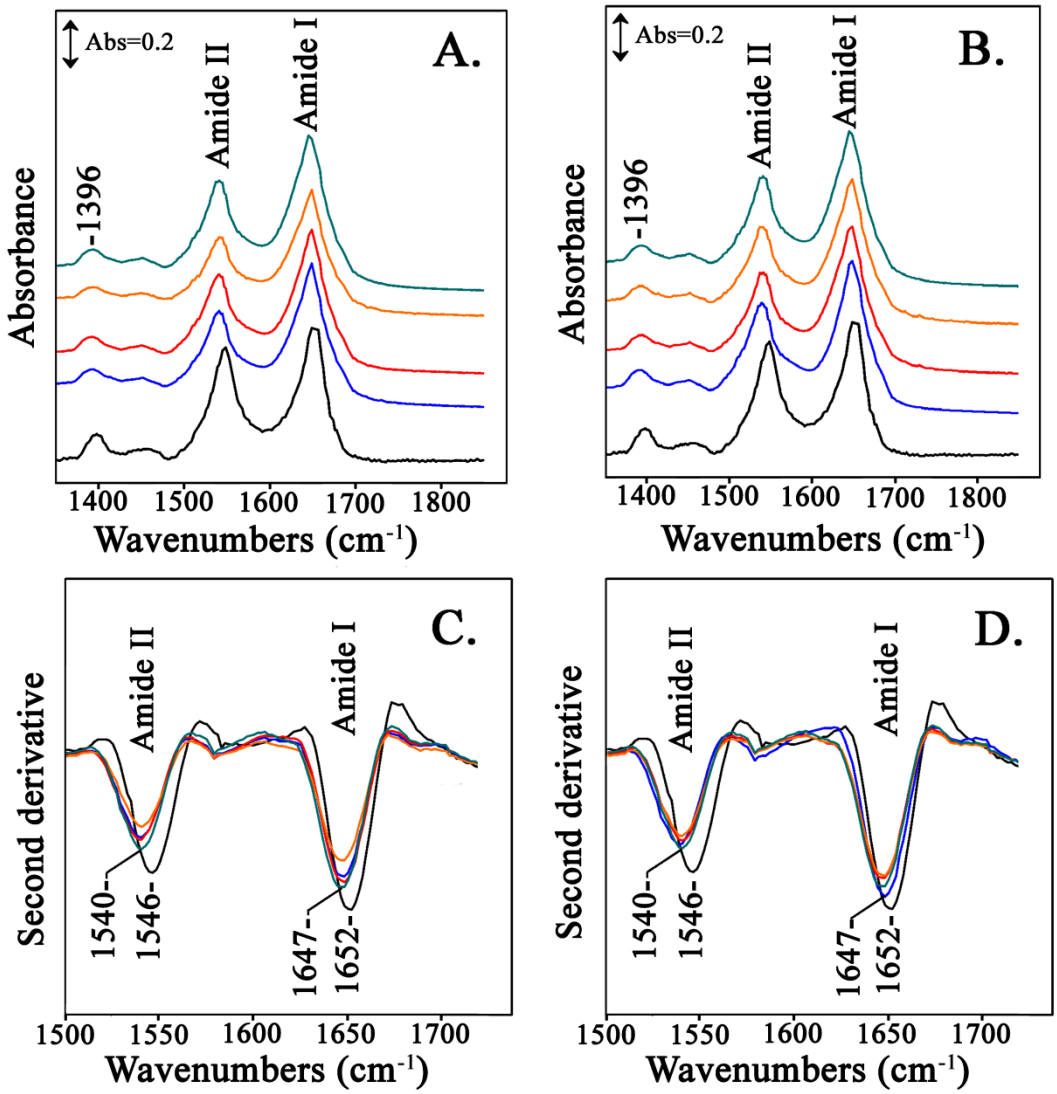

Figure 39. ATR-FTIR spectra of myoglobin (pH8.0) with added LC Fractions 2-5. **A.** Reaction of asparagine with glucose. **B.** Reaction of asparagine with fructose. **C.** Corresponding second derivative spectra of A. **D.** Corresponding second derivative spectra of B. (Black: Mb, Blue: Mb + Fraction 2, Red: Mb + Fraction 3, Orange: Mb + Fraction 4, Cyan: Mb + Fraction 5).

It was previously suggested that the coordination of distal histidine to the β iron produces a scissoring motion in helices E and F which results in modifications in the tertiary structure of the tetramer, mainly in the αβ interface [36]. Raman spectroscopy studies have indicated that this scissor-like motion of helices E and F is critical in the transition from the R to the T state [37-38]. An interesting fact is that in models with

mammalian (horse) and Antarctic fish hemoglobins is that the EF fragment modifications are related to a heme sliding motion that exposes the heme to a more solvent-exposed position [16-17]. This results in a shift of the heme group and a narrowing of the heme pocket as the E- and F-helices move toward each other. It is worth mentioning that these movements did not occur in a mutant myoglobin variant examining the function of the distal His [39].

Effector molecules can bind to liganded Hb and this process provides insight into Hb allosteric transition [40]. Previous studies have examined the interaction of polyphenols with serum proteins [41-42] and demonstrated that binding of these molecules to hemoglobin indicate that hydrogen-bonded interactions provide a means of transport of these substances in the blood. The results of protein glycation often vary according to the nature of the modified protein and also the type of carbohydrate molecule. Even though glucose plays the primary role in the formation of glycation products, other monosaccharides have been shown to be sufficient and even act more effectively than glucose to produce glycated variants. Among these, fructose has been shown to perform the glycation process at a much faster rate [43]. Here, we have described the effect of glucose and fructose derivatives and have shown that these also mediate structural and functional alterations on hemoglobin and myoglobin.

There seems to be a link between hemichrome formation and loss of protein functionality [44-45]. Certain reactive molecules, such as glyoxal and methylglyoxal (MG) have been shown to react with proteins to form advanced glycation end products (AGEs) following Maillard-like reaction [46]. Methylglyoxal modification enhanced the structural stability of hemoglobin but it lowered its iron-mediated oxidation reactions [47]. We suggest that tetrameric Hbs form a partial hemichrome state upon addition of MRP compounds as observed in the present spectroscopic investigations. On the same line, these Maillard reaction species act as external ligands binding to an external protein site triggering the formation of six-coordinated bis-histidyl hemichrome species. Bis-histidyl adducts seem to form not only in hemoglobin but also in a monomeric protein such as myoglobin. We have observed these effects in near physiological conditions and these events were not induced in any way by changing experimental conditions to extremes (e.g. temperature, pH, etc.). The heterogeneous and diverse

nature of AGE structures often makes the application of a universal biomarker method difficult since these compounds may be present as mixtures in human serum. When examining analytical methods, the effort is to optimize quantitative methods for AGE quantification, such as HbA1c, but not for qualitative analysis. Further investigations could include more detailed studies on exact binding sites and spectroscopic determination of other food-derived compounds with hemoglobin and myoglobin.

6.5 References

[1] Stadler, R. H., Blank, I., Varga, N., Robert, F., Hau, J., Guy, P. A., Robert, M. C., Riediker, S. (2002). Food chemistry: Acrylamide from Maillard reaction products. *Nature*, **419**, pp. 449-450.

[2] Zyzak, D. V., Sanders, R. A., Stojanovic, M., Tallmadge, D. H., Eberhart, B. L., Ewald, D. K., Gruber, D. C., Morsch, T. R., Strothers, M. A., Rizzi, G. P., Villagran, M. D. (2003). Acrylamide Formation Mechanism in Heated Foods. *Journal of Agricultural and Food Chemistry*, **51**, pp. 4782-4787.

[3] Amrein, T. M., Andres, L., Manzardo, G. G. G., Amado, R. (2006). Investigations on the Promoting Effect of Ammonium Hydrogencarbonate on the Formation of Acrylamide in Model Systems. *Journal of Agricultural and Food Chemistry*, **54**, pp. 10253-10261.

[4] Stadler, R. H., Robert, F., Riediker, S., Varga, N., Davidek, T., Devaud, S. P., Goldmann, T., Hau, J. R., Blank, I. (2004). In-Depth Mechanistic Study on the Formation of Acrylamide and Other Vinylogous Compounds by the Maillard Reaction. *Journal of Agricultural and Food Chemistry*, **52**, pp. 5550-5558.

[5] Hidalgo, F. J., Delgado, R. M., Navarro, J. L., Zamora, R. (2010). Asparagine Decarboxylation by Lipid Oxidation Products in Model Systems. *Journal of Agricultural and Food Chemistry*, **58**, pp. 10512-10517.

[6] Srikanth, V., Maczurek, A., Phan, T., Steele, M., Westcott, B., Juskiw, D., Münch, G. (2011). Advanced glycation endproducts and their receptor RAGE in Alzheimer's disease. *Neurobiology of Aging*, **32**, pp. 763–777.

[7] Gul, A., Rahman, M. A, Salim, A., Simjee, S.U. (2009). Advanced glycation end products in senile diabetic and nondiabetic patients with cataract. *Journal of Diabetes and its Complications*, **23**, pp. 343–348.

[8] Deli, G., Bosnyak, E., Pusch, G., Komoly, S., Feher, G. (2013). Diabetic neuropathies: diagnosis and management. *Journal of Neuroendocrinology*, **98**, pp. 267–280.

[9] Paneni, F., Beckman, J. A., Creager, M. A., Cosentino, F. (2013). Diabetes and vascular disease: pathophysiology, clinical consequences, and medical therapy: part I. *European Heart Journal*, **34**, pp. 2436–2443.

[10] Nass, N., Bartling, B., Navarrete Santos, A., Scheubel, R. J., Börgermann, J., Silber, R. E., Simm, A. (2007). *Zeitschrift für Gerontologie und Geriatrie*, **40,** p. 349.

[11] Little, R. R., Rohlfing, C. L. (2013). The long and winding road to optimal HbA1c measurement. *Clinical Chimica Acta*, **418**, pp. 63–71.

[12] Pan, T., Li, M., Chen, J., Xue, H. (2014). Quantification of glycated hemoglobin indicator HbA1c through near-infrared spectroscopy. *Journal of Innovative Optical Health Sciences*, **07**, p. 1350060.

[13] Shapiro, R., McManus, M. J., Zalut, C., Bunn, H. F. (1980). Sites of nonenzymatic glycosylation of human hemoglobin A. *Journal of Biological Chemistry*, **255**, pp. 3120-3127.

[14] Ahmed, N., Dobler, D., Dean, M., Thornalley, P. J. (2005). Peptide Mapping Identifies Hotspot Site of Modification in Human Serum Albumin by Methylglyoxal Involved in Ligand Binding and Esterase Activity. *Journal of Biological Chemistry*, **280**, pp. 5724-5732.

[15] Sugawara, V., Kadono, E., Suzuki, A., Yukuta, Y., Shibasaki, Y., Nishimura, N., Kameyama, Y., Hirota, M., Ishida, C., Higuchi, N., Haramoto, K., Sakai, Y., Soda, H. (2003). Hemichrome formation observed in human haemoglobin A under various buffer conditions. *Acta Physiologica Scandinavica*, **179**, pp. 49–59.

[16] Vergara, A., Vitagliano, L., Di Prisco, G., Verde, C., Mazzarella, L. (2008). Spectroscopic and crystallographic characterization of hemichromes in tetrameric hemoglobins. *Methods in Enzymology*, **436**, pp. 421–440.

[17] Robinson, V. L., Smith, B. B., Arnone, A. (2003). A pH-Dependent Aquomet-to-Hemichrome Transition in Crystalline Horse Methemoglobin. *Biochemistry,* **42**, pp. 10113-10125.

[18] Stadler, R. H., Blank, I., Varga, N., Robert, F., Hau, J., Guy, P. A., Robert, M. C., Riediker, S. (2002). Food chemistry: Acrylamide from Maillard reaction products. *Nature*, **419**, pp. 449-450.

[19] Ioannou, A., Varotsis, C. (2016). Real Time Monitoring the Maillard Reaction Intermediates by HPLC- FTIR. *Journal of Physical Chemistry and Biophysics,* **6**, p. 210.

[20] Ioannou, A., Daskalakis, V., Varotsis, C. (2017). Detection of Maillard reaction products by a coupled HPLC-Fraction collector technique and FTIR characterization of Cu(II)-complexation with the isolated species. *Journal of Molecular Structure,* **1141**, pp. 634-642.

[21] Ajandouz, E. H., Tchiakpe, L. S., Ore, F. D., Benajiba, A., Puigserver, A. (2001). Effects of pH on Caramelization and Maillard Reaction Kinetics in Fructose-Lysine Model Systems. *Journal Food Science,* **66**, pp. 926-931.

[22] Benjakul, S., Lertittikul, W., Bauer, F. (2005). Antioxidant activity of Maillard reaction products from a porcine plasma protein-sugar model system. *Food Chemistry*, **93**, pp. 189-196.

[23] Lertittikul, W., Benjakul, S., Tanaka, M. (2007). Characteristics and antioxidative activity of Maillard reaction products from a porcine plasma protein-glucose model system as influenced by pH. *Food Chemistry,* **100**, pp. 669-677.

[24] Sugiyama, K, Sakai, T. (2011). *Method of measuring glycated hemoglobin concentration*. U.S. Patent, 8,021,887.

[25] Litvinko, N. M., Andreiuk, G. M., Kisel, M. A., Kiselev, P. A., Akhrem, A. A. (1989). The use of hemoglobin for determination of phospholipase A2 activity. *Prikladnaia biokhimiia i mikrobiologiia*, **25**, pp. 847-852.

[26] Dousseau, F., Pezolet, M. (1990). Determination of the secondary structure content of proteins in aqueous solutions from their amide I and amide II infrared bands.

Comparison between classical and partial least-squares methods. *Biochemistry*, **29**, pp. 8771-8779.

[27] Barth, A., Zscherp, C. (2002). What vibrations tell about proteins. *Quarterly Reviews in Biophysics*, **35**, pp. 369-430.

[28] Bandekar, J. (1992). Amide modes and protein conformation. *Biochimica et Biophysica Acta*, **1120**, p. 123-143.

[29] Krimm, S., Bandekar, J. (1986). Vibrational Spectroscopy and Conformation of Peptides, Polypeptides, and Proteins. *Advances in Protein Chemistry*, **38**, pp. 181-364.

[30] Garidel, P., Schott, H. (2006). Fourier-transform midinfrared spectroscopy for analysis and screening of liquid protein formulations. *BioProcess International*, **4**, pp. 48-55.

[31] Litvinov, R. I., Faizullin, D. A, Zuev, Y. F, Weisel, J. W. (2012). The α-Helix to β-Sheet Transition in Stretched and Compressed Hydrated Fibrin Clots. *Biophysical Journal*, **103**, pp. 1020–1027.

[32] Baldwin, J., Chothia, C. (1979). Haemoglobin: The structural changes related to ligand binding and its allosteric mechanism. *Journal of Molecular Biology*, **129**, pp. 175-220.

[33] Alizadeh-Rahrovi, J., Shayesteh, A., Ebrahim-Habibi, A. (2015). Structural stability of myoglobin and glycomyoglobin: a comparative molecular dynamics simulation study. *Journal of Biological Physics*, **41**, pp. 349-366.

[34] Iannuzzi, C., Maritato, R., Irace, G., Sirangelo, I. (2013). Glycation Accelerates Fibrillization of the Amyloidogenic W7FW14F Apomyoglobin. *PLOS ONE*, **8**, p. e80768.

[35] You, Y., Liu, F., Du, K. J., Wen, G. B., Lin, Y. W. (2014). Structural and functional alterations of myoglobin by glucose-protein interactions. *Journal of Molecular Modeling*, **20**, pp. 2358.

[36] Riccio, A., Vitagliano, L., Di Prisco, G., Zagari, A., Mazzarella, L. (2002). The crystal structure of a tetrameric hemoglobin in a partial hemichrome state. *Proceedings of the National Academy of Sciences*, **99**, pp. 9801-9806.

[37] Rodgers, K. R., Spiro, T. G. (1994). Nanosecond dynamics of the R-T transition in hemoglobin: ultraviolet Raman studies. *Science*, **265**, pp. 1697-1699.

[38] Jayaraman, V., Rodgers, K. R., Mukerji, I., Spiro, T. G. (1995) Hemoglobin allostery: resonance Raman spectroscopy of kinetic intermediates. *Science*, **269**, pp. 1843-1848.

[39] Dou, Y., Admiraal, S. J., Ikeda-Saito, M., Krzywda, S., Wilkinson, A. J., Li, T., Olson, J. S., Prince, R. C., Pickering, I. J., George, G. N. (1995). Alteration of Axial Coordination by Protein Engineering in Myoglobin BISIMIDAZOLE LIGATION IN THE His64→ Val/Val68→ His DOUBLE MUTANT. *Journal of Biological Chemistry*, **270**, pp. 15993−16001.

[40] Chen, Q., Lalezari, I., Nagel, R. L., Hirsch, R. E. (2005). Liganded Hemoglobin Structural Perturbations by the Allosteric Effector L35. *Biophysical Journal*, **88**, pp. 2057-2067.

[41] Lu, Z., Zhang, Y., Liu, H., Yuan, J., Zheng, Z., Zou, G. (2007). Transport of a Cancer Chemopreventive Polyphenol, Resveratrol: Interaction with Serum Albumin and Hemoglobin. *Journal of Fluorescence*, **17**, pp. 580-587.

[42] Hegde, A. H., Sandhya, B., Seetharamappa, J. (2012). Investigations to reveal the nature of interactions of human hemoglobin with curcumin using optical techniques. *International Journal of Biological Macromolecules*, **52**, pp. 133-138.

[43] Schalkwijk, C.G., Stehouwer, C. D. A., van Hinsbergh, V. W. M. (2004). Fructose-mediated non-enzymatic glycation: sweet coupling or bad modification. *Diabetes Metabolism Research and Reviews*, **20**, pp. 369–382.

[44] Banerjee, S., Maity, S., Chakraborti, A. S. (2016). Methylglyoxal-induced modification causes aggregation of myoglobin. *Spectrochimica Acta Part A: Molecular and Biomolecular Spectroscopy*, **155**, pp.1-10.

[45] Sen, S., Bose, T., Roy, A., Chakraborti, A. S. (2007). Effect of non-enzymatic glycation on esterase activities of hemoglobin and myoglobin. *Molecular and Celular Biochemistry*, **301**, pp. 251-257.

[46] Banerjee, S., Chakraborti, A. S. (2014). Structural alterations of hemoglobin and myoglobin by glyoxal: A comparative study. *International Journal of Biological Macromolecules*, **66**, pp. 311-318.

[47] Banerjee, S., Chakraborti, A. S. (2016). Methylglyoxal modification enhances the stability of hemoglobin and lowers its iron-mediated oxidation reactions: An in vitro study. *International Journal of Biological Macromolecules*, **95**, pp. 1159-1168.

7 Fluorescence characterization of hemoglobin modification by Maillard reaction products

7.1 Abstract

Maillard reaction products (MRPs) are formed by reactions of carbohydrate intermediates with proteins, resulting in the formation of advanced glycation end-products (AGEs). Dietary Maillard reaction products are recognized as potential chemical modifiers of human proteins. The reaction of hemoglobin with MRPs from an asparagine-sugar model system was investigated by fluorescence spectrophotometry. The tryptophan-specific fluorescence obtained for glycated hemoglobin exhibited Stokes effect since the wavelength of the emission peak was shifted to a higher wavelength than that of native hemoglobin. The lowering of this energy level may be associated to ligand binding and hence subsequent structural modification of hemoglobin. To further support this, the fluorescence emission signals of the individual fractions were replaced by new emission features indicating the presence of intermediate species in the reaction mixture.

7.2 Introduction

Fluorophores are considered precursors of brown pigments and allow detecting the progress of the Maillard reaction before any visual change occurs. Browning development occurs after a characteristic induction period where fluorescent uncolored intermediates are formed. Methods based on visible spectrum absorbance measurements were widely employed as a universal technique for monitoring the progress of the global Maillard reaction [1-6]. Fluorescence measurement has been proposed as a reliable method to monitor protein damage at early stages in milk-related products [7-10]. Fluorescence was initially employed to evaluate the formation of MRPs in milk and in recent years it is used in the assessment of the processing of cereals, cookies, soybeans, infant formula, cooked salmon and bakery products. Fluorescent compounds may be present as free in the matrix or linked to the protein fraction. Some authors have demonstrated that fluorescent products attached to proteins were significantly more than

those generated by free fluorescent compounds, and they also exhibited a shift in the emission properties during the heating time [7-8].

However, the most substantial developments in explaining the formation of fluorescent compounds, in the evaluation of their structure and in the development of experimental techniques for their detection, have been performed in biomedical and biological areas [11-14]. In several disciplines the Maillard reaction has gained considerable importance, since much human pathology is derived of the non-enzymatic glycosylation of proteins [11, 15-19].

Fluorescence from the Maillard reaction is attributed to molecular structures with complex bonds between carbon and nitrogen, and the contribution of sugar caramelization to global fluorescence is insignificant in amino-acid containing systems [20-21]. Fluorescent compounds are precursors of for the brown pigments formed in the advanced stage of the Maillard reaction presenting a range of chemical structures [22-23]. The first authors that described the spectral characteristics of the fluorescent chromophores in a glucose-glycine browning system highlighted that the chromophore group was a Schiff-base in conjugation with an electron donating group [24]. Since then many other chemical structures of fluorescent MRPs have been identified. Most of the characterized structures of fluorescent compounds are based mainly on the amino-acids lysine and arginine, including Lys-hydroxy-triosidine, Arg-hydroxy-triosidine and Arg-pyrimidine [25-26]. One other characteristic example is pentosidine which is a protein-derived MRP formed when glucose reacts with ribonuclease and lysozyme. It is found in very low amounts in foods [27] but it is thought to store in tissues with age [28].

Maillard products are formed by reactions of both carbohydrate- and lipid-derived intermediates with proteins, leading to formation of advanced glycation and lipoxidation end-products (AGE/ALEs). AGEs can be classified by their ability to show fluorescence or to form cross links on proteins. AGEs formation occurs in a very slow time frame and naturally in the healthy organisms, nonetheless, this process is accelerated under certain conditions, such as hyperglycemia and oxidative stress. Dietary MRPs added to the intra and extracellular AGEs, contribute to the accumulation of these compounds in tissues. Dietary Maillard products are discussed as “glycotoxins” and thus as a nutritional risk, but also increasingly with regard to positive effects in the human body [29]. It is now generally accepted that plasma glucose levels are not a very reliable

factor when considering glycemic control in normoglycemic and hyperglycemic individuals since they often fluctuate depending on many factors. Measurement and development of improved analytical methods for determination of Hb-AGE are important in evaluating qualitatively and quantitatively glycation status.

The biochemical applications of fluorescence often utilize intrinsic protein fluorescence. Among biopolymers, proteins are unique in displaying useful intrinsic fluorescence [30]. The variable tryptophan quantum yields in proteins are affected by near environment quenchers in the protein, which may include lysine and histidine residues, as well as amide groups in the peptide backbone. In this study, we have investigated the effect of hemoglobin modification with discrete MRPs from asparagine-sugar model systems using fluorescence excitation/emission spectrophotometry to follow changes in hemoglobin mainly through tryptophan fluorescent characteristics.

7.3 Materials and Methods

7.3.1 Sample preparation of MRPs

Solutions of glucose and asparagine or fructose and asparagine (0.2 M, pH 8.0) were prepared in phosphate buffer (50 mM, pH 8.0). Samples were heated in closed screw-capped tubes at 180 °C in a heating oven (Memmert, Germany) for 2 hours.

7.3.2 HPLC-Fraction collector analysis of MRPs

The HPLC instrumental setup and the separation of individual MRP fractions were described in detail earlier [31]. HPLC analysis was performed on a 4.6 x 250 mm, 5 μm particle size, Zorbax SB-Aq analytical column (Agilent Technologies). Maillard reaction products (MPRs) were analyzed under aqueous conditions using a previously reported method [32].

7.3.3 Preparation of hemoglobin with added MRPs

Hemoglobin from bovine blood (Sigma) at pH 8.0 was immediately mixed with each individual LC fraction from the reaction between asparagine and glucose or fructose at 180 °C. The native and glycated hemoglobin samples were diluted to a final concentration of 5 mM. The dilution was prepared using 50 mM phosphate buffer (pH 8.0). The fluorescence spectra of the mixtures were collected up to 30 days incubation.

7.3.4 Fluorescence analysis

The Cary Eclipse Fluorescence Spectrophotometer (Agilent Technologies, USA) controlled from a PC using the Agilent Technologies WinFLR software (version 1.2) was used for obtaining the fluorescent signal. Fluorescence values of the native and glycated hemoglobin samples were measured using a clear four-sided quartz cuvette in the spectrophotometer sample compartment. The excitation and emission slit widths for both the excitation and emission monochromators were set with the value of 5.0 nm. The Excitation Emission Matrix (EEM) measurement and processing were generated by scanning emission spectra from 320 nm to 500 nm at 1 nm intervals, with 5 nm increments of the excitation wavelengths from 260 nm to 310 nm. The Milli-Q water blank was subtracted from the sample EEM spectra.

7.4 Results and Discussion

The formation of fluorescent products was previously investigated during the storage of various foods, food model and biological systems [33-36]. The excitation (340–370 nm) and emission (420–470 nm) wavelengths corresponding to the maxima of these systems are used to characterize the fluorescent products from Maillard reactions [37]. However, this is not always the case. An excitation wavelength of 400 nm yielded an emission peak at 468 nm in a study of sugar-lysine MRPs [38]. Additionally, fluorescent AGEs containing arginine in their structure present an excitation wavelength of 320 nm and an emission wavelength of 380 nm [39]. This wide range reveals the diversity of fluorescent species depending on the specific reaction being studied.

Proteins react with glucose to form a stable Amadori product through Schiff base adducts that are transformed to advanced glycation end products (AGEs) some of which exhibit fluorescence. Therefore, their fluorescence intensities indicate of the extent of AGE-modified proteins. These excitation-emission maxima are distinct from tryptophan fluorescence in proteins. The maximum excitation and emission wavelengths for tryptophan fluorescence in hemoglobin in hemoglobin are at 290 and 336 nm, respectively. A worthy feature of intrinsic protein fluorescence is the high sensitivity of the local environment of tryptophan. Alterations in the emission spectra of tryptophan

may occur in response to conformational transitions, subunit association, substrate binding, or denaturation.

Figure 40A shows the fluorescence emission spectra of native hemoglobin (pH 8.0). It is observed that native hemoglobin displays weak autofluorescence under these conditions when maximally excited around 280 nm. **Figure 40B** shows the corresponding fluorescence excitation-emission matrix (EEM) of native hemoglobin. The contour map enables the identification of peaks within a multi-component sample matrix. The different colors are associated with intensity with the deep red being the most intense. We observe that for native hemoglobin the maximum excitation/emission is 280nm/338 nm.

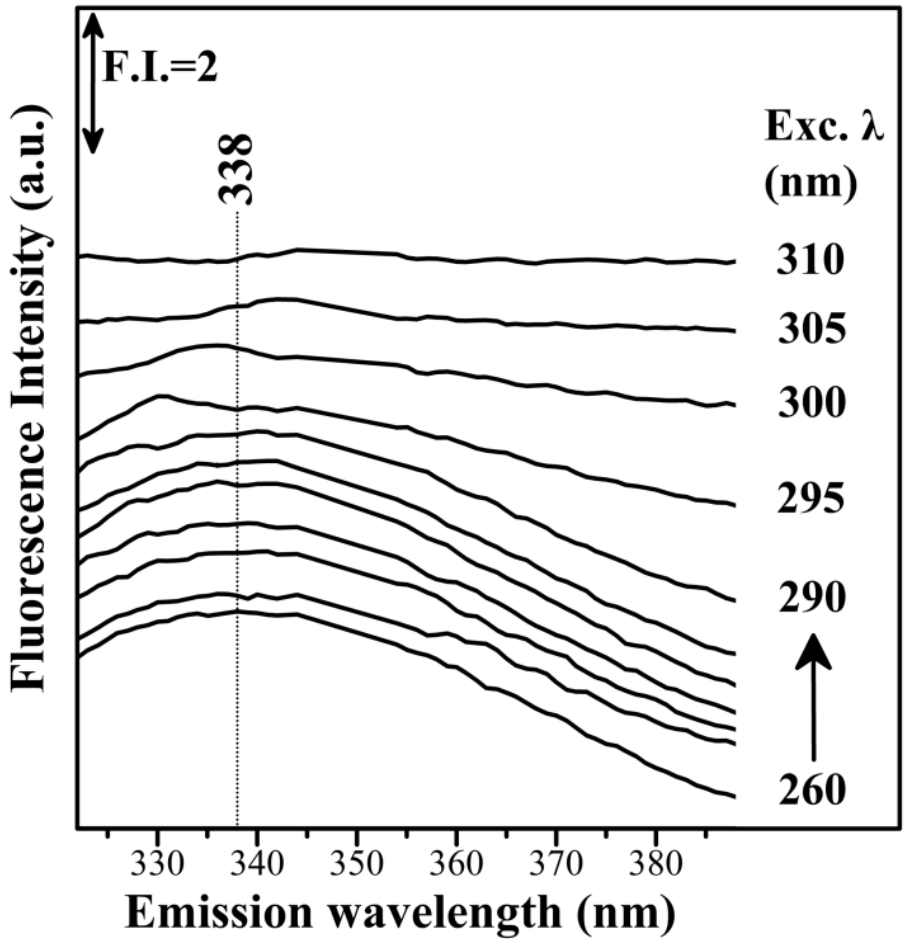

Figure 40A. Fluorescence emission spectra of native hemoglobin (pH 8.0). (Excitation wavelength range: 260-310nm).

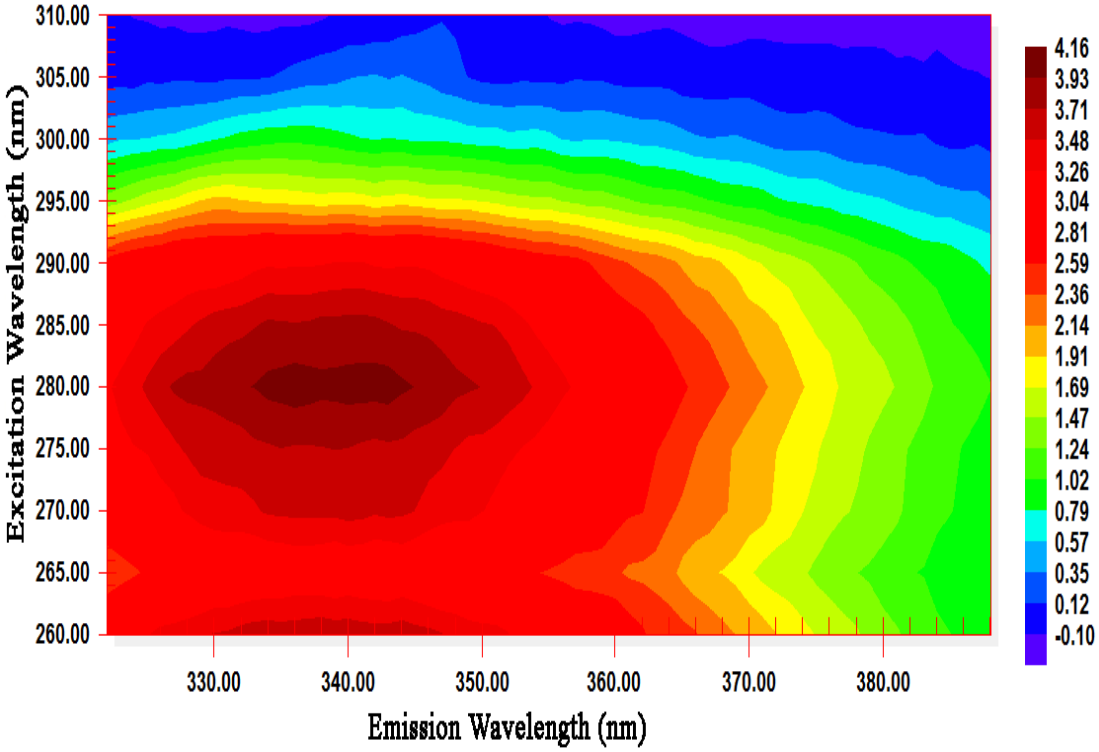

Figure 40B. Fluorescence excitation-emission matrix (EEM) of native hemoglobin (pH 8.0). (Excitation wavelength range: 260-310nm).

Figure 41 shows the corresponding fluorescence emission spectra of the individual LC fraction 2 of the reaction between asparagine-fructose (pH 8.0). It is observed that at least two dinstinct emission peaks are present in the emission range 380-500 nm which is characteristic for fluorescent food-derived products from Maillard reactions.

It was previously reported that the fluorescence analysis of glycated hemoglobin fractions exhibited a new emission peak at 345 nm when excited at 308 nm that was different from its non-glycated equivalent [40]. The authors discuss that this representative emission peak was associated with the formation of Hb-AGE and that the Amadori compound of glycated hemoglobin (HbA1c) failed to exhibit any fluorescence.

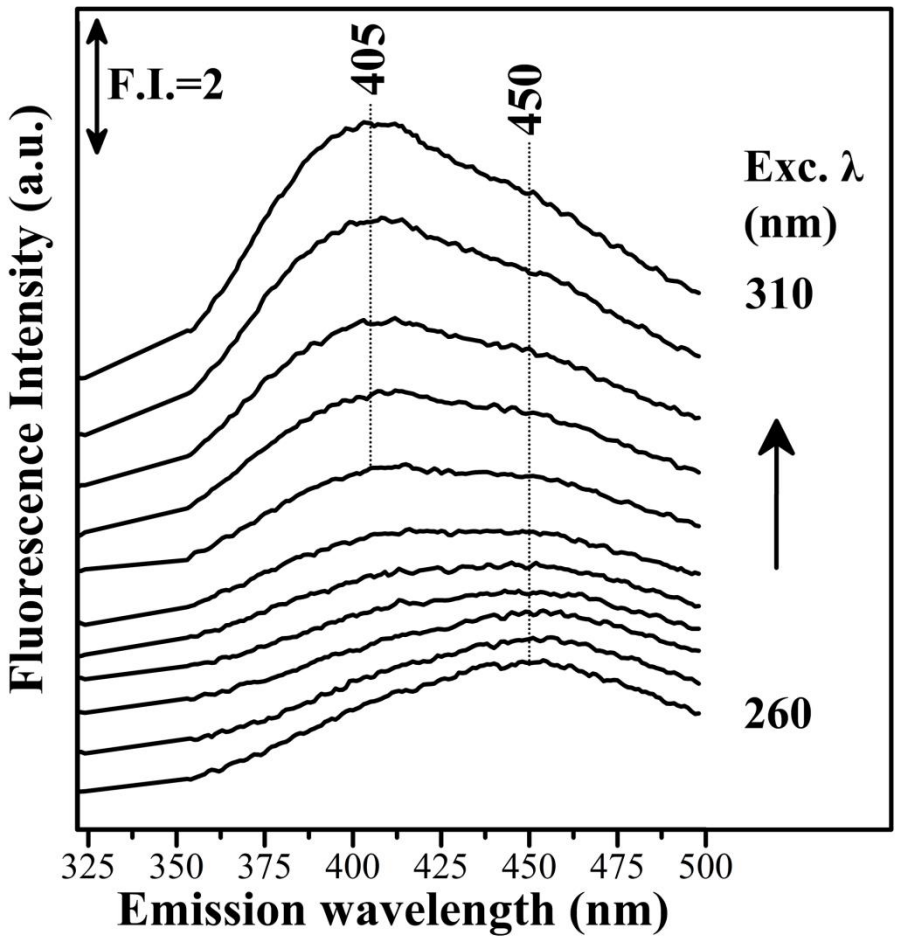

Figure 41. Fluorescence emission spectra of LC Fraction 2 from the reaction of Asn-Fruc (Excitation wavelength range: 260-310nm).

Figure 42A shows the fluorescence emission spectra of hemoglobin with LC Fraction 2 from the reaction of asparagine and fructose after 1 day incubation. **Figure 42B** shows the contour plot of excitation and emission wavelengths for the same sample. The emission maximum was located around 348 nm for the excitation range of 260-290 nm. The fluorescence obtained for this glycated Hb exhibited Stokes effect since the wavelength of the emission peak is 10 nm more than that of native hemoglobin (**Figure 40**). The lowering of this energy level can be associated to ligand binding and hence subsequent structural modification of hemoglobin. It is generally accepted that when the tryptophan residue becomes hydrogen bonded or increasingly exposed to water, its fluorescent emission shifts to longer wavelengths.

The second observation giving supporting evidence of hemoglobin-MRP binding is that for the excitation range of 260-290 nm we observe the decrease in the emission intensity of the 450 nm emission feature (as shown in **Figure 41**). Furthermore, there is the appearance of two broad emission maxima around 390 nm and 430 nm in the excitation range between 300-310 nm which were absent in the isolated fraction sample. This may suggest that there is a mixture of species arising from the interaction of hemoglobin and the individual MRP.

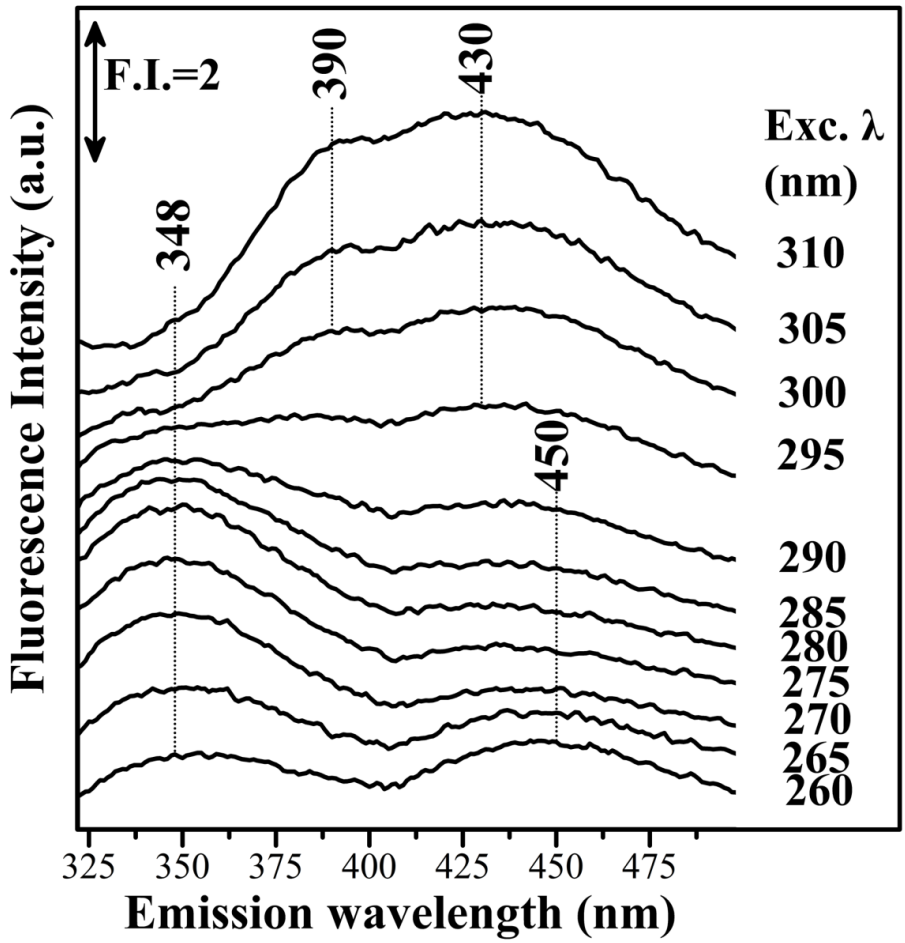

Figure 42A. Fluorescence emission spectra of hemoglobin with LC Fraction 2 from the reaction of Asn-Fruc after 1 day incubation (Excitation wavelength range: 260-310nm).

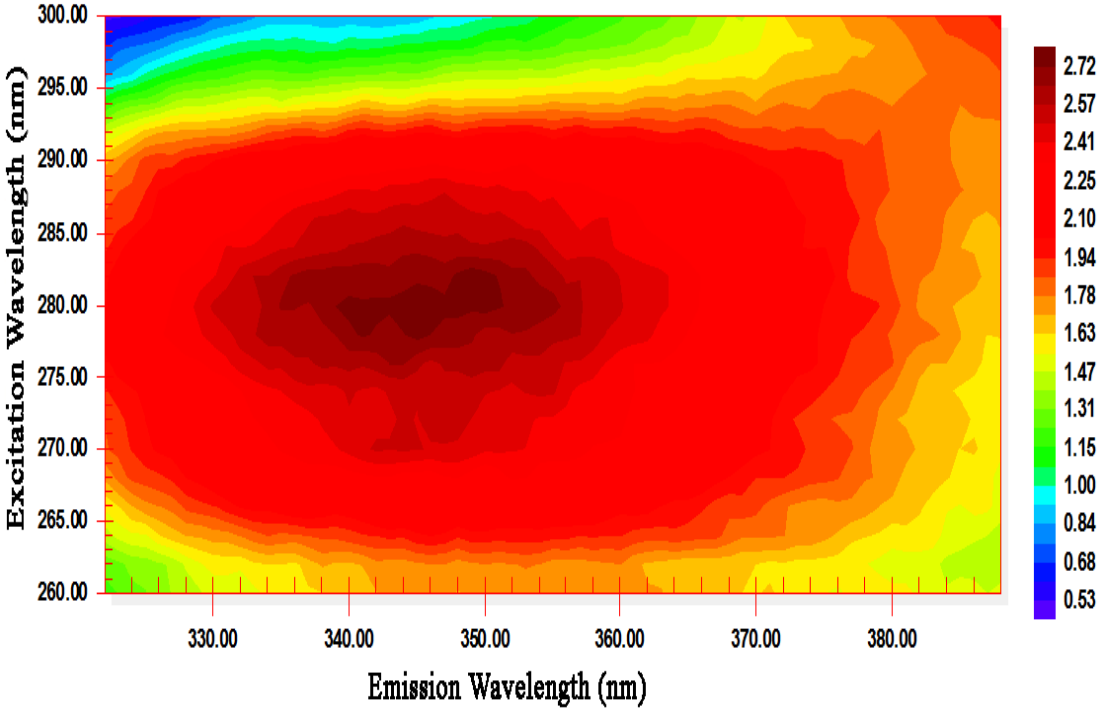

Figure 42B. Fluorescence excitation-emission matrix (EEM) of hemoglobin with LC Fraction 2 from the reaction of Asn-Fruc after 1 day incubation.

Figure 43 shows the fluorescence emission 3D spectra of the individual LC fraction 3 of the reaction between asparagine-fructose (pH 8.0). The first emission band is at 450 nm in the excitation range of 260-310 nm with the highest emission intensity at an excitation wavelength of 260 nm. The second emission band is at 408 nm in the excitation range of 290-310 nm. **Figure 44A** shows the fluorescence emission 3D spectra of hemoglobin with LC Fraction 3 from the reaction of asparagine and fructose after 1 day incubation. **Figure 44B** shows the fluorescence excitation-emission matrix (EEM) for the same sample. The emission maximum was located around 342 nm for the excitation range of 260-290 nm. In this case, the shift from the tryptophan-specific emission is less than that for the Hb-fraction 2. However, there is a clear additional emission at 370nm for the excitation range of 260-290 nm and another broad emission band at 390 nm for the excitation range of 295-310 nm. Additionally, there is a very weak and broad emission feature at 450 nm in the place of a much defined emission band observed of the individual LC Fraction 3 (**Figure 43**). These events suggest that

there is alteration on the structural features of the individual fraction with the simultaneous formation of new species in the mixture solution.

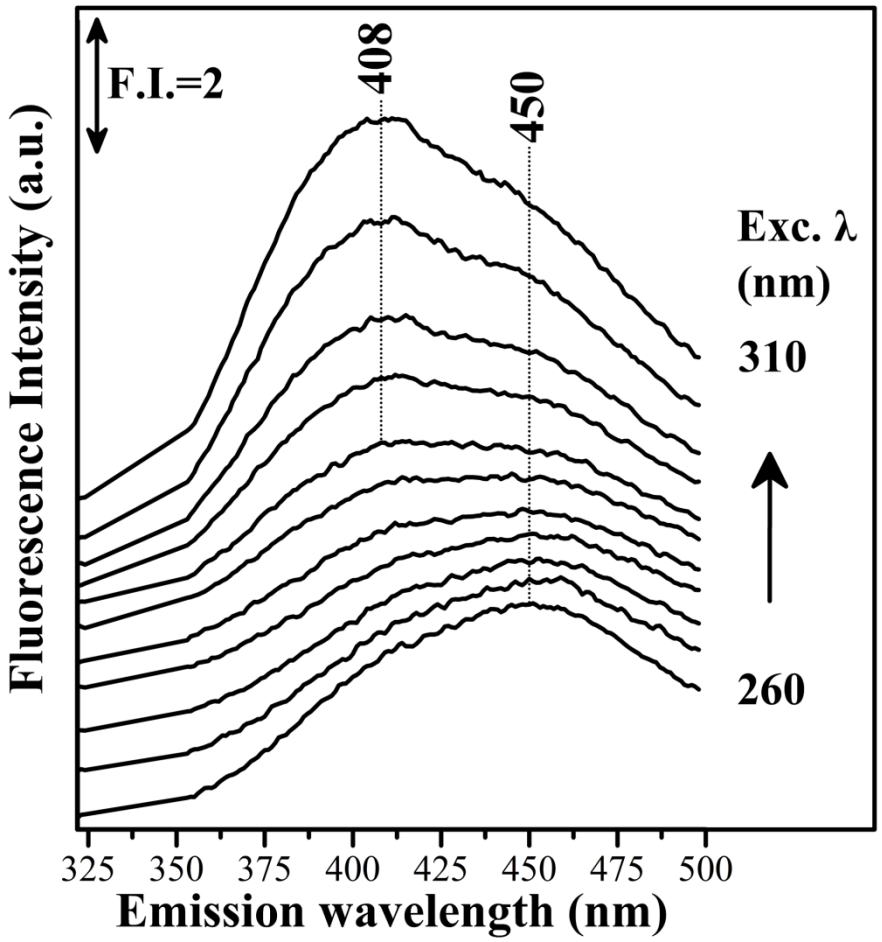

Figure 43. Fluorescence emission spectra of LC Fraction 3 from the reaction of Asn-Fruc (Excitation wavelength range: 260-310nm).

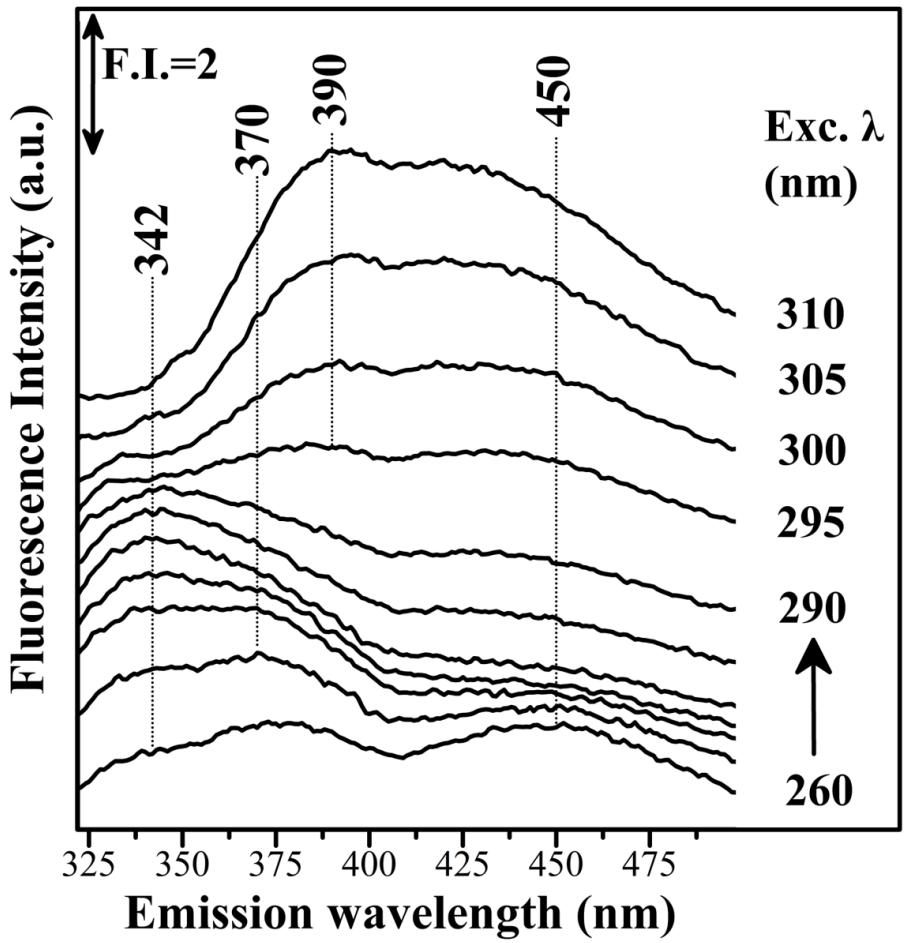

Figure 44A. Fluorescence emission spectra of hemoglobin with LC Fraction 3 from the reaction of Asn-Fruc after 1 day incubation (Excitation wavelength range: 260-310nm).

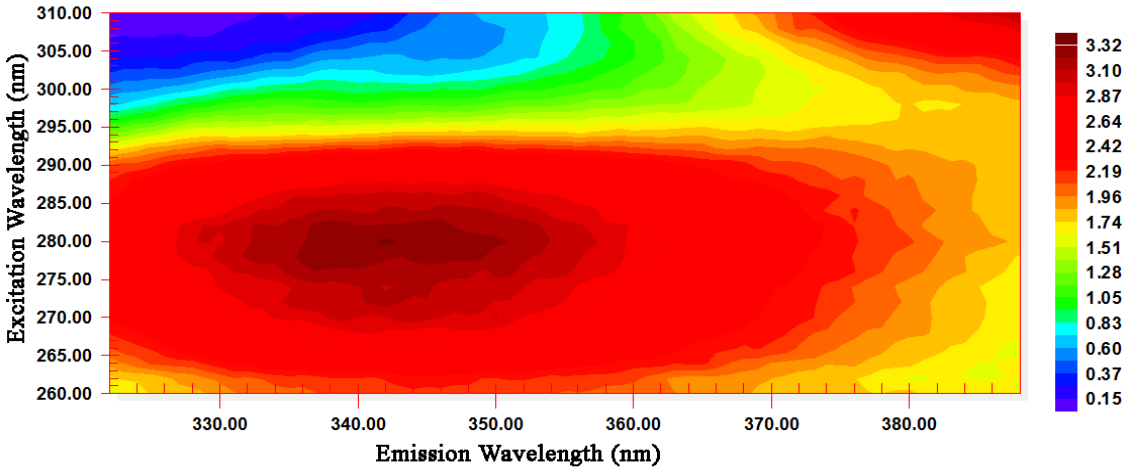

Figure 44B. Fluorescence excitation-emission matrix (EEM) of hemoglobin with LC Fraction 2 from the reaction of Asn-Fruc after 1 day incubation.

The fluorescence emission spectra of the individual LC fraction 4 of the same reaction are shown in **Figure 45**. It is observed that there are two main emissions lying at around 440 nm and 402 nm. The differences in the fluorescence spectra suggest that this fraction is structurally different from the previous fractions. When comparing with the fluorescence emission spectra of hemoglobin with LC Fraction 4 from the reaction of asparagine and fructose illustrated at **Figure 46A**, it is evident that the two emission bands corresponding to the individual fraction have disappeared and a very weak signal at 450 nm appears at an excitation wavelength of 260 nm only. The emission maximum was located around 342 nm for the excitation range of 260-290 nm as additionally shown in the fluorescence map in **Figure 46B**. For this case as well, the shift from the tryptophan-specific emission is not as large as that for the Hb-fraction 2. Nonetheless, there is a new emission at 387 nm for the excitation range of 295-310 nm.

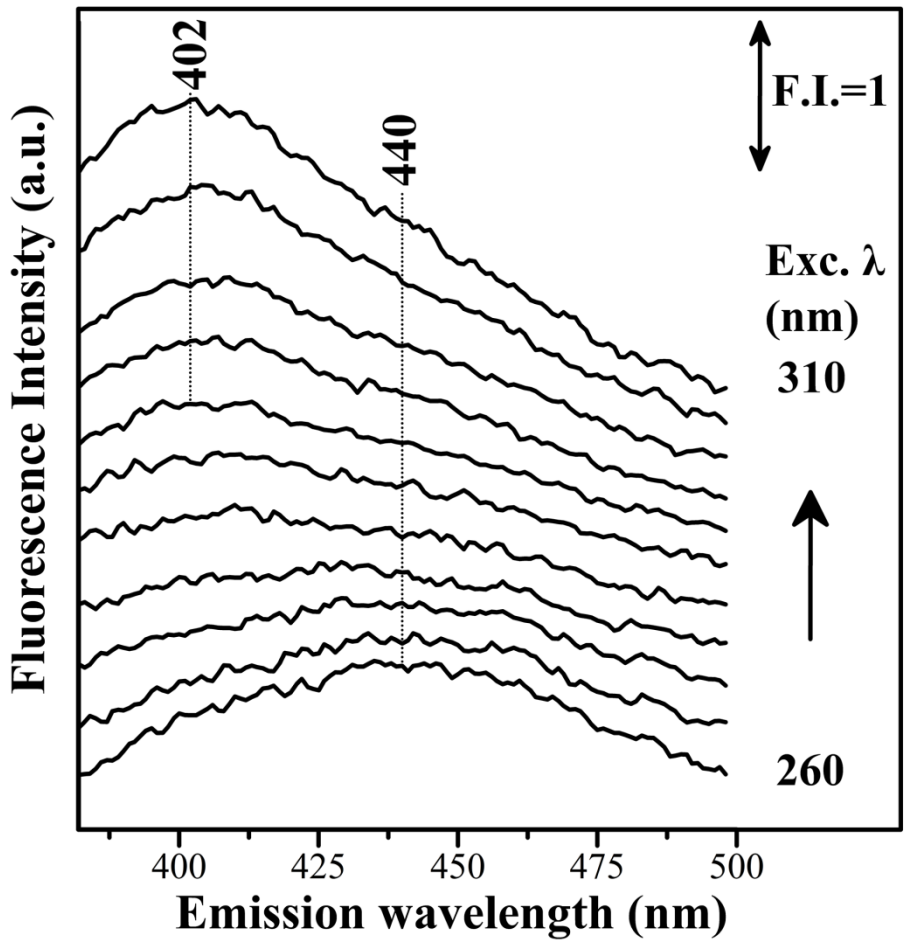

Figure 45. Fluorescence emission spectra of LC Fraction 4 from the reaction of Asn-Fruc (Excitation wavelength range: 260-310nm).

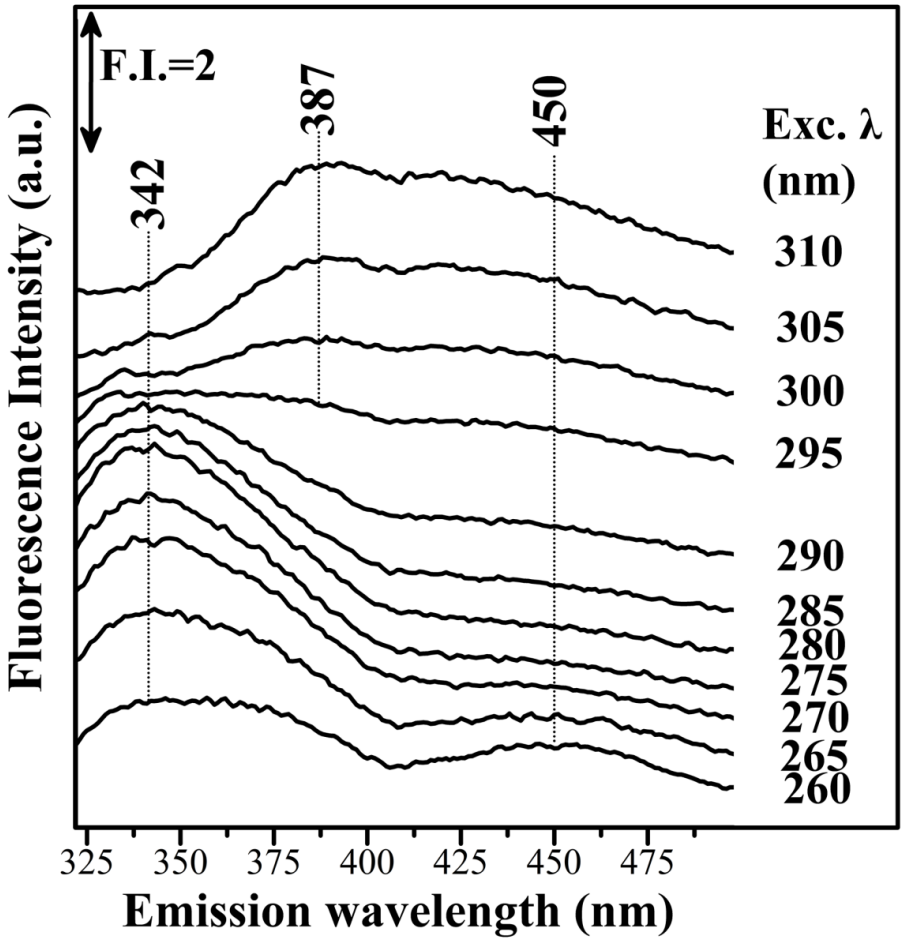

Figure 46A. Fluorescence emission spectra of hemoglobin with LC Fraction 4 from the reaction of Asn-Fruc after 1 day incubation (Exc. wavelength range: 260-310nm).

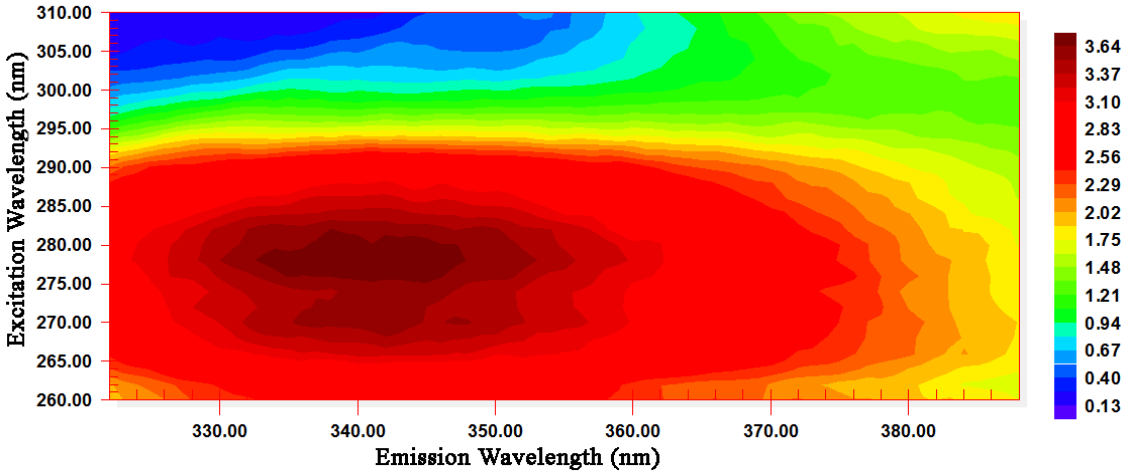

Figure 46B. Fluorescence excitation-emission matrix (EEM) of hemoglobin with LC Fraction 4 from the reaction of Asn-Fruc after 1 day incubation.

The fluorescence emission spectra of the individual LC fraction 5 of the reaction between asparagine-fructose (**Figure 47**) reveal that this is the exception since it failed to exhibit any specific fluorescence in the excitation range tested for the other fractions. This may be explained by the fact that this fraction probably has no chemical groups that fluoresce. It also seems to have no significant effect on the tryptophan specific fluorescence of hemoglobin after 1 day incubation (**Figure 48**). If we compare this result with the previous FTIR spectra, we conclude that this fraction presented the least effects when added to hemoglobin compared to other fractions. Nevertheless, a small emission band around 387 nm is evident for the excitation range 300-310 nm (**Figure 48**).

Figure 49 illustrates the fluorescent emission profiles of the hemoglobin-MRP mixtures after 1 month incubation. The major feature observed is the appearance of a new strong emission feature around 395 nm mainly at the excitation range of 290-310 nm. This emission band is increases with time since it was also observed after 1 day incubation as a smaller emission band (**Figure 42, 44, 46, 48A**). A fluorescence quenching effect on tryptophan fluorescence is also concurrently occurring. This effect was often utilized to demonstrate ligand-protein interactions [41-43].

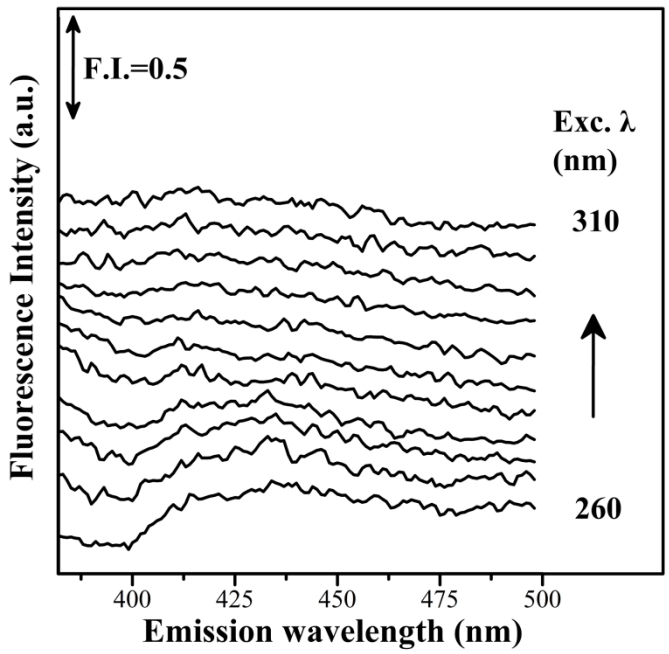

Figure 47. Fluorescence emission spectra of LC Fraction 5 from the reaction of Asn-Fruc (Excitation wavelength range: 260-310nm).

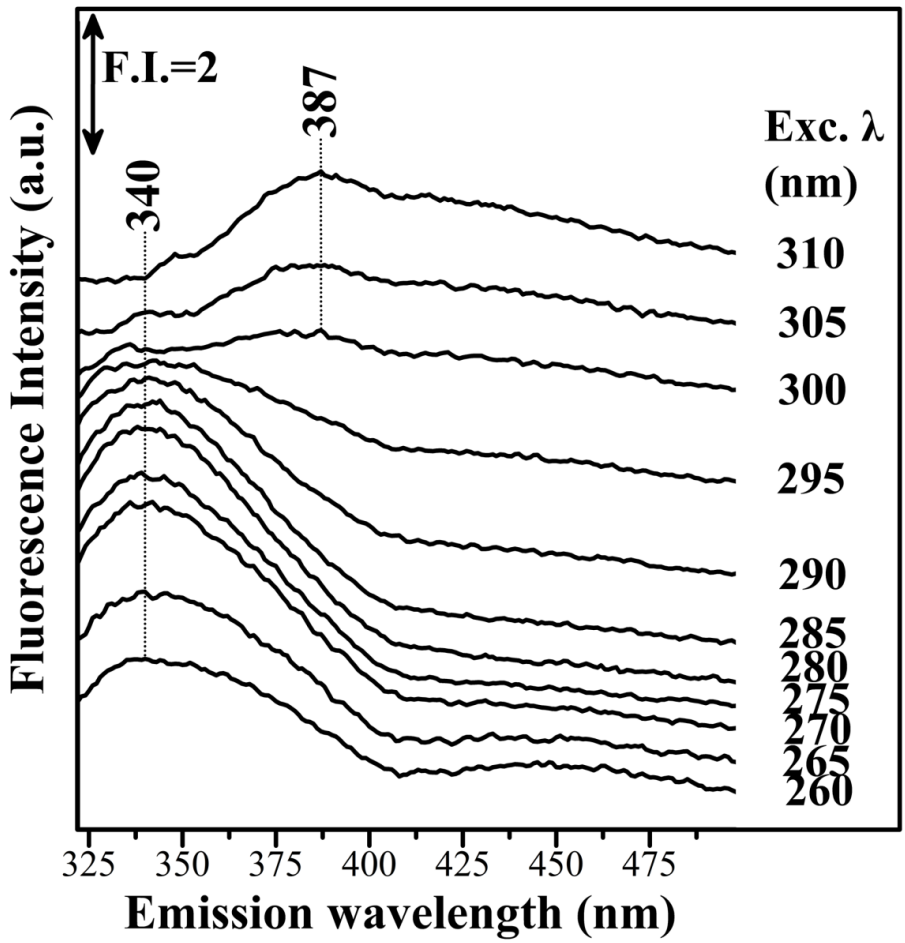

Figure 48A. Fluorescence emission spectra of hemoglobin with LC Fraction 5 from the reaction of Asn-Fruc after 1 day incubation (Exc. wavelength range: 260-310nm).

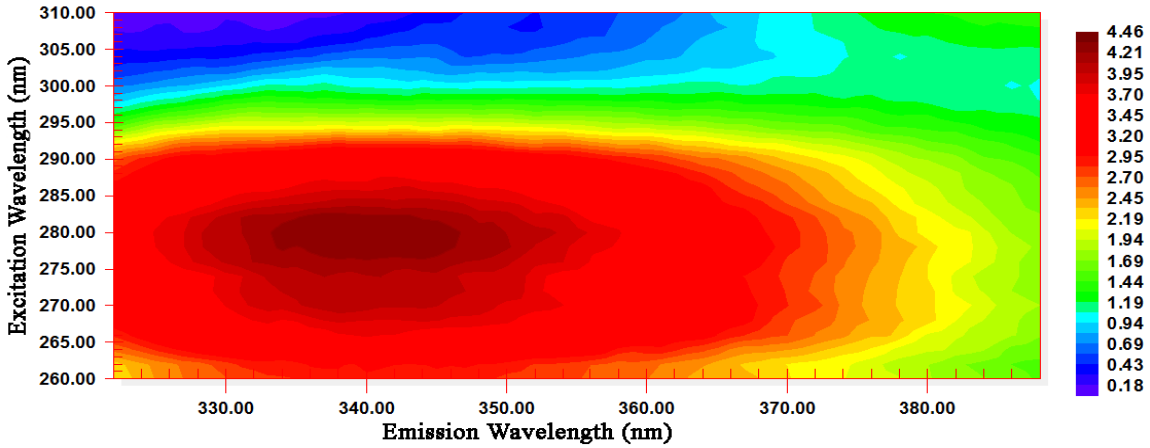

Figure 48B. Fluorescence excitation-emission matrix (EEM) of hemoglobin with LC Fraction 5 from the reaction of Asn-Fruc after 1 day incubation.

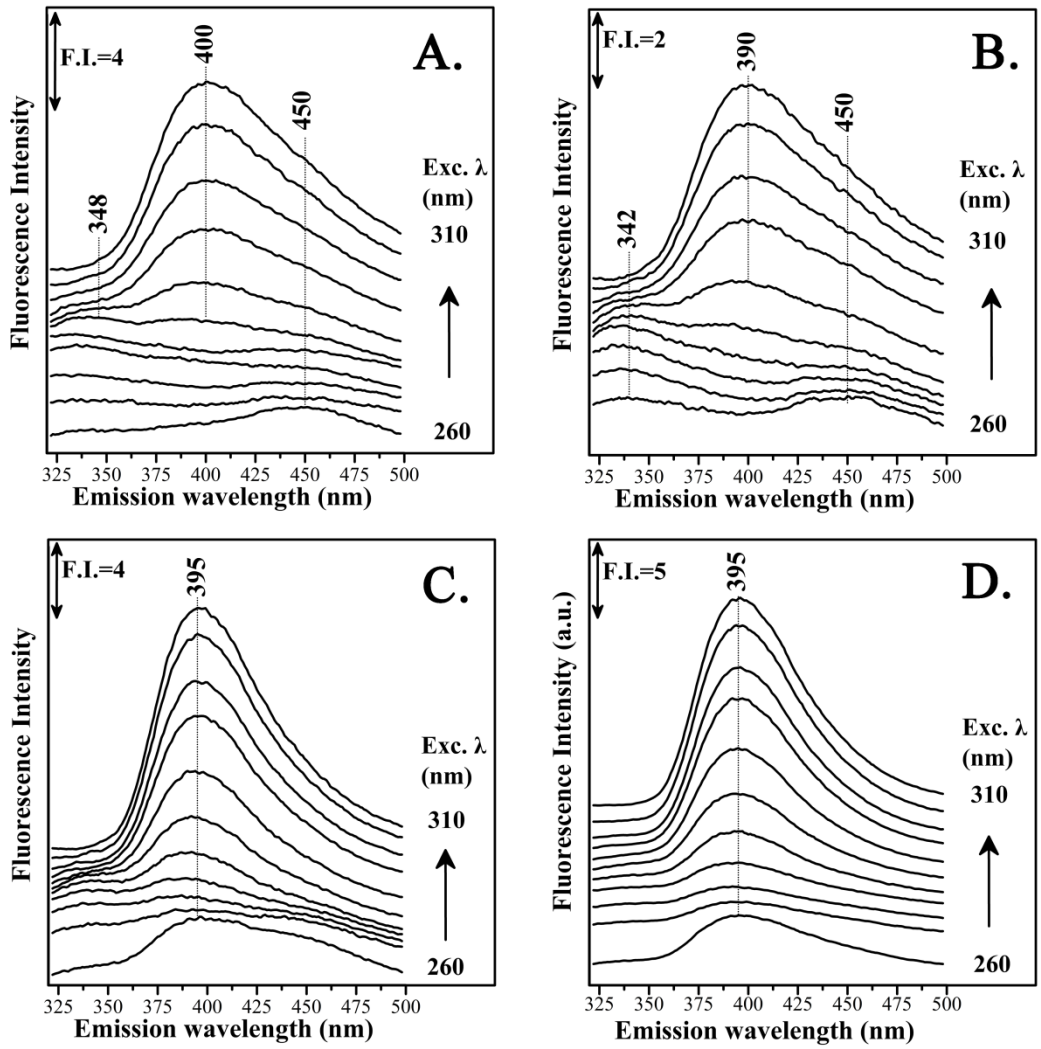

Figure 49. Fluorescence emission spectra of hemoglobin with: **A.** LC Fraction 2, **B.** LC Fraction 3, **C.** LC Fraction 2, **D.** LC Fraction 5, from the reaction of Asn-Fruc after 1 month incubation (Excitation wavelength range: 260-310nm).

It was recently identified from fluorescent intensity maps of degenerated cartilage from osteoarthritis patients that one of the fluorescent peaks appeared at the Ex./Em. 330/390 nm [44]. This is very similar to the 390 nm emission band appearing in the case of the spectra obtained in our investigation after prolonged incubation of the mixtures. The authors discuss that this is a result of non-enzymatic glycation reaction which is followed by the formation of several types of fluorescent crosslinks (AGEs) [44]. One example is pentosidine (Ex./Em. 335/385 nm) which is thought to be formed by

reactions of pentoses with lysine and arginine in model systems but also from glucose, fructose, ascorbate, Amadori compounds, 3-deoxyglucosone, and other sugars [45].

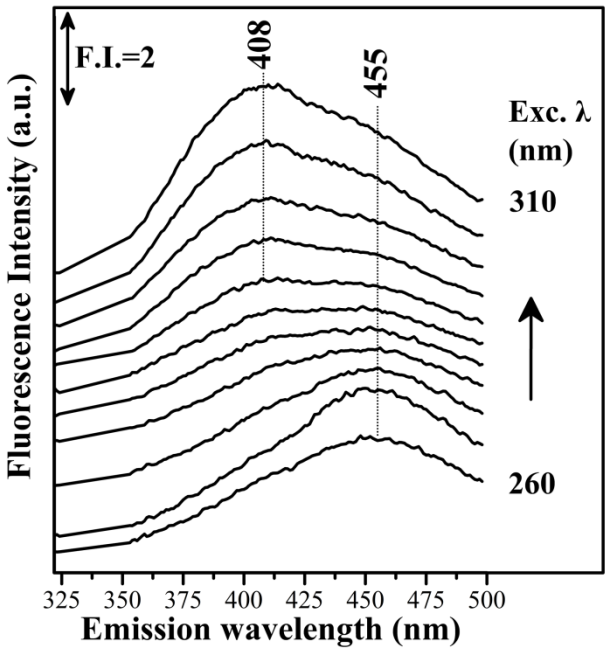

Figure 50. Fluorescence emission spectra of LC Fraction 2 from the reaction of Asn-Gluc (Excitation wavelength range: 260-310nm).

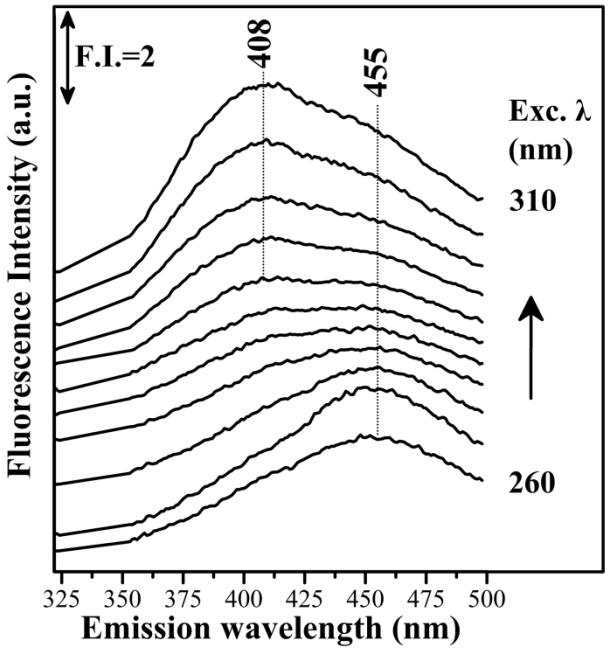

Figure 51. Fluorescence emission spectra of LC Fraction 3 from the reaction of Asn-Gluc (Excitation wavelength range: 260-310nm).

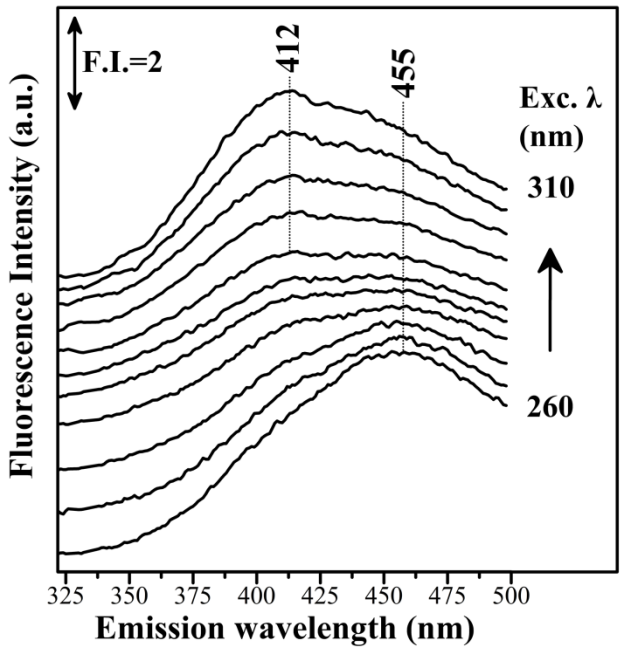

Figure 52. Fluorescence emission spectra of LC Fraction 4 from the reaction of Asn-Gluc (Excitation wavelength range: 260-310nm).

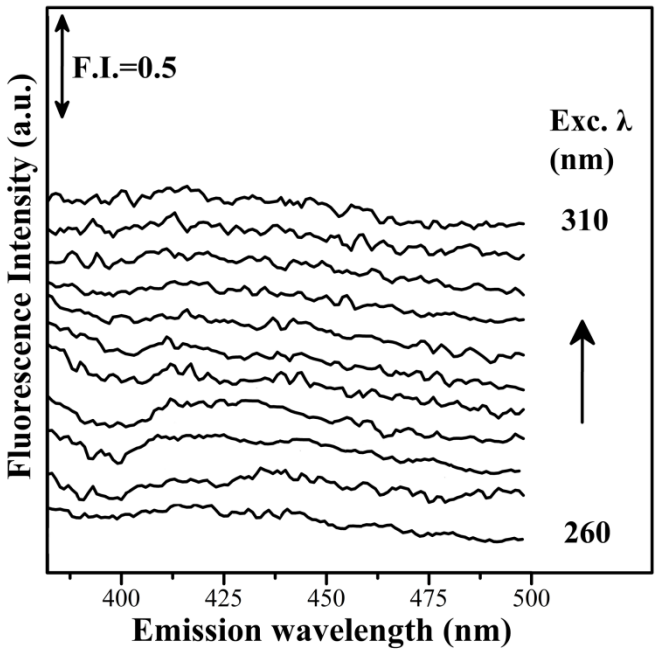

Figure 53. Fluorescence emission spectra of LC Fraction 5 from the reaction of Asn-Gluc (Excitation wavelength range: 260-310nm).

The fluorescence emission spectra of the individual LC fractions arising from the reaction of asparagine and glucose show similar fluorescent profiles as those from the asparagine and fructose reaction (**Figure 50-53**). The fluorescent signals arising from these individual LC fractions do not appear when these are mixed with hemoglobin (**Figure 54-55**).

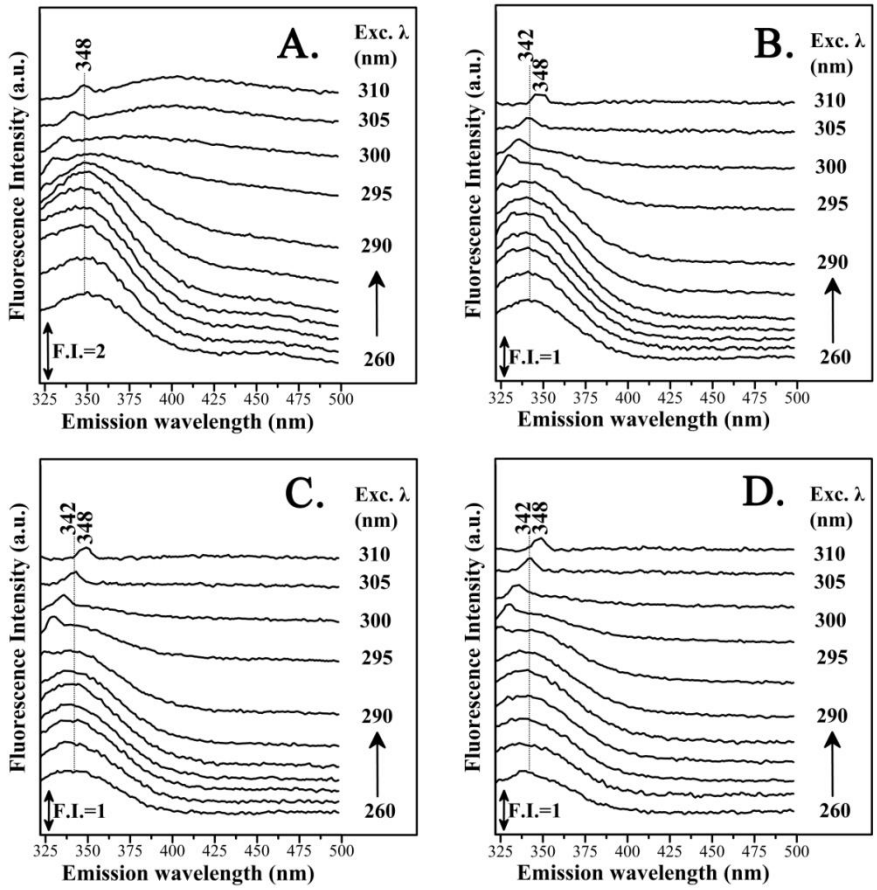

Figure 54. Fluorescence emission spectra of hemoglobin with: **A.** LC Fraction 2, **B.** LC Fraction 3, **C.** LC Fraction 4, **D.** LC Fraction 5 from the reaction of Asn-Gluc after 1 day incubation (Excitation wavelength range: 260-310nm).

The corresponding fluorescent emission spectra of the hemoglobin-MRP fractions from the asparagine-glucose reaction after 1 day incubation (**Figure 54**) exhibit to some extent a different effect on hemoglobin compared to their equivalent hemoglobin-MRP fractions from the asparagine-fructose reaction. For all the excitation wavelengths there

is a small shift in the tryptophan specific fluorescence from 338nm to 342 nm with the exception of fraction 2 which displays a shift to 348 nm. Additionally, there is a well-defined emission peak at approximately Ex./Em.: 310/348 nm present in all mixtures (**Figure 54**). The same emission features are observed after 1 month time period (**Figure 55**). The change after this time period is that there is a shift in the tryptophan-specific fluorescence of hemoglobin to 348 nm for fractions 2-4 and 353 nm for fraction 5 (**Figure 55**).

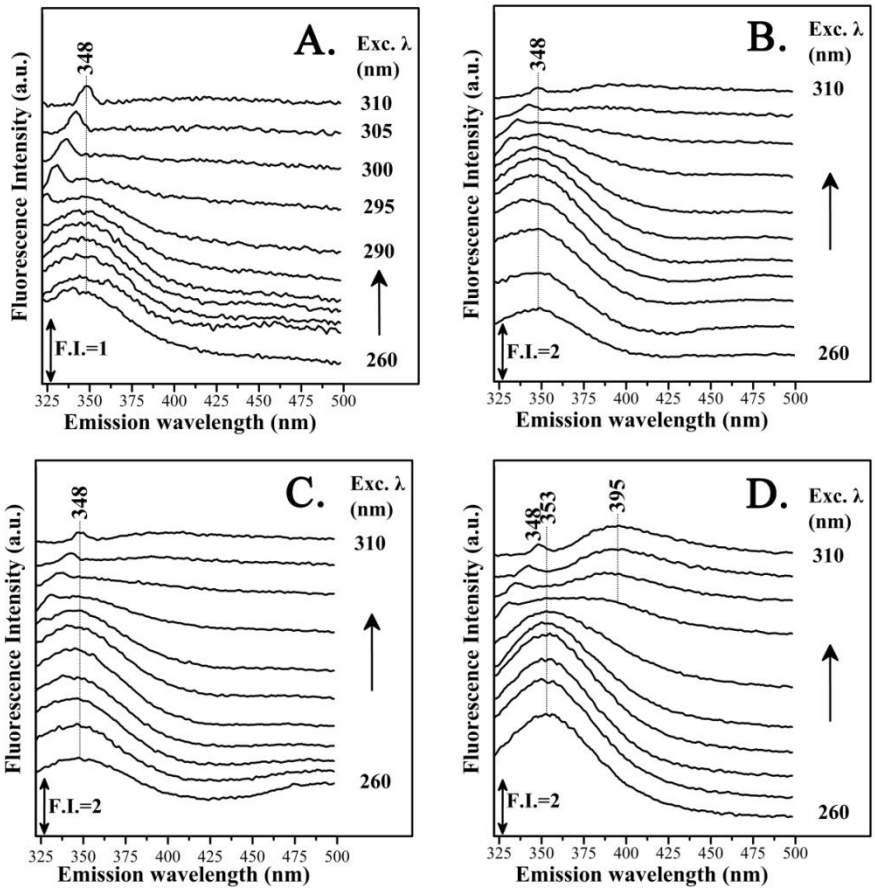

Figure 55. Fluorescence emission spectra of hemoglobin with: **A.** LC Fraction 2, **B.** LC Fraction 3, **C.** LC Fraction 4, **D.** LC Fraction 5 from the reaction of Asn-Gluc after 1 month incubation (Excitation wavelength range: 260-310nm).

The fact that similar red shifts were observed in the emission wavelength maximum of hemoglobin which was due to ligand binding [46] suggest a change in the microenvironment of the β-Trp 37 residue of hemoglobin towards a more polar side since it acts as a 'sensing' probe towards ligand binding in its proximity. The 348 nm species may relate to a stable Hb-AGE end-product though it has a comparatively lower quantum yield compared to hemoglobin intrinsic fluorescence.

Intrinsic fluorescence activity accompanied by fluorescent mapping were employed in this study to provide experimental evidence regarding the relationship of intrinsic protein fluorescence and the chemical events that follow ligand binding by glycated chemical species. The limitation of this study is the small number of Maillard reactions being addressed in model reactions and the lack of robust chemical standards. A larger in vivo study will extend these results and verify the ability of this fluorescence approach to a more heterogeneous in vivo system.

7.5 References

[1] Saguy, I., Kopelman, I.J., Mizrahi, S. (1978). Extent of non-enzymatic browning in grape fruit juice during thermal and concentration processes: Kinetics and prediction. *Journal of Food Processing and Preservation*, **2**, pp. 175–184.

[2] Toribio, J. L., Lozano, J. E. (1984). Nonenzymatic browning in apple juice concentrate during storage. *Journal of Food Science*, **49**, pp .889–892.

[3] Buera, M. P., Chirife, J., Resnik, S., and Wetzler, G. (1987). Nonenzymatic browning in liquid model systems of high water activity: Kinetics of color changes due to Maillard's reaction between different single sugars and glycine and comparison with caramelization browning. *Journal of Food Science*, **52**, pp. 1063-1067.

[4] Petriella, C., Chirife, J., Resnik, S. L., Lozano, R. D. (1988). Technical note: Correlation between induction time and rate of browning in heated model solutions of glucose and lysine. *International Journal of Food Science and Technology*, **23**, pp. 415–418.

[5] Labuza, T.P. 1994. Interpreting the complexity of the kinetics of the Maillard reaction. In: *Maillard reactions in Chemistry, Food and Health.* pp. 176-181. The Royal Society of Chemistry, Cambridge.

[6] Ajandouz, E. H. and Puigserver, A. (1999). Nonenzymatic browning reaction of essential amino acids: Effect of pH on caramelization and Maillard reaction kinetics. *Journal of Agricultural and Food Chemistry*, **47**, pp.1786–1793.

[7] Morales, F. J., Romero, C., Jimenez-Perez, S. (1996). Fluorescence associated with Maillard reaction in milk and milk-resembling systems. *Food Chemistry*, **57**, pp.423-428.

[8] Morales, F. J., van Boekel, M. A. J. S. (1997). A study on advanced Maillard reaction in heated casein/sugar solutions: Fluorescence accumulation. *International Dairy Journal*, **7**, pp.675–683.

[9] Leclere, J., Birlouez-Aragon, I. (2001). The fluorescence of advanced Maillard products is a good indicator of lysine damage during the Maillard reaction. *Journal of Agricultural and Food Chemistry*, **49**, pp.1682–1687.

[10] Birlouez-Aragon, I., Sabat, P., Gouti, N. (2002). A new method for discriminating milk heat treatment. *International Dairy Journal*, **12**, pp. 59–67.

[11] Vlassara, H., Brownlee, M., Cerami, A. (1986). Nonenzymatic glycosylation: Role in the pathogenesis of diabetic complications. *Clinical Chemistry*, **32**, pp. B37–B41.

[12] Cerami, A., Vlassara, H. and Brownlee, M. 1987. Glucose and aging. *Scientific American*, **256**, pp.90–96.

[13] Song, D. U., Jung, Y. D., Chay, D. O., Lee, K. H., Yang, S. Y., Shin, B. A., Ahn, B. W. (2002). Effect of drinking green tea on age-associated accumulation of Maillard type fluorescence and carbonyl groups in rat aortic and skin collagen. *Archives of Biochemistry and Biophysics*, **397**, pp.424–429.

[14] Ortwerth, B. J., Chemoganskiy, V., and Olesen, P. R. (2002). Studies on singlet oxygen formation and UVA light-mediated photobleaching of the yellow chromophores in human lenses. *Experimental Eye Research*, **74**, pp.217–229.

[15] Monnier, V.M., Cerami, A. (1982). Non-enzymatic glycosylation and browning of proteins in diabetes. *Journal of Clinical Endocrinology and Metabolism*, **11**, pp. 431-452.

[16] Monnier, V. M., Kohn, R. R., Cerami, A. (1984). Accelerated age-related browning of human collagen in diabetes mellitus. *Proceedings of the National Academy of Sciences U.S.A.*, **81**, pp. 583–587.

[17] Cerami, A. (1994). The role of the Maillard reaction in vivo. In: *Proceedings of the Fifth International Symposium on the Maillard Reaction*. The Royal Society of Chemistry, Cambridge.

[18] Baynes, J. W., Thorpe, S. R. (1999). The role of oxidative stress in diabetic complications: A new perspective on an old paradigm. *Diabetes*, **48**, pp. 1–9.

[19] Baynes, J. W. (2001). The role of the AGEs in aging: Causation or correlation. *Experimental Gerontology*, **36**, pp.1527–1537.

[20] Matiacevich, S. B., Buera, M. P. (2006). A critical evaluation of fluorescence as a potential marker for the Maillard reaction. *Food Chemistry*, **95**, pp. 423– 430.

[21] Rozycki, S. D., Buera, M. P., Piagentini, A. M., Costa, S. C., Pauletti, M. S. (2010). Advances in the study of the kinetics of color and fluorescence development in concentrated milk systems. *Journal of Food Engineering*, **101**, pp. 59–66.

[22] Morales, F.J., Van Boekel, M.A.J.S. (1998). A study on advanced Maillard reaction in heated casein/sugar solutions: colour formation. *International Dairy Journal*, **8**, pp. 907-915.

[23] Rufián-Henares, J.A., Delgado-Andrade, C. (2009). Effect of digestive process on Maillard reaction indexes and antioxidant properties of breakfast cereals. *Food Research International*, **42**, pp. 394-400.

[24] Chio, K.S., Tappel, A.L. (1969). Synthesis and characterization of the fluorescent products derived from malonaldehyde and amino acids. *Biochemistry*, 8, pp.2821-2827.

[25] Tessier, F., Monnier, V. M., Kornfield, J. A. (2002). Characterization of novel chromophores, fluorophores and cross-links from glyceraldehyde, lysine and arginine. In: *International Congress Series*. Elsevier, pp. 303-311.

[26] Shipanova, I.N., Glomb, M.A., Nagaraj, R.H. (1997). Protein modification by methylglyoxal: chemical nature and synthetic mechanism of a major fluorescent adduct. *Archives of biochemistry and biophysics*, **344**, pp. 29-36.

[27] Henle, T., Schwarzenbolz, U., Klostermeyer, H. (1997). Detection and quantification of pentosidine in foods. *Zeitschrift für Lebensmitteluntersuchung und-Forschung A*, 204, pp. 95-98.

[28] Booth, A. A., Khalifah, R. G., Todd, P., Hudson, B. G. (1997). In vitro kinetic studies of formation of antigenic advanced glycation end products (AGEs) Novel inhibition of post-Amadori glycation pathways. *Journal of Biological Chemistry*, **272**, pp. 5430-5437.

[29] Hellwig, M., Henle, T. (2014). Baking, Ageing, Diabetes: A Short History of the Maillard Reaction. *Angewandte Chemie International Edition,* **53**, pp. 10316-10329.

[30] Lakowicz, J. R. (1983). Protein fluorescence. In: *Principles of fluorescence spectroscopy* (pp. 341-381). Springer.

[31] Ioannou, A., Daskalakis, V., Varotsis, C. (2017). Detection of Maillard reaction products by a coupled HPLC-Fraction collector technique and FTIR characterization of

Cu(II)-complexation with the isolated species. *Journal of Molecular Structure*, **1141**, pp. 634-642.

[32] Ioannou, A., Varotsis, C. (2016). Real Time Monitoring the Maillard Reaction Intermediates by HPLC- FTIR. *Journal of Physical Chemistry and Biophysics*, **6**, p. 210.

[33] Iida, T., Yoshiki, Y., Akiyama, Y., Okubo, K. (2002). Photon emission properties of roasted soybean as related to reactive oxygen scavenging activities. *Food Chemistry*, **77**, pp. 471–477.

[34] Masaki, H., Okano, Y., and Sakurai, H. (1999). Generation of active oxygen species from advanced glycation end-products AGEs during ultraviolet light A UVA irradiation and a possible mechanism for cell damaging. *Biochimica and Biophysica Acta*, **1428**, pp. 45–56.

[35] Morales, F., Jimenez-Perez, S. (2001). Free radical scavenging capacity of Maillard reaction products as related to colour and fluorescence. *Food Chemistry*, **72**, pp. 119-125.

[36] Park, C. K., Kim, D. H. (1983). Relationship between fluorescence and antioxidant activity of ethanol extracts of Maillard browning mixture. *Journal of the American Oil Chemists' Society*, **60**, pp. 22–26.

[37] Matiacevich, S. B., Santagapita, P. R., Buera, M. P. (2005). Fluorescence from the Maillard reaction and its potential applications in food science. *Critical reviews in food science and nutrition*, **45**, pp.483-495.

[38] Jing, H., Kitts, D. D. (2004). Antioxidant activity of sugar–lysine Maillard reaction products in cell free and cell culture systems. *Archives of Biochemistry and Biophysics*, **429**, pp. 154-163.

[39] Ferrer, E., Alegria, A., Farre, R. (2000). Advanced glycosilation end products (AGEs) and colour in milk and milk resembling systems. A review. *Recent Research Developments in Agricultural & Food Chemistry*, **4**, pp. 269–290.

[40] Vigneshwaran, N., Bijukumar, G., Karmakar, N., Anand, S., Misra, A. (2005). Autofluorescence characterization of advanced glycation end products of

hemoglobin. *Spectrochimica Acta Part A: Molecular and Biomolecular Spectroscopy*, **61**, pp. 163-170.

[41] Sil, S., Kar, M., Chakraborti, A. S. (1997). Studies on the interaction of hematoporphyrin with hemoglobin. *Journal of Photochemistry and Photobiology B: Biology*, **41**, pp.67-72.

[42] Mahesha, H. G., Singh, S. A., Srinivasan, N., Rao, A. G. (2006). A spectroscopic study of the interaction of isoflavones with human serum albumin. *The FEBS journal*, **273**, pp.451-467.

[43] Böhl, M., Tietze, S., Sokoll, A., Madathil, S., Pfennig, F., Apostolakis, J., Fahmy, K., Gutzeit, H. O. (2007). Flavonoids affect actin functions in cytoplasm and nucleus. *Biophysical journal*, **93**, pp.2767-2780.

[44] Padilla-Martinez, J. P., Lewis, W., Ortega-Martinez, A., Franco, W. (2017). Intrinsic fluorescence and mechanical testing of articular cartilage in human patients with osteoarthritis. *Journal of Biophotonics*, pp.1-10.

[45] Dyer, D. G., Blackledge, J. A., Thorpe, S. R. and Baynes, J. W. (1991). Formation of pentosidine during nonenzymatic browning of proteins by glucose. Identification of glucose and other carbohydrates as possible precursors of pentosidine in vivo. *Journal of Biological Chemistry*, **266**, pp.11654-11660.

[46] Chakraborty, S., Chaudhuri, S., Pahari, B., Taylor, J., Sengupta, P. K., Sengupta, B. (2012). A critical study on the interactions of hesperitin with human hemoglobin: Fluorescence spectroscopic and molecular modeling approach. *Journal of luminescence*, **132**, pp.1522-1528.

8 Conclusions

The objective of the experimental work was to detect intermediates in the acrylamide formation pathway mainly by means of the ATR-FTIR technique and provide insight about how these are formed with respect to temperature, pH and chemical composition of the employed system. FTIR is an extremely structure-sensitive technique and our experimental setup was suited for real-time determination of the transient intermediates formed in modeled Maillard reactions especially under physiological aqueous conditions resembling food systems. The application of analytically independent methods for the separation and identification of discrete chemical species and the construction of chemical fingerprint mapping techniques such as illustrated by fluorescence spectroscopy was a prerequisite for this work.

In the first section, the direct coupling of a chromatographic system such as high performance liquid chromatography (HPLC) with a structure sensitive detector like on-line FTIR employing an ATR flow cell was demonstrated as a unique analytical technique. The HPLC-FTIR technique can be a useful tool in the analysis of Maillard reaction products. The first stage in the classical Maillard reaction is the formation of Schiff base and Amadori adducts to amino acids and/or proteins. However, these are difficult to detect in an aqueous environment. The Schiff base intermediate of a fructose/asparagine model system was identified by difference time-dependent spectra. We have characterized specific FTIR marker bands corresponding to the Schiff base intermediate. This approach of the HPLC-FTIR application to the Maillard reaction has the potential to be implemented to other similar chemical reactions in a range of disciplines without the need to isolate the species and characterize them separately. The limitation of this method is that it is mainly a qualitative analysis method and the detection limit of the FTIR detector is not as low as a typical chromatographic technique.

From this point, it was followed that there was a requirement for increasing the sample concentration in order to detect small amounts of low-yield chemical species like the Amadori compound in these reactions. Solid phase extraction (SPE) was then utilized in combination with ATR-FTIR spectroscopy in order to identify these products from a

complex chemical composition mixture. We have identified the vibrational marker bands primarily of the C=O group of the Amadori compounds in the FTIR spectra after methanolic SPE elution. This resulted from enhanced detection of these chemical species after separation from their initial reactants.

Furthermore, a novel analytical technique with respect to Maillard reactions involving a combination of high performance liquid chromatography (HPLC) with a fraction collector was described. This methodology was aimed towards the effective isolation and subsequent spectroscopic analysis of MRPs. The FTIR experimental evidence presented structure-sensitive changes as depicted by a deamination event and formation of asparagine glycoconjugates. Density functional theory calculations were also performed to further support the experimental findings.

Schiff bases and Amadori adducts also undergo facile oxidation, especially in the presence of transition metal ions, and fragment to yield shorter chain sugars and reactive intermediates thus accelerating the diversity of generated species. Metal complexes with saccharides and their derivatives are of increasing importance in medicine and pharmacy and their significance lies in the oxidative pathways and the loss of anti-oxidant activity by MRP/metal complexes. Nevertheless, there are limited spectroscopic insights about their coordination function. We have attempted to provide spectroscopic evidence of Cu (II) metal ion complexation with MRPs as depicted by changes in the UV-vis and FTIR spectra in characteristic vibrational marker bands.

It is well established that Maillard products are formed by reactions of both carbohydrate- and lipid-derived intermediates with proteins, leading to formation of advanced glycation and lipoxidation end-products (AGE/ALEs). AGEs can be described by their ability to form cross links on proteins. Dietary Maillard products as these resembling from model systems are being discussed as “glycotoxins” and thus pose a nutritional risk. To take a step further we devised an experimental investigation involving the interactions of these compounds with proteins, namely hemoglobin and myoglobin. The spectroscopic investigation upon addition of discrete MRPs to hemoglobin and myoglobin led to the modification of Amide I band and formation of a modified protein adduct known as a hemichrome. Hemichromes are known to occur through hexa-coordination of the heme iron when the distal histidine irreversibly blocks the heme ligand binding site. As a consequence of loss of functionality it is

hypothesized that protein aggregation occurs identified through a distinct FTIR absorption band. Nevertheless, an issue to be considered is that the extent of this modification is limited under the experimental conditions presented as illustrated by the percentage of the new species forming against the native protein concentration. However, in our opinion, these findings are very significant because the spectral events did occur without any induction of any sort in the course of the experimental work. It is therefore of great interest to extent this investigation in a prolonged time setting. Additionally, it is worth investigating the interactions of several lipids and lipid derivatives with human serum proteins and likewise with other protein targets. This could be performed through a series of structure-sensitive techniques, such as Raman and fluorescence spectroscopies.

The latter was already being used as a complementary technique to study the glycation reaction of hemoglobin with MRPs from an asparagine-sugar model system. The structural alteration of hemoglobin was demonstrated through shifts in the characteristic tryptophan fluorescence and the parallel loss of MRP signals. These events support the preceding spectral events confirming protein modification monitored by the UV-vis and ATR-FTIR techniques.